

https://dspace.org/

Heat-Induced Changes to Porcine Bone at Different Taphonomic Conditions

Rathokane, Thato Portia

2024

University of the Witwatersrand, Johannesburg

https://hdl.handle.net/10539/47072

Rathokane, Thato Portia. (2024). Heat-Induced Changes to Porcine Bone at Different Taphonomic Conditions [Master`s dissertation, University of the Witwatersrand, Johannesburg]. WIReDSpace. https://hdl.handle.net/10539/47072

Downloaded from a DSpace repository. https://dspace.org/

Heat-Induced Changes to Porcine Bone at Different Taphonomic Conditions



UNIVERSITY OF THE
WITWATERSRAND,
JOHANNESBURG



Thato Portia Rathokane

A Dissertation submitted to the Faculty of Health Sciences, University of the Witwatersrand, Johannesburg, in fulfilment of the requirements for the degree of Master of Science in Medicine.

FACULTY OF HEALTH SCIENCES
UNIVERSITY OF THE WITWATERSRAND, JOHANNESBURG

2024

Declaration

I, Thato Portia Rathokane, declare that this dissertation entitled “Heat-induced changes to porcine bone at different taphonomic conditions” is my own unaided work. It is being submitted for the Degree of Master of Science in Medicine at the University of the Witwatersrand, Johannesburg. It has not been submitted before for any degree or examination at any other University.

_____

Thato Portia Rathokane

30 August 2024 at Parktown, Johannesburg

Abstract

Heat exposure to bone results in physical and chemical alterations thus making victim identification and the circumstances surrounding their death difficult to determine. There is conflict in understanding how the expression of macroscopic heat-induced changes relate to microstructural heat-induced alterations of collagen with specific reference to burnt bone. The aim of this study was to investigate the relationship between heat-induced macroscopic and histological alterations at different taphonomic conditions cremated at different temperatures.

The study was done with incrementally heated (300°C, 400°C and 500°C) bones (N=3, experimental n=27; control n=6) at different taphonomic conditions (fleshed, wet/defleshed and dry bone) using a muffle furnace. Bone samples were weighed, and analysed for macroscopic changes (colour, mass loss, fracturing and fragmentation). Post-cremation, 3mm bone blocks were extracted and fixed in 10% neutral buffered formalin, decalcified (10% formic acid) then processed and sectioned. Sections were stained with Sirius Red-Fast Green (SFRG) stain to investigate collagen presence and distribution. Additionally, 1mm blocks were extracted for ground bone sectioning and photomicrographs were taken for micro-fracture assessment.

Wet and dry bones cremated at 400°C and 500°C were partially calcined and had more macroscopic and microscopic fractures compared to fleshed bones. Only fleshed and wet bones presented misaligned fragmentation, indicative of plastic deformation. The SRFG stain was shown to reveal both collagenous and non-collagenous proteins; however, with polarized light in combination with SRFG staining it was possible to identify areas of putative collagen even at higher temperatures (400°C and 500°C) in fleshed but not in wet and dry bones. Further studies using more specific approaches to identifying collagen degradation are proposed, in order to understand the mechanisms of fracturing and bone deformation.

The present study was able to propose a role for soft tissue and moisture in protecting bone during cremation and provide insights into the biomechanics of thermal alterations of porcine bone. Before application can be made in a human forensic setting, further research in human bone and across more varied conditions is required. This study is seminal to the understanding of both macro and microscopic bone heat-induced changes, a relationship rarely assessed in burnt bone studies.

Dedication

This dissertation is dedicated to:

my unwavering pillars of support – my mother, father, and grandmother:

Lorraine Tebello Rathokane

Joseph Tebogo Mlambo

Elizabeth Ntswaki Rathokane

Special gratitude to my resilient source of motivation amidst challenges, my daughter:

Kganyang Daisy Rathokane

Acknowledgements

I thank my supervisors' grant (RINC) from the School of Anatomical Sciences for funding the materials I needed to conduct the study. I thank the Gauteng City Region Academy bursary for funding my studies throughout the course of my degree.

A special thanks to the School of Chemical and Metallurgy Engineering for allowing me to use the muffle furnace for cremating the bones. Thanks to the School of Anatomical Sciences for providing consumables and allowing me to use the tissue processing, decalcification and maceration equipment.

Special thanks to my supervisors, Dr Nicholas Bacci, Professor Tanya Augustine and Dr Brendon Billings for their consistency in guiding me, for being reliable and supportive throughout. I humbly thank Mr Paul den Hoed from School of Chemical and Metallurgy Engineering for his guidance throughout conducting cremation trials and his knowledge on thermodynamics. I also thank Mrs Hasiena Ali and Mr Bradley Khoza from the School of Anatomical Sciences for assistance and training in histological and staining methods throughout the course of the laboratory work conducted for this study.

Contents Page

Declaration i
Abstract ii
Dedication iii
Acknowledgement iv
Table of Contents v
List of figures viii
List of tables x
Abbreviations xi
1.Introduction 1
1.1 A brief description of fire 1
1.2 Bone composition and histology 3
1.3 Effects of heat-induced macroscopic changes 7
1.4 Effects of heat-induced microscopic changes 8
1.5 Relationship of macro and microscopic heat-induced changes 10
1.6 Aims and Objectives 13
2.Materials and Methods 14
2.1 Ethics 14
2.2 Sampling 14
2.3 Bone Specimen Groups and Preparation 14
2.4. Weighing and Photography 16
2.5. Furnace preparation and Cremation Process 16
2.6. Pilot Study 18
2.6.1. Optimising atmospheric composition - nitrogen use 18
2.6.2. Optimising heating temperatures 18
2.6.2.1. Selection of parameters 19
2.6.3. Optimizing decalcification solutions 21
2.6.3.1. Bone block extraction 21
2.6.3.2. Decalcification 22
2.7. Experimental Study 24

2.7.1. Sampling 24
2.7.2. Macroscopic analyses 25
2.7.3. Heat-induced fragmentation 25
2.7.4. Heat-induced colour changes 26
2.7.5. Heat-induced fracturing 27
2.8. Microscopic Analysis 30
2.8.1. Bone block extraction and decalcification 30
2.8.2. Decalcified bone tissue processing, cutting, and staining 30
2.8.3. Ground bone sectioning 31
2.8.4. Histological analysis of stained and ground bone sections 31
2.9. Data analysis 33
3.Results 35
3.1. Optimization of heating experimental parameters 35
3.1.1. The use of nitrogen gas during cremation 35
3.1.2. Optimising the cremation temperature 35
3.1.3. Determination of optimal decalcification solution 37
3.2. Experimental Study - Macroscopic Results 39
3.2.1. Repeatability 39
3.2.2. Heat-induced macroscopic colour change and fragmentation 39
3.2.3. Heat-induced mass loss 40
3.2.4. Heat-induced macroscopic fracturing 41
3.3. Experimental study - Microscopic Results 44
3.3.1. Repeatability 45
3.3.2. Histological Morphology of bone, tendon and muscle 45
3.3.2. Qualitative assessment of collagen 48
3.3.3. Microfracture assessment 54
4.Discussion 58
4.1. Cremation trials in closed and open systems 58
4.2. Bone heat transfer 60
4.3. Heat-induced bone macroscopic changes and proposed associated microstructural mechanisms 61

4.3.1. Colour changes **61**
4.3.2 Mass changes **63**
4.3.3 Fragmentation and fracturing **64**
5. Conclusion **75**
5.1. Limitations **75**
5.2. Findings **77**
References **80**
Appendix A: Waiver from Animal Ethics Research Committee **100**
Appendix B: Solutions **103**
Appendix C: Ground Bone Sectioning and other methods **106**
Appendix D: Optimization Results **107**
Appendix E: Thermocouples temperature graph **110**
Appendix F: Heat-induced colour change and fragmentation **110**
Appendix G: Heat-induced mass loss **115**
Appendix H: Heat-induced macro-fracturing **116**
Appendix I: Experimental microfracture **118**
Appendix J: Plagiarism – Turnitin Report **119**

List of Figures

Figure Number	Title of Figures	Page
Figure 1.2	Photomicrograph showing unaltered juvenile porcine bone histology and human bone histology.	**6**
Figure 2.3.1	Flow diagram showing the experimental procedure from cremation to analysis including the pilot study and experimental components of the study.	**15**
Figure 2.5.1	Image showing the bone prepared for cremation by drilling, inserting thermocouple and putting the bone into the furnace.	**17**
Figure 2.6.2.1	Image of pre- and post-cremation of pig tibia bones at 200°C, 600°C and 800°C.	**20**
Figure 2.6.3.1	Left Porcine (Sus scrofa domesticus) tibiae showing block extraction regions.	**22**
Figure 2.6.3.2.1	Examples of decalcification checks of dry bone blocks on different days.	**23**
Figure 2.6.3.2.2	Example of undecalcified and decalcified cremated bone block damage.	**24**
Figure 2.7.4.1	Images showing heat lines, heat border, charring and calcination colour change.	**27**
Figure 2.7.5.1	A left dry macerated treated dry tibia bone with labelled location.	**28**
Figure 2.7.5.2	Types of heat-induced macroscopic fractures on cremated bones.	**29**
Figure 2.8.4.1	Image showing the division of slide section.	**33**
Figure 3.1.2.1	Graphs showing the cremation temperatures of samples, furnace, and the ambient temperature during cremation for 30 minutes at different maximum temperatures.	**37**
Figure 3.1.3.1	Decalcification time in relation to acid decalcification solutions and successful embedding of blocks.	**38**
Figure 3.2.3.2	Pre and post-cremation mass of bone cremated at specific temperature under different bone conditions.	**41**
Figure 3.2.4.1	Macrofracture type prevalence and location across all experimental	**43**

	parameters (taphonomic conditions and temperatures)	
Figure 3.3.2.1	Representative photomicrographs of tendon and muscle stained with Haematoxylin and Eosin	**46**
Figure 3.3.2.2	Representative photomicrographs of bone stained with Haematoxylin and Eosin	**47**
Figure 3.3.3.1	Representative photomicrographs showing sections of tendon and muscle stained with Sirius Red – Fast Green	**50**
Figure 3.3.3.2	Representative photomicrographs showing Sirius Red – Fast Green stained sections of decalcified unburnt bone (control).	**51**
Figure 3.3.3.3	Representative photomicrographs of Sirius Red – Fast Green stained decalcified bone sections obtained from fleshed bones cremated at different temperatures.	**52**
Figure 3.3.3.4	Representative photomicrographs showing the Sirius Red – Fast Green staining of decalcified sections from wet and dry bones cremated at different temperatures.	**53**
Figure 3.3.4.1	Representative photomicrographs of ground bone sections at different temperatures and taphonomic conditions showing micro-fracturing.	**56**
Figure 3.3.4.2	Graph showing the micro-fracturing extent on bones at different taphonomic condition cremated at different temperatures.	**57**

List of Tables

Table Number	Title of Table	Page
Table 2.6.2.1	Pilot study bone sample distribution.	**19**
Table 2.7.1	Total bone sample for each bone condition and cremation temperature.	**25**
Table 2.7.4.1	Scoring system of heat-induced colour changes.	**26**
Table 2.7.5.1	Refined heat-induced macroscopic fracture types and their descriptions	**28-29**
Table 2.8.4	Proposed microfracture definition criteria	**32**
Table 3.2.4.1	Frequency of fractures and fracture type for bones at different taphonomic conditions cremated at different temperatures.	**44**

Abbreviations

ANOVA – Analysis of Variance

APES - Aminopropyltriethoxysilane

FA – Formic acid

FCA – Formic citric acid

H&E – Haematoxylin and eosin

NA – Nitric acid

NBF – Neutral buffered formalin

SRFG – Sirius Red-Fast Green

WHO – World Health Organization

Chapter 1: Introduction

1.1. A brief description of fire

According to World Health Organisation (WHO), exposure to fire, smoke and flame has been found to be the main cause of 2 328 (6.8%) deaths in South Africa in 2016 (WHO, 2016) which has increased from 1993 to 2020, on global scale, to approximately 401,000 deaths per year (Murray and Lopez, 1996; Brushlinsky *et al*., 2022). Fire is known to be one of the most destructive forces in our society (Correia, 1996), destroying any material ranging from buildings, and vehicles to body tissues including bones. Fire is defined as an exothermic oxidation reaction between fuel and an oxidizer (most often oxygen) that generates sufficient heat to be self-sustaining and yields readily detectable heat and light (DeHaan, 2007).

Fire as a result of heat can be caused by vehicle accidents (Correia and Beattie, 2002), house fires (Dirkmaat, 2002) and mass destruction (Mundorff, 2008). These causes may also include areas with dangerously exposed electrical cables, highly explosive liquids and chemicals which can result in smoke and/or flames which induce fire (Imaizumi, 2005). Globally, about 2.7 billion people lack clean and safe cooking facilities and 1.2 billion have no access to electricity (Byers, 2004), and therefore, cooking has been reported to be one of the major causes of fire, resulting in 80% of fires being kitchen-related (Spearpoint and Hopkin, 2021). In South Africa, as a developing nation (de Klerk and de Villiers, 2012), there are many low-income settlements where highly flammable fuels like paraffin are used due to energy poverty (Gevaart-Durkin *et al*., 2014) and often lead to burn injuries/fatalities (Schwebel *et al*., 2009; Kimemia *et al*., 2014; Kimemia and Niekerk, 2017).

Fire is described as a chemical process through which heat and light are generated (Reidsma *et al*., 2016) while heat is described as the energy transferred when there is temperature difference, moving from regions of higher temperature to lower temperature (Cho *et al*., 1998). There are three types of heat transfer: conduction, radiation, and convection. Conduction is the transfer of heat through physical contact. The process of conduction occurs at a molecular level transferring energy from more energetic molecules to lower energetic molecules (Cho *et al*., 1998). Radiation is electromagnetic energy emitted by a body at the expense of its internal energy and does not require a medium for conduction (Cho *et al*., 1998). Convection occurs through movement of fluid

(including air) due to a density difference between temperatures (Cho *et al*., 1998). Heat effects on bone can occur without inducing fire, through processes such as bone drilling operations which cause a rotational speeding (Davidson, 1999). Temperature and thermal damage have been found to increase with increasing heat effects such as drilling with rotational speed (Davidson, 1999).

The heat exposure on bodies results in thermal destruction ranging from damage in physical, mechanical, and behavioural functioning of the body as well as destruction of skin, muscle, cartilage, and underlying fats and tissues (DeHaan, 2015, 2018). Heat exposure on incomplete burnt remains (cremains) is a critical taphonomic challenge as it alters the skeletal remains by changing their colour, shape and structure (Correia, 1996). These changes make it difficult to identify cremains and thereby complicating the measurements and analysis of the number of individuals, sex, age, living stature, and population affinity estimation as well as perimortem conditions and trauma (Krogman 1943a, 1943b; Wells, 1960; Liebenberg *et al*., 2023). Fire can also be used to hide evidence, by simulating natural fires (Imaizumi, 2015), making victim identification and interpretation of the circumstances surrounding death difficult (Mamede *et al.,* 2019). Forensic anthropologists can aid in victim identification of burnt remains by constructing a biological profile and providing information on trauma and taphonomy (Hackman, 2016). Being able to study cremated bone fragments when fire is used as a murder weapon or to hide evidence, as opposed to natural fires (e.g., veldt fires), is crucial in order to assess intentionality around death. Hence, it is vital for forensic anthropologists to know the bone composition and different taphonomic bone conditions (fleshed, wet, and dry) in order to understand the changes that occur when skeletal remains are exposed to heat (Galtés & Scheirs, 2019). Fleshed bone taphonomic condition refers to the bone that is completely covered by soft tissues (skin, muscles, tendons and ligaments) whereas wet bone is covered by minimal or remnants of soft tissues. Dry bones are not covered by any soft tissue and they contain little to no organic components (Mahon *et al*., 2021) of the bone such as fats which have a melting point temperature of 45°C - 55°C (Alabdalall *et al*., 2021)

According to Eckert *et al*. (1988), cremated remains' composition varies according to tissue survival. There is charred cremation where the internal organs are still preserved, followed by partial cremation where the soft tissues are still preserved, then incomplete cremation where the bone pieces are the only remains and complete cremation where there is only ash left. Cremation

research has focused on three categories: analysis of visual characteristics, histological analysis and the demographic analysis of cremated remains such as age, sex and population affinity estimation (Correia, 1996). Heat exposure can induce macroscopic changes in bone size and colour, as well as deformation (warp) and fragmentation (fracture) of bone (Ubelaker, 2009; Goncalves *et al*., 2011).

1.2. Bone composition and histology

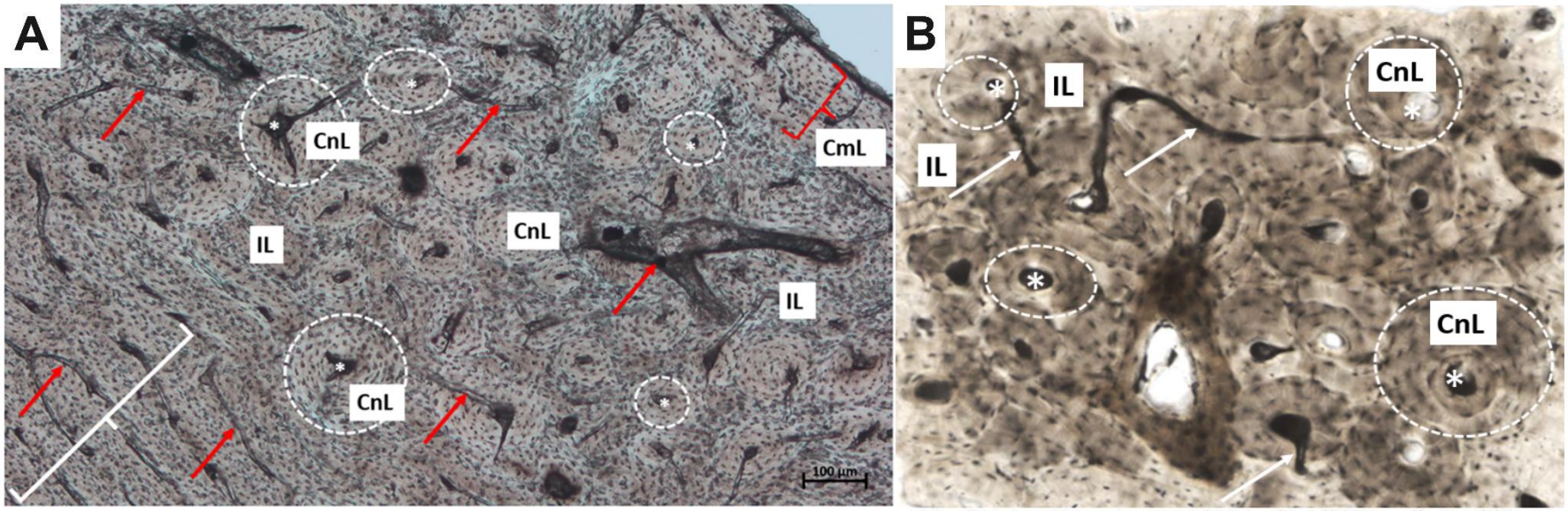
Bone *in vivo*, is a specialised connective tissue characterised by cells within a mineralised extracellular matrix (Kerr, 2010). Although a hard tissue, bone can contain between 10% and 20% water (Currey, 1990; Sanz *et al*., 2023). Within the extracellular matrix, 65% of the matrix is made of an inorganic component, mineral hydroxyapatite ($Ca_{10}(PO_4)_6(OH)_2$), and 25% is composed of organic material (Lowenstam and Weiner, 1989; Currey *et al*., 2001; Currey, 2003), type I collagen and to a lesser extent, type III collagen, bone cells (osteoblasts, osteocytes, and osteoclasts) and non-collagenous proteins (Boskey *et al*., 2001; Lee & Einhorn, 2001; Wang, *et al*., 2001; Thompson, 2015; Ellingham *et al*., 2016). Osteoclasts, osteoblasts and osteocytes work together to balance the resorption and absorption during bone remodelling (Frost, 1996). Osteoclasts degrade the bone matrix through enzymatic activity resulting in resorption lacunae, followed by programmed cell death of osteocytes where required, once resorption is complete (Ross & Pawlina, 2006). Osteoblasts secrete collagen and bone matrix proteins forming uncalcified bone matrix known as osteoid (Ross & Pawlina, 2006), which then mineralises approximately ten days after deposition (Ross & Pawlina, 2006, Stout and Crowder, 2011). Certain developing bones, for example long bones, may require a hyaline cartilage scaffold on which to lay osteoid down, known as endochondral ossification, as opposed to the process of intramembranous ossification whereby bone develops directly from a mesenchyme (intramembranous ossification) (Ross and Pawlina, 2006). As osteoid is being secreted, the bone begins to mineralise trapping the osteoblasts within bone matrix spaces called lacunae and differentiating into osteocytes (Ross & Pawlina, 2006; Horocholyn, 2013). Osteocytes maintain and monitor the bone matrix by communicating with each other through cytoplasmic processes contained within canaliculi (Ross & Pawlina, 2006; Horocholyn, 2013). Immature bone, also termed woven bone, reflects mineralised bone that has an irregular arrangement of collagen, with greater hydration and cellular content. Immature bone undergoes remodelling with further growth and becomes lamellar (mature layered bone) which

contains orderly layers of collagen and mineralised bone, less water and less cells (Ross and Pawlina, 2006; Kerr, 2010; Horocholyn, 2013; Labuschagne, 2020). Juvenile bones have more trabecular bone (low compact bone density) and more organic material such as collagen compared to adult mature bones which could alter how bone responds to heat (Waterhouse, 2013).

Collagen is an extracellular protein consisting of triple helical tropocollagen molecules (Lambri *et al*., 2018). The collagen molecules form fibrils which are arranged to form collagen fibres (Bozec and Odlyha, 2011), in which carbonated apatite crystals are embedded during the process of mineralisation (Mano, 2005; Lau *et al*., 2013; Lambri *et al*., 2016). Collagen provides elasticity (Lambri *et al*., 2018), and is responsible for resisting deformation (Ma *et al*., 2021) by providing structural and mechanical support to the bone through toughness and stiffness (Lee *et al*., 2001; Bozec *et al*., 2007). As such, the microstructure of bone, specifically collagen, is proposed to be highly affected by heat and involved in bone heat-induced alterations (Zioupos *et al*., 1999; Gonçalves *et al*., 2011, 2015; Vassalo *et al*., 2016).

The structural integrity of bone is linked to the presence of orderly layers of bone matrix called lamellar bone. Lamellar bone is divided into two: cortical (compact) bone and trabecular (spongy or cancellous bone). In humans, cortical bone is arranged in elongated and roughly cylindrical structures called osteons or Haversian systems (Frost, 1973; Parfitt, 1994), considered the structural units of cortical bone (Brits *et al*., 2014). Primary osteons form during development, particularly with appositional growth whereas secondary osteons are created during bone remodelling, a dynamic process (Matsuo *et al*., 2019). Within the centre of each osteon, there is an osteon canal which contains blood vessels, lymphatics and nerve bundles. These neurovascular structures are surrounded by concentric lamellae of bone matrix (Ross & Pawlina, 2006). Between the osteons, there are remnants of concentric lamellae, reflecting normal bone turnover, called interstitial lamellae (Ross & Pawlina, 2006). Trabecular bone in humans, is similarly layered but typically lacks the presence of osteons. Trabecular bone, found deep to cortical bone, has a porous appearance with thin spicules that make up a bone network forming marrow cavities (Martini *et al*, 2008) that contain blood vessels which nourish the bone and bone marrow (Horocholyn, 2013). Red bone marrow is where haematopoiesis occurs, and yellow marrow contains lipids stored in adipocytes (Ross & Pawlina, 2006). The arrangement of the bone matrix is different in non-human animals (Horocholyn, 2013).

Although bones of non-human animals are made up of the same bone constituents as in humans, their arrangement and composition proportions differ depending on the species (Horocholyn, 2013). Domestic pigs are artiodactyls, and their bone microstructure is mainly plexiform (Horocholyn, 2013) (Figure 1.2). Plexiform bone is described as primary bone containing a dense network of vascular canals that are arranged longitudinally, radially and circumferentially forming a brick-wall appearance (Francillon-Vieillot *et al*., 1990; Enlow, 1996; Horocholyn, 2013; Labuschagne, 2020) (Figure 1.2). In pig bone, vascular canal structures identified as canals, similar to primary osteons, that are lacking concentric lamellae (Francillon-Vieillot *et al*., 1990; Hillier and Bell, 2007) (Figure 1.2). The primary osteons in plexiform bone are few, small and concentric in shape with no clear demarcation of cement line while secondary osteons are large, dense and elliptical shaped with a clear demarcation of cement line (Francillon-Vieillot *et al*., 1990; Hillier and Bell, 2007; Labuschagne, 2020). On the cortical bone of artiodactyls, the plexiform structures originate near the periosteum while the osteons extend to the endosteum forming osteon banding (Francillon-Vieillot *et al*., 1990; Hillier and Bell, 2007). Osteon banding is described as a distinct row of five or more primary and/or secondary osteons (Mulhern and Ubelaker, 2001). Although mature pigs (and cows) also contain dense osteon systems, structures such as plexiform, osteon banding and resorption lacunae (found between osteons), are the main structures that differentiate pig bone from human bone (Martiniaková *et al*, 2006a; Martiniaková *et al*, 2006b). These resorption lacunae indicate that pigs have a high rate of turnover compared to other artiodactyls (Martianikova *et al*, 2006b). The justification for the use of the selected animal model (i.e. domestic pigs) includes similarity to human bone composition and histology (Aerssens *et al*., 1998; Horocholyn, 2013).



https://histologyslides.med.umich.edu/Histology/Basic%20Tissues/Cartilage%20and%20Bone/093B_HISTO_40X.htm. Accessed: 08 August 2024.

Figure 1.2: Photomicrograph showing unaltered juvenile porcine and human bone histology.

A) Unaltered juvenile porcine bone showing plexiform morphology (white bracket) with vascular canals (red arrow) arranged in parallel and connecting the osteon structures (dashed white circle). The osteon canals (white asterisk) are surrounded by concentric lamella (CnL). In between the osteons there are interstitial lamellae (IL) and from the outer (periosteum) side of the bone there is a layer of bone matrix called circumferential lamellae (red bracket - CmL). **B)** Human bone image showing osteon structures (dashed white circle) that are closely packed together with larger and more visible osteon canals (white asterisk) surrounded by concentric lamella (CnL). The osteon canals are connected by a transverse (Volkmann's) canal (white arrow). Image B was sourced from an open access website under CC- BY-SA-NC Creative Commons license 4.0, underwent cropping and editing (increased contrast and added labels), however, the original license terms remain unchanged.

1.3. Effects of heat-induced macroscopic changes

Heat exposure can induce macroscopic changes in bone size and colour, as well as deform (warp), fragment and fracture the bone (Ubelaker, 2009; Goncalves *et al*., 2011). When bone is exposed to heat between 100°C and 300°C, dehydration occurs leading to 1-2% reduction in volume (Castillo *et al*., 2013). This dehydration can also be seen as a change in colour, visible as heat lines and heat borders, at sites where soft tissues retract during burning (Krap *et al*., 2017b) exposing the bone to heat (Ellingham *et al*., 2015). Change in colour is affected by temperature, exposure duration, position of heat source, distance from the heat source, oxygen availability as well as the surrounding medium which influences the degree of combustion (Correia, 1996; Bennett, 1999; Walker & Miller, 2005; Imaizumi *et al*., 2014; Krap *et al*., 2017a). The blackening of the bone, also known as charring, is associated with carbonization of the skeletal material, while grey and grey-white is associated with decomposition of the bone organic components and chalk white is only associated with final calcination, where the water and organic components of the bone are completely lost (Shipman *et al*., 1984; Correia, 1996; Whyte, 2013; Snoeck *et al*., 2016). Other colours have been associated with inorganic materials surrounding the environment like zinc, copper and iron (Shipman *et al*., 1984). Therefore, Symes *et al*. (2015) suggest that colour changes do not give sufficient information on heat-exposure dynamics, specifically in relation to bone without soft tissue shielding. Heat-induced warping and fracturing, however, have been found to be reliable indicators of pre-burning taphonomic conditions (fleshed, wet and dry) (Lemmers, 2012; Ulguim, 2015).

Warping is described as a severe, irregular change in alignment of the bone resulting in bone losing its usual shape and become deformed in appearance (Goncalves *et al*., 2015). Warping/deformation is affected by shrinkage (Christensen *et al*., 2022). Shrinkage occurs when the bone is reduced in size (de Oliveira Coelho, 2015), due to contraction of the polymers (bone collagen) during cooling rates (Li *et al*., 2020), which changes the visual appearance of the bone as stress is applied to the bone tissue. The stress experienced by the bone, is the force applied that changes the bone as it undergoes elastic deformation (Christensen *et al*., 2022). This type of deformation is recoverable when a force is no longer applied and the bone returns to its original shape (Christensen *et al*., 2022). However, as the stress increases, so does the strain on the bone which eventually results in the bone reaching the yielding point. The bone will respond by undergoing plastic deformation

where the bone shape will permanently change and thereafter resulting in failure or fracture of the bone (Christensen *et al*., 2022).

Heat-induced fractures in bone can be visualised as fracture lines. There are six common type of heat-induced fractures that have been classified and defined by researchers (Krogman, 1939, 1943; Baby, 1954; Binford, 1963; Mayne, 1990; Symes *et al*., 1996, cited by Symes *et al*., 2008). Longitudinal fractures are generally seen on the diaphysis of long bones, running along their long axis (Varvares, 2016) and are proposed to occur when the diaphysis of the bone is exposed to heat until the protein in the bone matrix collagen dehydrates and denatures reducing the elasticity of the bone (Herrmann and Bennett, 1998). Step fractures extend from the margin of the longitudinal fracture across the bone shaft to the intersection of another longitudinal fracture (Symes *et al*., 2008). Transverse fractures are seen in a horizontal direction on the diaphysis of the long bone and are suggested to occur across the grain of the bone (Varvares, 2016) as a result of structural failure due to unilateral heat exposure and are common in bodies showing a pugilistic posture (Symes *et al*., 2008). Patina fractures appear as fine cracks on the surface of the bone and are suggested to occur as a result of flat areas exposed to increased amounts of heat, following the destruction of protective soft tissues and proposed contraction of the cortical bone (Symes *et al*., 2008). Delamination fractures, where the inner cortical bone layers of the compact bone separate from outer cortical bone layers, are thought to occur when dry skeletonised bone is exposed to heat (Symes *et al*., 2008; Keough *et al*., 2015). Curved-transverse, or thumbnail, fractures appear as concentric and/or half concentric fractures and have been associated with fleshed bones and appear in areas where there is muscle shrinkage during cremation (Symes *et al*., 2008; Gonçalves *et al*., 2015). This suggests an association between thumbnail fractures occurrence and muscle attachment sites.

1.4. Effects of heat-induced microscopic changes

Despite the heat-induced macroscopic changes occurring as a result of the bones' physical and chemical composition changing (Castillo *et al*., 2013), few studies tried to associate microstructural changes to macroscopic changes (Castillo *et al*., 2013; Imaizumi, 2015). Heat-induced bone diagenesis is a process involving a series of stages at which bone breaks down (Thompson, 2004). The first stage is dehydration which occurs between 100°C-300°C, there is breakage of hydroxyl bonds, with water molecules between adhering bioapatite crystals and

organic constituents removed (Marques *et al*., 2018). In the second stage, organic components such as lipids and proteins chemically decompose between temperatures 400°C and 500°C (Marques *et al*., 2018). In the third stage, the carbonate formed is released as the temperature increases to 700°C (Marques *et al*., 2018). Lastly, in the fusion stage (> 700°C), bioapatite crystals increase in size and fuse around or within the pores created by water and organic component loss (Marques *et al*., 2018). These microscopic changes reflect biochemical changes that result in physical and mechanical alterations (Thompson, 2004).

When bone is exposed to heat, assessment of histological parameters show that osteons decrease in size (diameter, area, and perimeter), with a corresponding increase in the size of osteon canals (Horocholyn, 2013). Carbonisation limited the measurements of the osteons and osteons canals as it interfered with the bone tissue, however, Horocholyn (2013) found a significant decrease of 21318.6 μm^2 to 15831.7 μm^2 in osteon area while osteon canals had no significant difference. When the bone matrix is exposed to increasing heat, it develops microscopic fractures at temperatures as low as 100°C-300°C (Castillo *et al*., 2013). These heat-induced micro-fractures have been identified in other studies on burnt bone but not described in detail (Symes *et al*., 2008; Gonçalves *et al*., 2011, Castillo *et al*., 2013; Imaizumi *et al*., 2014; Gonçalves *et al*., 2015; Vassalo *et al*., 2016). Therefore, there is lack of understanding on the how micro-fractures are identified and how they develop. A recent study defines different types of bone micro-fractures resulting from high impulse current application (Bacci *et al*., 2021) based on previous observations in burnt bone (Brain, 1991). These micro-fractures include radiating, interstitial, irregular, circumferential and circumferential irregular (Bacci *et al*., 2021). While these micro-fractures have been defined in a high impulse current context (Bacci *et al*., 2021), their definitions could be applied to heat-induced micro-fracturing considering similarities with respect to thermal and pressure associated parameters of trauma propagation.

Collagen provides elasticity and resistance (Lambri *et al*., 2018; Ma *et al*., 2021), in addition to providing structural and mechanical support to the bone (Lee *et al*., 2001; Bozec *et al*., 2007). As such, it has been suggested that a relationship exists between heat-induced microscopic changes and macroscopic changes. Several quantitative studies of collagen have been conducted to find the relationship between the collagen destruction due to heat and heat-induced bone changes (Zioupos *et al*., 1998; Wang *et al*., 2001; Gonçalves *et al*., 2011; Lambri *et al*., 2018; Marques *et al*., 2018).

Quantification of collagen was conducted by staining the bone sections with Sirius Red-Fast Green (SRFG) stain (Houghton *et al*., 1996; Gopinathan *et al*., 2020). The SRFG stain stains the collagen red and non-collagenous proteins green, subsequent elution of the dye and spectrophotometer analysis of the wavelengths of the colours emitted permitted quantification (Houghton *et al*., 1996). However, the stain has been found to be more effective when using polarized light as the Sirius red stained collagen is birefringent (Lattouf *et al*., 2014). Birefringence, shown by anisotropic structures, can be described as a measure of the difference of refractive indices that result from a beam of light splitting into two (Caamaño *et al*., 2010; Rittié, 2017; Liu *et al*., 2020). This birefringence occurs when picrosirius red elongated molecules bind to collagen molecules, the picrosirius red molecules thus become oriented parallel to the long axis of the collagen fibres (Wolman, 1975; Liu *et al*., 2021)

1.5. Relationship of macro and microscopic heat-induced changes

It is suggested that there is a relationship between macroscopic warping and heat-induced fractures and microscopic change in the amount of collagen present in bones (Castillo *et al*., 2013). Bone collagen content is proposed to vary between different pre-heating taphonomic condition (fleshed, wet and dry) (Zioupos *et al*., 1999; Gonçalves *et al*., 2015). Collagen content has been found to differ among modern and archaeological bone (Vassalo *et al*., 2016), biological sexes (Vassalo *et al*., 2016) and ages (Zioupos *et al*., 1999). Heat-induced warping was seen more commonly in modern bones (more collagen) as opposed to archaeological bones (less collagen) (Vassalo *et al*., 2016). Other studies also found warping present on fleshed bones and no warping on archaeological dried bones (Baby, 1954; Etxeberria, 1994; Vassalo *et al*., 2019), while another study identified warping across fleshed, recently defleshed and dried faunal bones cremated in an open-air experiment (Whyte, 2001). These conflicting results highlight the debate on the relationship between bone collagen content, subsequent denaturation and loss, the involvement of associated fascia and tendon, and thus the mechanisms of heat-induced warping. It is thus suggested that collagen content alone may not ensure warping, however, preservation of collagen-apatite bonds has been suggested as an additional driving force of warping (Gonçalves *et al*., 2015; Vassalo *et al*., 2016).

It is hypothesised that well preserved collagen-apatite bonds result in the development of collagen contractile forces when exposed to heat gradually (Zioupos *et al*., 1999; Gonçalves *et al*., 2015). As a result, the bone will have greater elasticity and will therefore be more likely to deform and fracture (Gonçalves *et al*., 2015; Vassalo *et al*., 2016). While no study has directly investigated fractures in relation to collagen, heat-induced thumbnail fractures are suggested to be common in fleshed bones at muscle attachment sites and are thought to occur as the muscles shrink during burning (Symes *et al*., 2008). However, thumbnail fractures were not present on dried bones in some studies (Baby, 1954; Binford, 1963), whereas others found thumbnail fractures in both dry and wet bone (Spennemann & Colley, 1989; Gonçalves *et al*., 2011). Thumbnail fractures were, however, found more often on bones burnt at lower temperatures in comparison to bones burnt at higher temperatures (Gonçalves *et al*., 2015). It has been suggested that at 800°C, the temperature is enough to ensure bone warping (Vassalo *et al*., 2019). However, shrinkage and warping were also found to be positively related to cooling rates of a semi-crystalline polymer (Li *et al*., 2020), such as bone bioapatite (Kroeze *et al*., 2009). This is due to an increase in crystallinity as the cooling rate increases causing recrystallization-induced strain and therefore leading to increased warping and shrinkage (Li *et al*. 2020). Additional proposed factors contributing to heat-induced changes are bone shape and weight (Vassalo *et al*., 2019), but require further testing and confirmation. Experimental design differences to induce thermal bone alterations between these studies could have contributed to variation and discrepancies of results, with certain studies making use of open field fires (Glazewski, 2006; Whyte, 2013; Keough *et al*., 2015; Carrolla and Smith, 2018) and others closed system heating, such as electric ovens or furnaces (Imaizumi et al., 2014; Gonçalves *et al*., 2015; Reidsma *et al*., 2016; Vassalo *et al*., 2016, 2019).

The use of muffle furnace makes the experiment more controlled by controlling variables such as the cremation temperature and cremation time. To test these relationships, it is important to conduct a controlled experimental study that can eliminate as many of the confounding variables such as the atmospheric air which may contain different level of gases, wind, humidity as well as different weather conditions on different days. Other studies for the most part attempt to recreate realistic settings (Walker *et al*., 2008; Gonçalves *et al*., 2015; Reidsma *et al*., 2016), making interpretation of results harder. Using a controlled experimental setting, such as a furnace can aid in controlling the experimental parameters providing a better understanding on how temperature in isolation may have an effect on heat-induced changes in bone.

As discussed above, controversy exists around bone collagen content at different taphonomic conditions (fleshed, defleshed (wet), or dry (degreased)) and its effect on heat-induced fracturing and warping. Despite their controversial findings, Gonçalves *et al*., (2015) hypothesized that warping and fractures occur as a result of the same event of bone contraction depending on the preservation of collagen-apatite bonds. Warping and fracturing are thought to occur more often when collagen bonds are well preserved, allowing collagen to contract, compared to when fewer preserved collagen bonds exist (Gonçalves *et al*., 2015). There is little to no definitive information regarding where the different types of heat-induced fractures are more commonly found on bones and how they are affected by different taphonomic conditions, temperature and time exposed to heat. Therefore, understanding the relationship between macroscopic and microscopic bone changes in relation to temperature, heat exposure time and bone taphonomic conditions would add to the dearth of knowledge on this relationship, and aid in a better interpretation of forensic anthropology cases of human burnt skeletal remains.

Aim and Objectives

The aim of the study was to investigate the relationships between heat-induced macroscopic and microscopic changes of domestic pig (*Sus scrofa domesticus*) tibiae at different taphonomic conditions (fleshed, wet/defleshed, and dry bone) and controlled temperatures. All objectives were investigated in relation to the taphonomic conditions and furnace temperature setting.
The objectives were thus as follows:

1. To determine, through a pilot study:
   1.1. The effect of nitrogen gas during cremation.
   1.2.The optimal furnace temperatures for subsequent experimentation.
   1.3. The effect of different decalcification solutions on burnt bone structural integrity for downstream analysis.
2. Assessment of associations between heat-induced macroscopic bone fracture patterns, their location on the bone and the experimental conditions.
3. Assessment of associations between heat-induced bone colour changes, fragmentation, and physical mass loss across the experimental conditions.
4. Determination of the relationship between heat-induced microscopic bone fractures and the experimental conditions.
5. Determination of the relationship between bone collagen content, experimental conditions and fracture location on the bone.

Chapter 2: Materials and Methods

2.1. Ethics

Ethical clearance was granted by the Animal Research Ethics Committee under the waiver 04-11-2021-O for experimental study conducted on commercial porcine bones (Appendix A1) and waiver 02-08-2022-O for dry pig skeletal material obtained from the School of Anatomical Sciences, Faculty of Health Sciences, University of the Witwatersrand (Appendix A2).

2.2. Sampling

This study made use of commercially obtained tibiae from juvenile (5 - 8-month-old) domestic pig (*Sus scrofa domesticus*) from Highway Meat Market, Ontdekkers Road, Johannesburg. Pig tibiae were selected due to their relative fully fleshed size being able to fit into the muffle furnace available, as well as the similar morphology and histological composition to human tibia (Aerssens *et al*., 1998; Horocholyn, 2013). Pigs commercially slaughtered in Gauteng, South Africa are of juvenile ages, as such no adult pig bones could be obtained. However, it has been suggested that adult pigs contain more distinct and denser plexiform and osteon banding systems than juvenile pigs (Martiniaková *et al*, 2006a; Martiniaková *et al*, 2006b; Horocholyn, 2013). The study included tibiae from both left and right hindlimbs that had been slaughtered less than a week before acquisition and did not show any visible pathology or trauma. After acquisition, the tibiae were stored in a fridge between 0°C and 4 °C for no longer than 3 days prior to cremation. The sample size for the pilot component of the study included 15 tibiae, while for the experimental study a total of 33 tibiae were used, with detailed subdivisions described in the sections below.

2.3. Bone Specimen Groups and Preparation

Fleshed bones were defined as bones covered with soft tissue (including skin, subcutaneous adipose, muscles, ligaments, and tendons) and wet bones were covered by minimal soft tissue (terminal muscle, ligament, tendon attachments and periosteum). For the purpose of the study, macerated bones were referred to as dry bones. Dry bones were prepared by macerating wet bones to mimic skeletonized bones with minimal presence of fat and soft tissues. Maceration was done by immersing wet bones in a solution of 2.54% commercial OMO auto detergent in tap water (1.5 L per bone) (Triaca *et al*., 2022), heated to 55°C for 24 hours (Triaca *et al*., 2021). Maceration was

checked manually by removing the remnants of soft tissue using forceps under running tap water. Where soft tissue remained attached to the bone, the maceration was continued in fresh solution for another 24 hours. Thereafter, bones were washed and soft tissue remnants were removed manually. The bones were placed on a paper towel on top of a metal tray to dry at room temperature for three days in a dedicated sunlit drying room with a ventilation system. After 48 hours, all the macerated bones were immersed in 5 L embalming fluid (The Great Supply (Pty) Ltd) for 24 hours and thereafter left to dry in the same conditions for two weeks. To prevent sample contamination, the dry macerated bones were individually double bagged in resealable plastic bags until they were used for experimentation. The experimental study was conducted after carrying out a pilot study to test and optimise the experimental parameters (Figure 2.3.1).

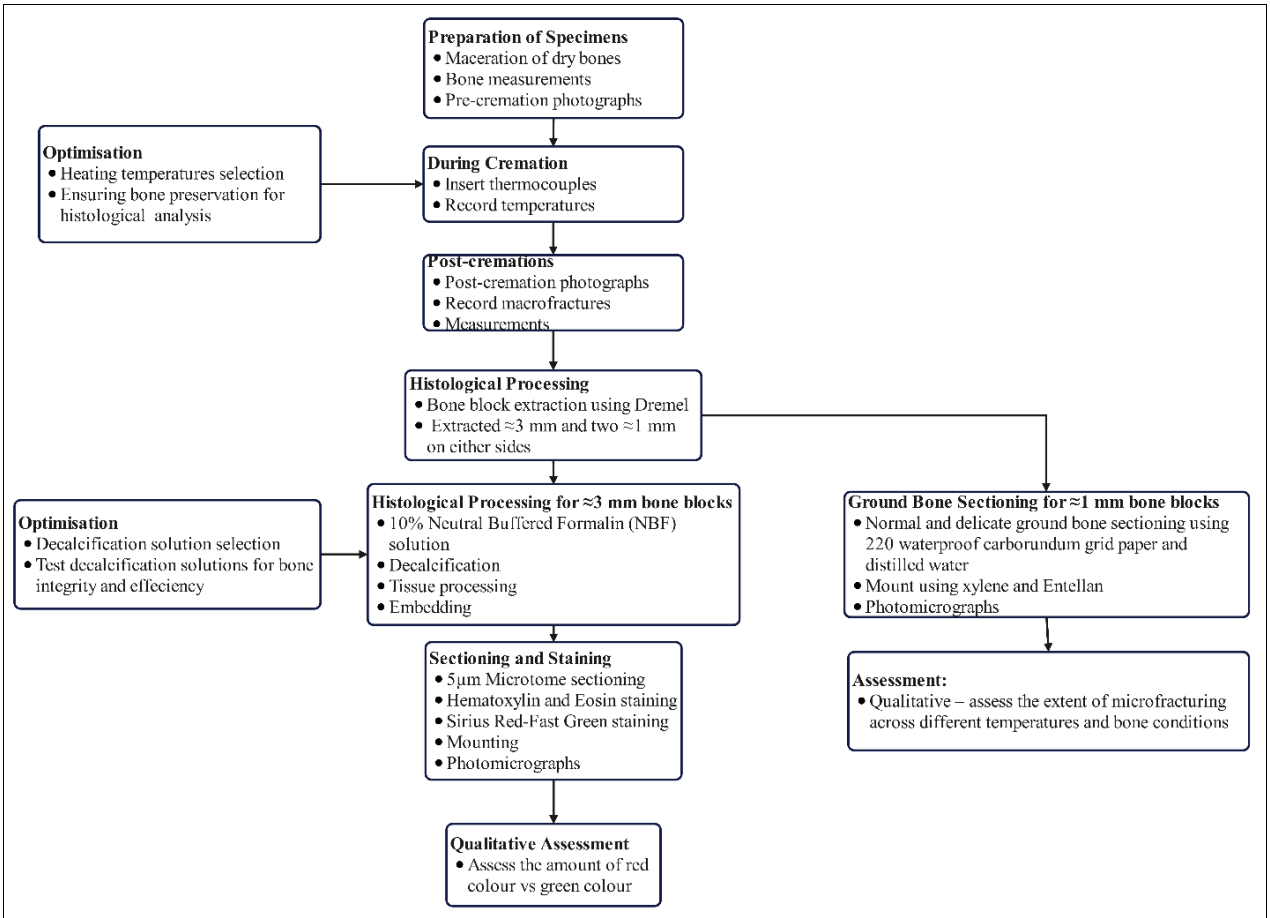


Figure 2.3.1: Flow diagram showing the experimental procedure from cremation to analysis including the pilot and experimental components of the study.

2.4. Weighing and Photography

Bones were photographed using a Canon EOS 750D camera (lens at 55mm, F10, 1/500 shutter speed, ISO-100 and flash on) on a blue grid (5 mm grid squares) background paper with Kaiser RS1 camera copy stand. To maintain a consistent angle, distance, and scale before and after experimentation, the camera was placed at a distance of 675 mm from the grid paper where the bone was placed. The tibiae were photographed from the anterior, posterior, medial, and lateral aspects with a specimen label. A 5 mm scale was represented on the photographs by each square on the background blue grid paper. The mass of each bone, placed in a resealable plastic bag of negligible weight, was measured before and after cremation using an analogue scale in triplicate and the average taken. Measurement of mass was taken to observe the difference between mass loss before and after cremation at different cremation conditions. The mass for fleshed and wet bones included fibula as it was difficult to separate from the tibia without compromising the sample integrity.

2.5. Furnace preparation and Cremation Process

A 0.6mm hole was drilled into the approximate mid-point of the distal end of each bone to be cremated, using a handheld electric drill (Figure 2.5.1.A), in order to insert a thermocouple, which was connected to a Key Sight 34972A data logger via LXI Data Acquisition Switch Unit channel box. Samples were placed in a muffle furnace (Celsius Scientific, serial number 250/19/918/2) fitted with a temperature controller unit (TOHO TTM-P4) (School of Chemical and Metallurgical Engineering, University of the Witwatersrand, Johannesburg). The furnace was set to increase at 10°C/minute to allow a gradual increase in temperature and prevent heat shock. Once the furnace reached 100°C, it was set to be on hold for 5 minutes to allow for the insertion of the bone samples and thermocouples (Figure 2.5.1. B and C). A maximum of three K-type thermocouples were used in each trial: one in the muscle (adjacent to cranial tibial muscle, fibular muscle and digital extensor muscle) of fleshed bones, one inside all bone types through the drilled hole on distal end, and one inside the furnace to measure the furnace temperature (Figure 2.5.1. C). A J-type thermocouple was placed outside the furnace to record the ambient temperature. The wet and dry bones were placed on top of a chalk tray while the fleshed bones were placed in a foil tray to avoid the moisture dripping into the furnace. The bones were positioned with the proximal end of the bone directed deep into the furnace and the anterior side facing the roof of the furnace to keep the testing

conditions consistent with heat exposure (Figure 2.5.1. C). After the insertion of thermocouples, the furnace temperature increased at a standard 10°C/minute rate until the furnace reached each selected heating temperature. Once the target temperature was reached, the furnace was set to hold at that specific temperature for 30 minutes. The datalogger recorded the thermocouple temperatures every 30 seconds. After the 30 minutes hold, the cremation trial ended and the furnace heating elements automatically switched off, allowing for the furnace to cool.

The door of the furnace was opened immediately after the trial had ended for temperatures at 400°C and less, allowing the bone to cool before being removed from the furnace. However, for temperatures at 500°C and above, the furnace was left to cool to 450°C before the door was opened to reduce the risk of combustion that could result from pyrolysis of gases being in contact with atmospheric oxygen (Emmons, 1986). Thereafter, the bones were removed from the furnace using tongs when the temperature reached 200°C. The bones were left to cool overnight on a ceramic tile.

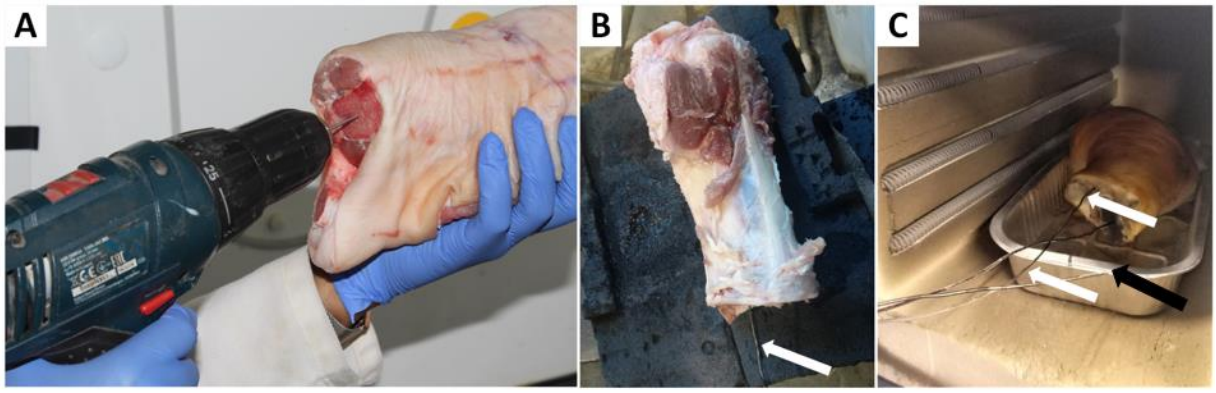


Figure 2.5.1: Image showing the bone prepared for cremation by drilling, inserting thermocouple and putting the bone into the furnace.

A) shows a hole being drilled into the distal end of the bone using a drill. **B)** shows the thermocouple inserted in the drilled hole (white arrow). **C)** shows the position in which a fleshed bone was inserted into the furnace (superior view of the bone went deep into the furnace and anterior of the bone facing the roof of the furnace). Image C also shows a thermocouple in the flesh of the fleshed bone, a thermocouple in the distal end of the bone (white arrow) and another thermocouple inside the furnace (black arrow).

2.6. Pilot Study

The pilot study took place to confirm the controlled parameters such as cremation temperature needed to cause heat-induced changes. The macroscopic heat-induced alteration analysis including heat-induced colour scoring criteria and fracture definitions were refined in the pilot study. Histology techniques such as decalcification and staining were also optimised.

2.6.1. Optimising atmospheric composition - nitrogen use

Fleshed and wet bones were exposed to 600°C heat for 30 minutes with an influx of nitrogen gas into the furnace. Nitrogen is an inert gas which does not undergo chemical reaction (Adamus, 2001; Forster, 2006). Fire extinguishers used in class A, B and C fires, contain Inergen made up of 52% nitrogen, 40% argon, and 8% carbon dioxide, these gases are considered as a fire suppresent by acting as oxygen diluting gases (Taheri, 2015). The temperature 600°C was chosen because it was expected to see more fractures and warping (Castillo *et al*., 2013; Gonçalves *et al.,* 2015; Vassalo *et al*., 2016), while also being the maximum temperature in which to investigate the presence of collagen, as collagen is expected to fully denature in bone heated above these temperatures (Trebacz and Wojtowicz, 2005; Wang *et al*., 2016). Nitrogen gas was used in order to avoid combustion by diluting the air and reducing the amount of oxygen (Moore and Yamada, 1998). The following day, both fleshed and wet bone were exposed to the same experimental conditions but without nitrogen gas (normal air). The heat-induced changes (colour, fracturing, and fragmentation) of both fleshed and wet bones heated with nitrogen influx were similar to bones heated without nitrogen and no combustion took place in either trial. Therefore, for the rest of the pilot and experimental study, the bones were cremated without the use of nitrogen gas.

2.6.2. Optimising heating temperatures

The pilot study sample for temperature optimisation initially consisted of 15 tibiae (Table 2.6.2.1). Certain inconsistencies in the sampling procedure for the pilot study resulted from observing the samples after each cremation trial and eliminating temperatures that, for example, were too destructive or did not present any macroscopic heat-induced changes.

Table 2.6.2.1: Pilot study bone sample distribution.

Temperature	*Tibia*			*Total*
	Fleshed	*Wet*	*Dry*	
200°C	1	1	0[a]	2
400°C	0	1[f]	1[f]	2
500°C	1[f]	1[f]	0	2
600°C	1[b]	1[b]	1	7
	1[c]	1[c]		
		2[d]		
800°C	1	1	0[e]	2
Total	5	8	2	**15**

a– The fleshed and wet conditions at 200°C did not present change in colour, macro and micro-fracturing, hence no further cremations at these temperatures were conducted.
b – Bones were cremated at the same time with the influx of nitrogen (N) into the furnace.
c – Bones were cremated at the same time without the influx of nitrogen.
d – Bones were cremated separately to observe any changes in expected results.
e – The fleshed and wet bones were highly fragmented at 800°C. Therefore, a dry bone sample was not cremated at this temperature.
f – The heating temperatures were reduced to 500°C and 400°C due to fragmentation when heated at 600°C and 800°C. The reduced temperatures showed less fragmentation and simulated expected results adequately hence, no further cremation of dry bone was conducted for optimisation.

2.6.2.1. Selection of temperature parameters

At the lowest temperature of 200°C for 30 minutes, no heat-induced changes on either fleshed or wet bones were identified, therefore this temperature was excluded from the experimental parameters. At the highest temperature of 800°C for 30 minutes, both the fleshed and wet bones were too fragmented to reconstruct (Figure 2.6.2.1). In addition, during the 800°C cremation trials, the furnace consistently short-circuited resulting in inconsistent heating of samples. As such, the temperature of 800°C was excluded from the study, and no further testing on a dry bone sample was conducted at this temperature. The effects of 600°C were tested for 30 minutes on both fleshed and wet bones, which were also too fragmented for analysis. Therefore, 600°C and 800°C were excluded as experimental parameters from the study. Cremation trials at 400°C and 500°C were then conducted to observe whether expected heat-induced changes would occur without destruction of bone beyond analysis. These temperatures yielded macroscopic heat-induced changes, with good preservation of bone integrity for analysis. Therefore, for the subsequent experimentation, the following temperatures were selected: 300°C, 400°C and 500°C for a duration of 30 minutes.

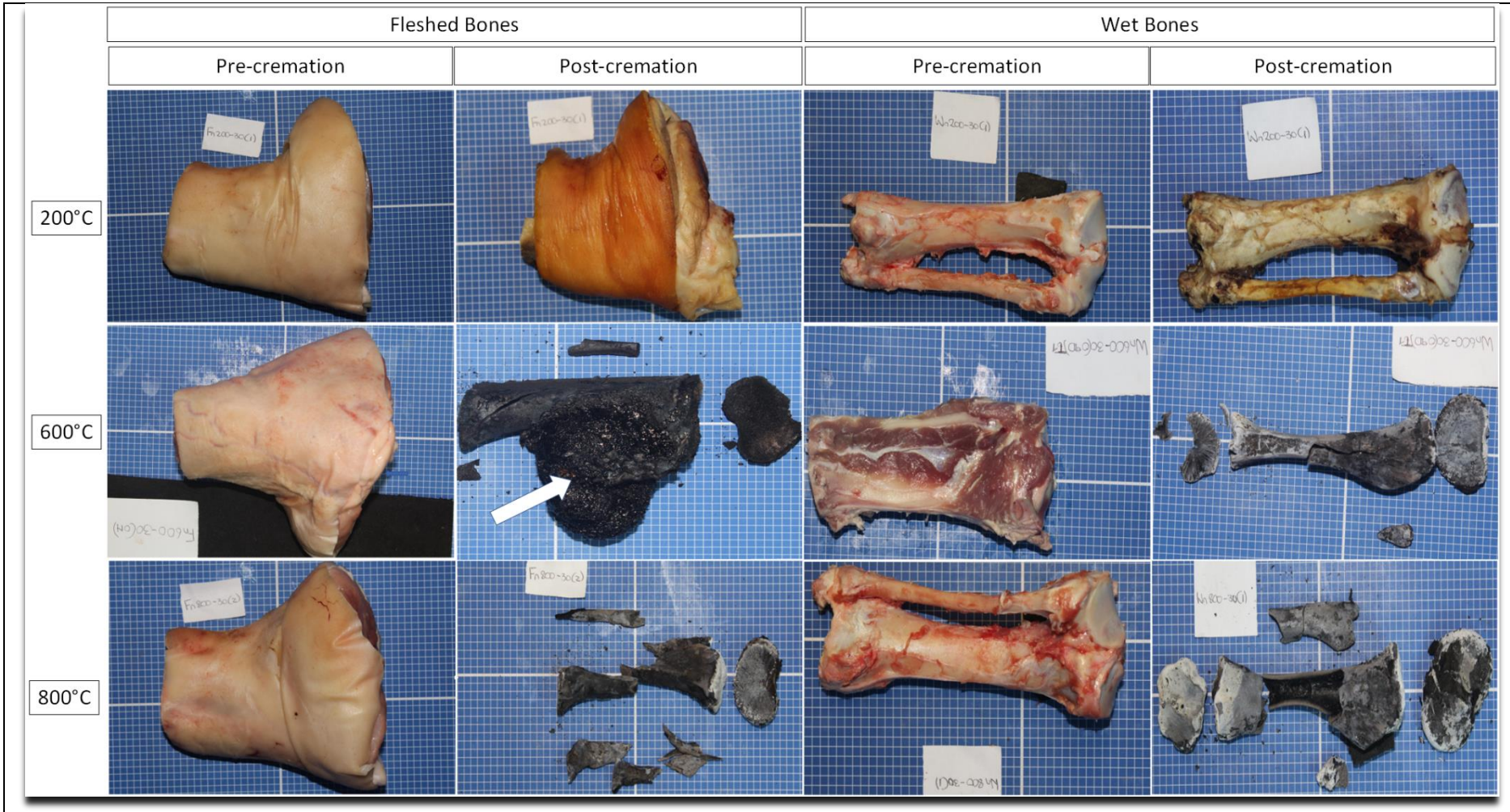


Figure 2.6.2.1: Image of pre- and post-cremation of pig tibia bones at 200°C, 600°C and 800°C.

At 200°C, there were no heat-induced changes post-cremation. At 600°C, the fleshed bone had an area that was unburnt underneath a mass of burnt tissue (white arrow). The fleshed bone showed heat-induced changes and little fragmentation in comparison to wet bone cremated at 800°C; however, wet bone at 600°C demonstrated more fragmentation. Both the wet and fleshed bone at 800°C, showed substantial fragmentation and colour changes. Scale: 1 block from the grid background = 5 mm

2.6.3. Optimising decalcification solutions

2.6.3.1. Bone block extraction

One ≈ 3 mm thick block was extracted using a Dremel rotary multi-tool (4000 Platinum) with cut-off wheels (size 409), from two sites: a muscle attachment site and a non-muscle attachment site (Figure 2.6.3.1). The location of choice for the non-muscle attachment site was the medial midshaft and for the muscle attachment site was the extensor groove (attachment site of the long digital extensor muscle, lateral digital extensor muscle, and long extensor muscle of the first digit) (Leibich *et al*., 2020).

All fleshed samples cremated at 300°C and 400°C still had soft tissue covering the bone while at 500°C and above, the soft tissue had retracted exposing the bone surface which became too fragile. Therefore, two methods of extraction were used, a 'normal' and 'delicate' bone block extraction method adapted from Maat *et al*., 2001. Delicate bone block extraction was applied for the fragile cremated wet and dry bones. A normal extraction method was made by cutting through the bone using the Dremel rotary tool until the bone block was extracted. For the delicate method, a drop of Alcolin super glue (generic cyanoacrylate glue) was applied to the area of interest and once dried, a single cut was made using the Dremel. An additional drop of glue was applied after every cut until successful extraction to avoid the separation of the compact bone layers. As previously mentioned, bones cremated at 800°C were in small fragments. The delicate extraction method also resulted in flaking of pieces of the cortical bone, hence this temperature was excluded from further experimentation.

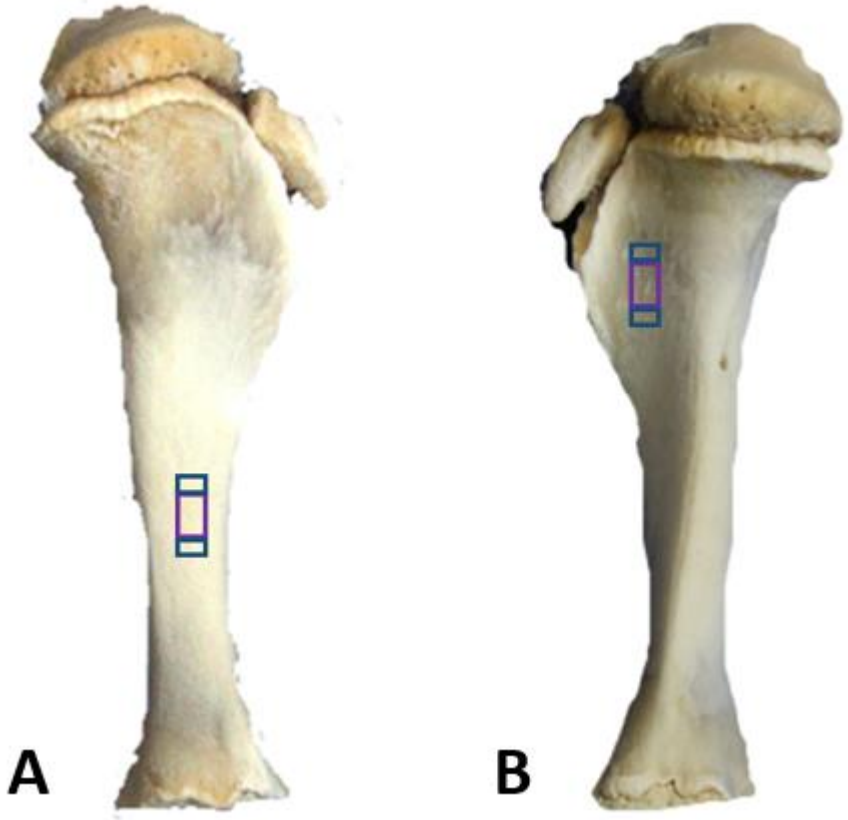


Figure 2.6.3.1: Left Porcine (*Sus scrofa domesticus*) tibiae showing block extraction regions.

Image showing bone block extraction sites of 3 mm block (purple) and two 1 mm blocks (blue) on either side of 3 mm block. **A)** extraction on the medial side at the midshaft which is the non-muscle attachment site **B)** extraction on the lateral side at the extensor groove site which is the muscle attachment site. Block size is not to scale.

2.6.3.2. Decalcification

The ≈ 3 mm blocks were fixed in a 10% neutral buffered formalin (NBF) solution (Layton *et al*., 2019) (Appendix B1) for 3 days. Thereafter, the fixed blocks were placed in cassettes and then placed inside the staining jars filled with 15ml of decalcification solution. Decalcification checks were done using a handheld Nomad portable dental X-ray (Aribex Inc., East Orem, USA). The x-ray showed calcium pockets that were visible as opaque white portions and when decalcification was complete, the bone blocks appeared translucent (Figure 2.6.3.2.1). After the first decalcification check, the blocks were rinsed for 10 minutes under running tap water and immersed in fresh decalcification solution until the bone blocks had completely decalcified. Once

decalcified, the bone blocks were rinsed for 30 minutes under running tap water. The bone blocks that decalcified earlier than others were stored in 10% NBF after rinsing until the rest of the blocks in a given batch had decalcified to be further processed together.

A total of 71 blocks were decalcified using four types of decalcification solutions, namely formic citric acid (FCA), 10% formic acid (FA), 5% nitric acid (NA), and 3% nitric acid (NA) (Appendix B1) to test which solution was most suitable for the experimental study. Decalcification was first conducted on dry skeletal bones using 10% formic acid (FA) and formic citric acid (FCA) which took a maximum of 6 days and 8 days to decalcify, respectively. Therefore, FCA was excluded due to taking more time to decalcify. For bones cremated at 500°C and 600°C, the bone blocks decalcified after a maximum of 2 days using 5% NA and 4 days using 10% FA. However, more bone blocks turned into powder (Figure 2.6.3.2.2) when decalcified with 5% NA than when decalcified with 10% FA. The 3% NA was used only on unburnt dry bones to test the effect of lower concentration of NA which had similar results as 5% NA. Therefore, 10% FA was chosen as the decalcification solution of the study to ensure preservation of bone tissue and a reasonable amount of time to decalcify in comparison to NA and FCA.

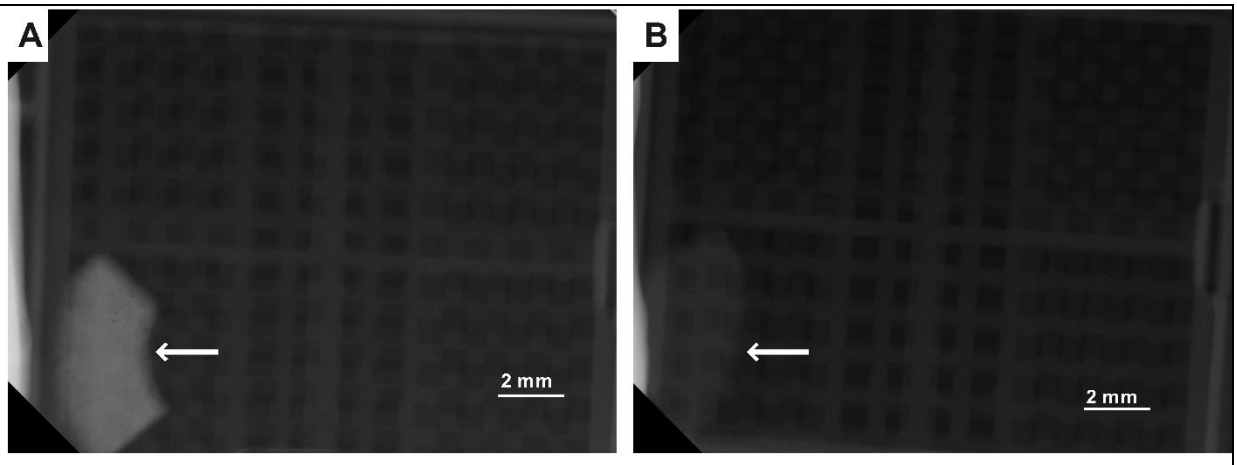


Figure 2.6.3.2.1: Examples of decalcification checks of dry bone blocks on different days.

A) shows the decalcification check of a dry bone block treated with 10% NBF for 3 days visible as an opaque white calcified tissue block (white arrow). **B)** shows a decalcified bone block after 4 days appearing as a semi-translucent block (white arrow) illustrating the progress of the decalcification process. The scale shows that one small square of the cassette is ≈ 1 mm.

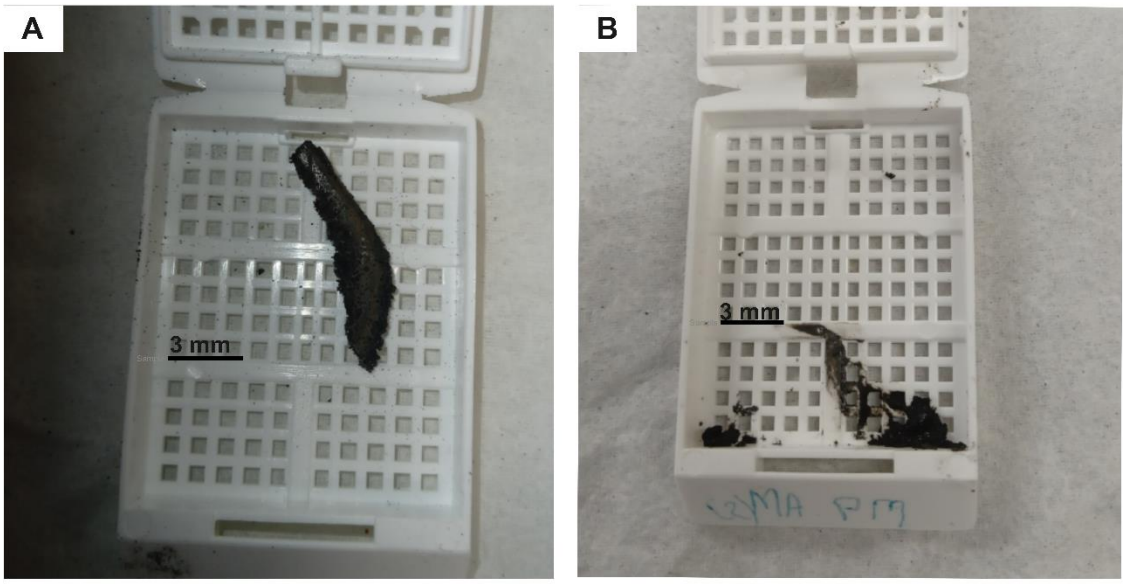


Figure 2.6.3.2.2: Example of undecalcified and decalcified cremated bone block damage.

A) shows the undecalcified bone block cremated at 600°C fixed with 10% NBF only and **B)** showing the decalcified bone block that turned into powder during decalcification. The scale bar shows that one small square of the cassette is ≈ 1 mm.

Following the completion of the pilot study and optimisation of the parameters for cremation (including air and furnace temperature) as well as determining the appropriate decalcification solution for histological analysis of fragile burnt bone, the experimental study was then conducted as below.

2.7. Experimental Study

2.7.1 Sampling

The experimental study included a sample size of 33 juvenile pig tibiae which were divided into three groups of fleshed, wet, and dry tibiae with each group consisting of three repeats for each cremation temperature group (300°C, 400°C and 500°C), including three wet and three dry bone controls (Table 2.7.1). As mentioned in section 2.3, fleshed bones were defined as bones covered with soft tissue (including skin, subcutaneous adipose, muscle, ligaments and tendons), wet bones were covered by minimal soft tissue (terminal muscle, ligament, tendon attachments and

periosteum) and dry bones were prepared by macerating wet bones. Due to obtaining the bones commercially, almost half of the distal ends in all the bone samples were cut off. The bones were prepared as per section 2.4 and section 2.5. Thereafter bones were exposed to heat at three different temperatures, previously chosen during the pilot study (section 2.6.2.1) namely 300°C, 400°C, and 500°C for a period of 30 minutes (Table 2.7.1). The control bones were retained at room temperature (25°C).

2.7.2. Macroscopic analyses

Photography, weighing bones, and cremation was conducted as described in section 2.4 and 2.5. The pre-cremation and post-cremation physical mass (bone and soft tissue), macro-fracturing, heat-induced colour changes, and fragmentation were recorded in Microsoft Excel. The thermocouple temperature readings were also recorded in a Microsoft Excel spreadsheet and the data presented as heat line graphs. However, the data for all fleshed bones cremated at 400°C, one trial of fleshed at 500°C and one trial of wet at 300°C were lost due to an error with the data logger.

Table 2.7.1: Total bone sample for each bone condition and cremation temperature.

Type of Bone	*Bone Condition*	*Controls*	*Cremation Temperatures*			*Total*
			300°C	*400°C*	*500°C*	
Tibia	*Fleshed*	0	3	3	3	9
	Wet	3	3	3	3	12
	Dry	3	3	3	3	12
	Total	6	9	9	9	**33**

a – The fleshed and wet bones were bought and had same microscopic bone composition material. The difference was the tissue covering the bone which was minimal on wet bones hence there were no controls for fleshed bones.

2.7.3. Heat-induced fragmentation

At all temperatures employed, there was no heat-induced warping identified. Warping is described as a severe, irregular change in alignment of the bone resulting in bone losing its usual shape and become deformed in appearance (Goncalves *et al*., 2015). However, heat-induced fragmentation was present. Fragmentation was scored based on whether the bone fragments could be aligned in their original position. The scores were defined as follows: (0) No fragments; (1) fragments were present and could be aligned; (2) fragments were present and could be partially aligned, and (3) fragments were present but could not align. When fragments were not aligned, or partially aligned this was considered an indicator of plastic deformation of the bone.

2.7.4. Heat-induced colour changes

Heat-induced colour changes were assessed based on a progression from heat lines to heat borders followed by charring and then calcination using an adjusted colour scale (based on: Schafer, 2001; Symes *et al*., 2008; Iscan and Steyn, 2013; Ellingham *et al*., 2015; Keough *et al*., 2015; Reidsma *et al.,* 2016; Rosa *et al*., 2023) (Table 2.7.4.1 and Figure 2.7.4.1). Heat lines are described as thin white lines marking the initial transition from unburnt to burnt area of the bone (Keough *et al*., 2015). A heat border is a thick off-white or light brown band between the burnt and unburnt area of the bone (Keough *et al*., 2015). Charring appears as the black colouring of the bone surface sometimes with a tint of blue, orange, and green colours (Keough *et al*., 2015). Calcination appears as a wide range of colours varying from grey, milky white, white and ash-brown (Keough *et al*., 2015).

Table 2.7.4.1: Scoring system of heat-induced colour changes.

Score	Definition	Definitions adapted from
0	Natural bone colour Colour - yellowish-white	Schafer, 2001
1	Heat lines: a thin line on the periphery of the heat border marking the transition from unburnt to burnt bone. Colour – thin white or black line	Symes *et al*., 2008; Iscan and Steyn, 2013; Ellingham *et al*., 2015; Keough *et al*., 2015
2	A thin line on the periphery of an off-white/brown thick band marking the transition from unburnt to burnt bone Colour – white/black thin line on periphery of thick brown band	Symes *et al*., 2008; Iscan and Steyn, 2013; Ellingham *et al*., 2015; Keough *et al*., 2015
3	An off-white colour transition to a black colour with the presence of a thin line and brown border in between. Colour - white/black thin line on periphery of thick brown band transitioning to black	Ellingham *et al*., 2015; Reidsma *et al*., 2016; Rosa *et al*., 2023
4	Less than half of the bone is black and the rest appears off-white Colour – light brown black with yellowish-white	Ellingham *et al*., 2015; Rosa *et al*., 2023
5	More than half of the bone is black and the rest appears off-white Colour – dark brown-black with yellowish-white	Reidsma *et al*., 2016; Rosa *et al*., 2023
6	The bone is entirely black sometimes with a tint of blue, orange, and green colours Colour – black with a tint of blue, yellow	Ellingham *et al*., 2015; Keough *et al*., 2015; Reidsma *et al*., 2016; Rosa *et al*., 2023
7	Less than half of the bone is grey and the rest appears black Colour – bluish-black patched with varying shades of grey	Ellingham *et al*., 2015; Rosa *et al*., 2023
8	More than half of the bone is grey and the rest appears black Colour – light brown with varying shades of grey	Ellingham *et al*., 2015; Rosa *et al*., 2023
9	The bone is entirely white-grey. Colour – chalk white/grey - white	Keough *et al*., 2015; Rosa *et al.*, 2023

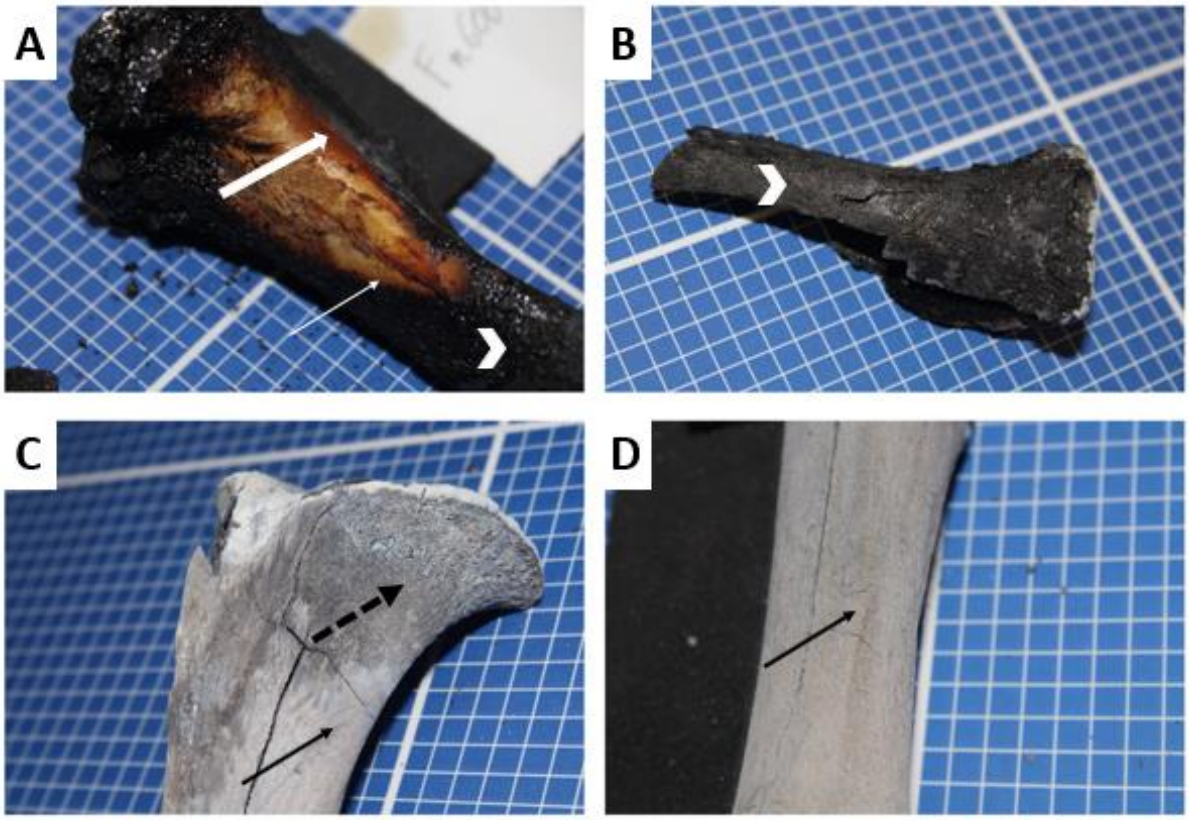


Figure 2.7.4.1: Images showing heat lines, heat border, charring and calcination colour change.

A) showing the heat border (thick white arrow) and heat lines (thin white arrow) on a fleshed bone cremated at 500°C with complete charring (white arrowhead). **B)** Complete charring was seen on wet bones cremated at 600°C. **C)** The dry bone cremated at 400°C presented different shades of calcination (dashed black arrow). **D)** Dry bone cremated at 600°C showed complete calcination. Scale: 1 block from the grid background = 5 mm

2.7.5. Heat-induced fracturing

Macroscopic fractures were recorded in order starting from the anterior side then lateral side followed by posterior side and lastly the medial side. For each side, fractures were recorded on three separate locations namely: proximal metaphysis, diaphysis, and distal metaphysis (Figure 2.7.5.1). For each side and each location, fractures were recorded from left to right. Fractures that were extending to different sides or locations were only recorded on the side and location on which they first appeared. The number and type of fracture (Table 2.7.5.1) were recorded based on their locations, whether on a muscle attachment site (e.g., extensor groove) or non-muscle attachment site (e.g., medial midshaft). Photographs for each side and each location were taken for macrofracture (Figure 2.7.5.2) inter-observer analysis.

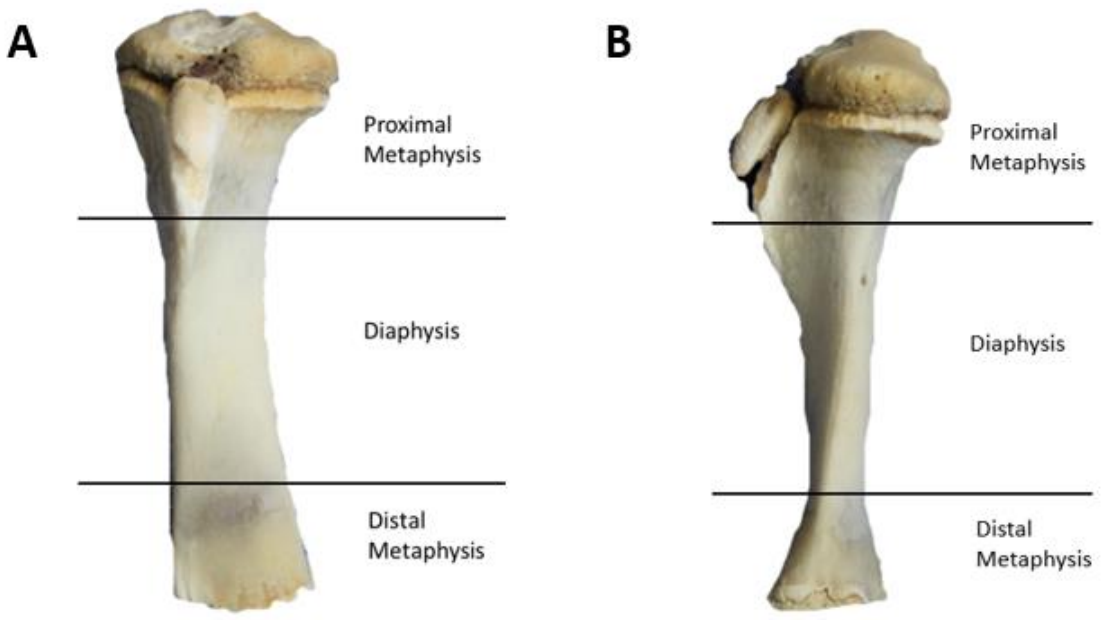


Figure 2.7.5.1: A left dry macerated treated dry tibia bone with labelled location.

A) Shows the anterior view of a dry tibia while image **B)** shows the lateral side. The upper section of the bone is proximal metaphysis which houses the muscle attachment site known as extensor groove. The middle section is the diaphysis (shaft) of the bone which houses the non-muscle attachment site known as medial diaphysis on the medial side of the bone. Lastly, the distal metaphysis which had its distal end cut out for all the experimental samples.

Table 2.7.5.1: **Refined heat-induced macroscopic fracture types and their descriptions** (adapted from Krogman, 1939, 1943a,b; Baby, 1954; Binford, 1963; Mayne, 1990; Symes *et al.,* 1996, cited by Symes *et al.,* 2015):

Fracture	Definitions
Longitudinal	Deep fracture in the cortical bone and appears to be parallel to the longest/longitudinal axis. May also appear as oblique fractures that are closer and/or approximately less than 45° to the longitudinal axis of the bone.
Transverse	Deep fracture in the cortical bone that appears to be perpendicular to the longitudinal axis of the bone. May also appear as oblique fractures that are closer and/or approximately less than 45° to the transverse axis of the bone.
Step	Irregular fracture where two longitudinal fractures merge with a transverse fracture in between them.
Curvilinear/Thumb-nail fracture	Deep fracture through the cortical bone forming a single or multiple concentric half-rings with relatively equal proportion of width to length.
Delamination	Separation of cortical bone layers from trabecular bone and/or the exposure of cancellous bone on epiphysis or metaphysis.

Patina	Superficial fine narrow linear cracks on the bone that does not cut deep into the cortical bone. They may appear irregular like a mosaic or mimicking the characteristics of other fractures. They can be further subdivided into: ● Patina longitudinal – a patina fracture in the longitudinal axis and may also appear as oblique superficial fractures that are closer and/or approximately less than 45° to the longitudinal axis of the bone. ● Patina transverse – a patina fracture in perpendicular to the longitudinal axis and may also appear as oblique superficial fractures that are closer and/or approximately less than 45° to the transverse axis of the bone. ● Patina curvilinear – a patina fracture that forms a single or multiple concentric half-rings with relatively equal proportion of width to length. ● Patina step – appears as patina longitudinal fractures that merge with patina transverse fracture forming a step fracture made of patina fractures only, or either patina transverse or patina longitudinal merging with a longitudinal or transverse fracture to form a step fracture that is not entirely made of patina fractures only. ● Patina mosaic – appear as very small fine mosaic superficial cracks in large numbers around one area.

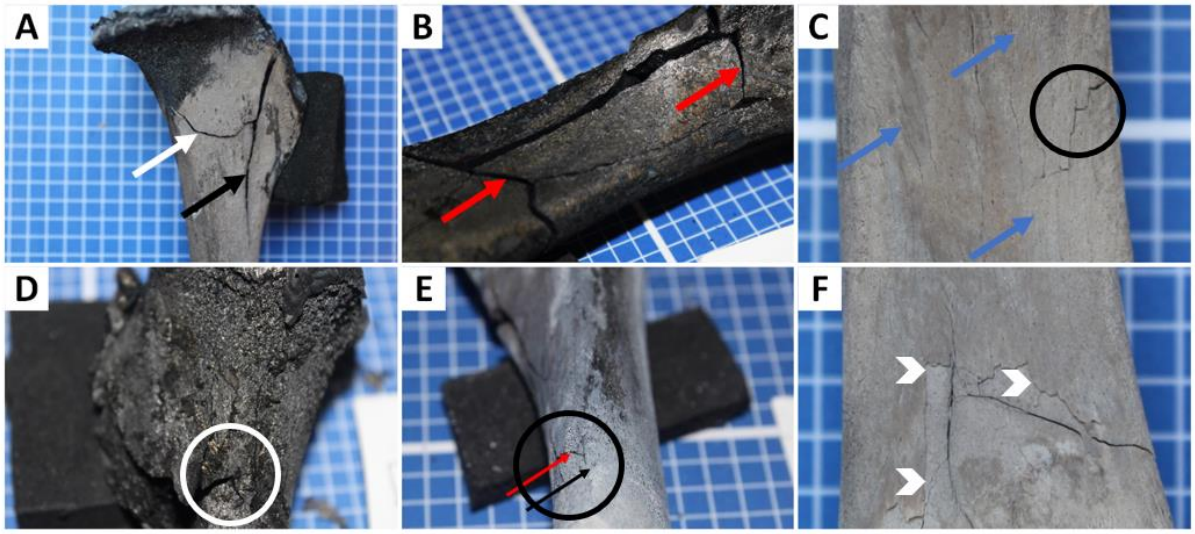


Figure 2.7.5.2: Types of heat-induced macroscopic fractures on cremated bones.

A) A curvilinear fracture (thick white arrow) merging with a longitudinal fracture (thick black arrow). **B)** A transverse fracture (thick red arrow) extending from longitudinal fracture. **C)** Patina longitudinal and patina transverse fractures merging to form a patina step fracture (black circle) and mosaic patina fractures (thick blue arrows). **D)** A step fracture as result of transverse fracture merging with two longitudinal fractures on either side (white circle). **E)** A patina step fracture (black circle) due to a patina transverse (thin red arrow) merging with two patina longitudinal fractures (thick black arrow) on either side. **F**) The white arrowhead indicates the separation of cortical bone layers as a result of heat forming a delamination fracture. Scale: 1 block from the grid background = 5 mm

2.8. Microscopic Analysis

2.8.1. Bone block extraction and decalcification.

Bone blocks were extracted using the same method as conducted in section 2.6.3.1. The ≈ 3 mm bone blocks were flanked by ≈ 1 mm bone blocks that were used for ground bone sectioning (Figure 2.6.3.1). The same methods of normal and delicate bone block extraction were used under similar conditions. All the ≈ 3 mm bone blocks were decalcified using 10% formic acid using the same method presented in section 2.6.3.2.

2.8.2. Decalcified bone tissue processing, cutting, and staining

Decalcified bone blocks were processed using a standard tissue processing machine (Thermo Scientific Citadel 2000) with a series of graded alcohols and chloroform, following which they were embedded in paraffin wax (Tissue-Tek Console, Miles Scientific) for subsequent serial sectioning using a rotary microtome (Leica RM2125 RTS). A series of 5µm sections were cut from each bone block and deparaffinised with xylene, rehydrated through a graded series of alcohols and distilled water to enable staining. Half of the sections were stained with Haematoxylin and Eosin (H&E) stain and the other half with a Sirius Red-Fast Green (SRFG) stain, mounted on glass slides coated with 3% 3-aminopropyltriethoxysilane (APES) (Appendix B2). The H&E stains the cell nuclei basophilic (purple-blue) while the cytoplasm stains eosinophilic in varying shades of pink (Bancroft and Layton, 2019). The SRFG was expected to stain collagen red and non-collagenous protein green (Houghton *et al*., 1996; Segnani *et al.,* 2015). For confirmation of staining of collagenous and non-collagenous proteins, sections from two muscles (cranial tibial muscle and long digital extensor muscle) and two tendons (tendon of gastrocnemius muscle/Achilles tendon and patellar tendon) were dissected from a fully fleshed pig tibia and histologically processed as negative and positive controls, respectively. As a negative control, muscle was expected to show greater green stain due to the presence of contractile proteins, with only connective tissue sheaths staining red (Ross and Pawlina, 2016). Tendon, conversely, made up of primarily type I collagen fibres, was expected to stain more red.

When collagen fibres are stained SRFG, they birefringe under polarized light (Lattouf *et al*., 2014). Birefringence is a measure of the difference of refractive indices that result from a beam of light

splitting into two (Caamaño *et al*., 2010; Rittié, 2017; Liu *et al*., 2021). The polarised photomicrographs of tendon were expected to birefringe yellow, yellowish-orange, yellowish-red, and red associated with type I collagen, and green to greenish-yellow which are colours associated with type III collagen (Montes and Junqueira, 1991; Hirshberg *et al*., 1999; Allon *et al*., 2006). Muscles were not expected to be birefringent on contractile proteins, with only connective tissue sheaths being birefringent. Fleshed bones were expected to birefringe at lower temperatures, with the intensity of birefringence decreasing as temperature increases. The wet and dry controls were expected to be birefringent with colours associated with collagen, which decreases with intensity as cremation temperature increases.

2.8.3. Ground bone sectioning

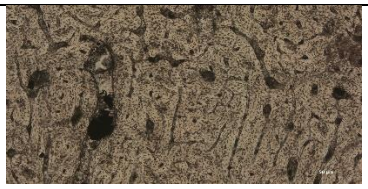
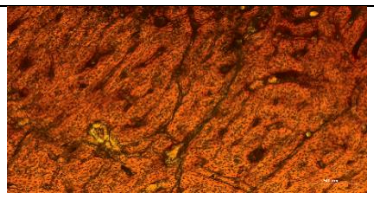
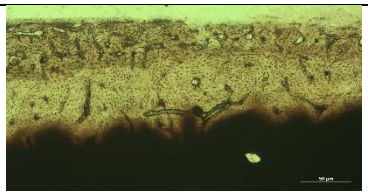
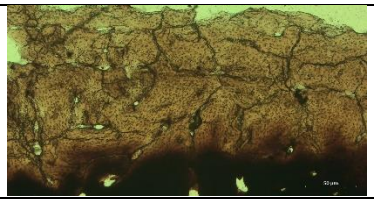
For preparation of normal ground bone sections, 1 mm blocks were ground down on 220-grit waterproof carborundum paper lubricated with distilled water, until sections were thin and smooth on both sides. Thereafter, a Frost's gripping device was applied by folding a slip of abrasive paper across the glass slide and using rotational motion with moderate pressure on the section, the section was ground further (Appendix C1). The thickness was monitored using light microscopy until histological features could be resolved (Maat *et al,* 2001; Bacci, 2016). For the delicate bones burnt between 300°C - 500°C, one side of the block was ground down on 220 grit paper until it become flat and smooth then the block was rinsed in soapy water (Sunlight liquid detergent). After the block had dried, it was placed onto a drop or two of cyanoacrylate glue that had been applied to a glass slide and left to dry for 2 hours, while weighed down. Thereafter, the unfinished side was ground down lubricated with distilled water by applying moderate pressure using the index and middle finger. Finished sections were then rinsed with distilled water three times and placed in fresh distilled water to prevent dehydration prior to mounting and analysis (Maat *et al,* 2001).

2.8.4. Histological analysis of stained and ground bone sections

All stained and ground bone sections were mounted with Entellan and photomicrographs were taken using Zeiss Axioskop 2 plus with a Zeiss Axiocam 208 colour (Zen 2010) at 5x magnification. Polarised images were also taken 5x magnification using the same microscope but changed the lighting to polariser. For both stained and ground bone sections the slide section was divided into 5 parts and photomicrographs were taken from the first, the third, and the fifth block

sections of the slide (Figure 2.8.4.1). Microfractures were classified according to the extent at which they fractured (Table 2.8.4 and Figure 2.8.4.2). The photomicrographs included sections of which the morphology of the tissue was present and visible, and excluded sections where more than 80% of the tissue was not present.

Table 2.8.4: Proposed microfracture definition criteria

Extent of Micro-fracturing	Description	Examples
No micro-fracturing	No visible micro-fractures present. Other artefacts, such as superficial scratches and vascular canals may be seen, but these are distinct from fractures.	
Low	The micro-fractures are few, individual and generally visible throughout the bone tissue.	
Moderate	Micro-fractures are visible throughout the bone section and may form few networks of merging fractures while other fractures are individual.	
High	Micro-fractures are arranged in complex networks with multiple merging micro-fractures across large areas of the visible tissue morphology (crazing-like patterns) (Pol and Gosavi, 2014).	

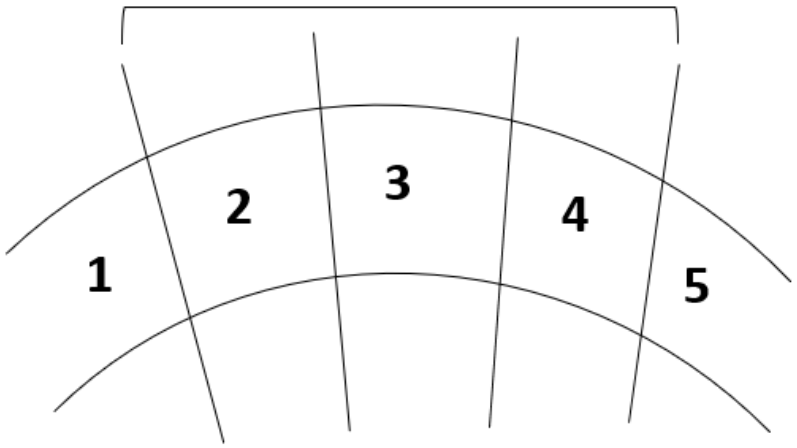


Figure 2.8.4.1: Image showing the division of slide section.

The slide section was divided into five areas and the photomicrographs were taken from the second, the third, and the fourth block represented by the bracket above the sections.

2.9. Data analysis

Data was managed in Microsoft Excel and statistical analyses undertaken using Statistical Package of Social Sciences (SPSS) (IBM Corporation, 2020, IBM SPSS Statistics for Windows, Armonk, New York, Version 27).

All the repeatability tests were conducted on a subset of 10 bone samples. For intra-observer, the data collection was repeated three times by the primary investigator with a waiting period of two weeks in between repeats. The inter-observer error data was collected by two additional observers and their data was compared with the first set of intra-observer data. Inter- and intra-observer error was assessed using intraclass correlation coefficient for macroscopic data (heat-induced colour, and the number, type, and location of heat-induced fractures). The intra- and inter-observer error for the extent of micro-fracturing was assessed using Fleiss's Kappa test.

The pilot (optimisation) study was only qualitatively assessed to confirm if the controlled parameters and experimental variables caused heat-induced changes that could be analysed downstream. Descriptive statistics of the macroscopic heat-induced fractures (number, location and type), colour and fragmentation were presented in a frequency table.

For experimental data, normality was determined using the Shapiro-Wilk test for continuous variables (pre- and post-cremation mass, mass loss percentage and total number of macrofractures). A Fisher-Freeman-Halton Exact test was conducted for heat-induced colour, fragmentation, macro-fracture type and location, and micro-fracturing, followed by a pair-wise Fisher's exact *post hoc* test to confirm where significant associations between those variables and experimental conditions were found. The difference between the pre- and post-cremation mass measurements was non-parametric, hence, Wilcoxon signed-rank tests was used to test for differences. The mass loss percentage across different temperatures and bone conditions were parametric and an ANOVA, followed by Dunn's *post hoc* test with Bonferroni correction was used to test differences. The relationship between total number of macrofractures and cremation temperature was non-parametric, thus the Kruskal Wallis ANOVA by ranks was used and followed by a pairwise Mann Whitney U *post hoc* test. However, the relationship between total number of macrofractures and bone taphonomic condition was parametric, thus an ANOVA followed by Dunn's *post hoc* test with Bonferroni correction was used to test for differences.

Chapter 3: Results

3.1. Pilot study: Optimisation of heating experimental parameters

Optimisation was done on 15 tibiae (5 fleshed, 8 wet and 2 dry) to confirm the control parameters that were used for the experimental study. Optimisation was conducted to test the use of nitrogen, cremation temperatures (200°C, 400°C, 500°C, 600°C and 800°C) and decalcification solutions. Data recorded included pre-cremation and post-cremation mass, heat-induced colour change, fragmentation, macrofracture prevalence, and thermocouple temperature readings.

3.1.1. The use of nitrogen gas during cremation

Two cremation trials were conducted on fleshed and wet tibia bones at 600°C, with and without the influx of nitrogen. Both trials had similar heat-induced colour change (charring) with heat lines and heat borders on fleshed bones (Appendix D2.1) and similar prevalence of macrofracture types (Appendix D1). Importantly, there was no physical sign of combustion in both trials with and without nitrogen gas. As a result, experimental cremations were conducted without nitrogen gas.

3.1.2. Optimising the cremation temperature

The cremation temperatures were optimised to check if there were heat-induced changes and ensure sample preservation for further analyses. Cremation on both fleshed and wet bones at 200°C did not present any heat-induced macroscopic changes, while at 400°C, 500°C, 600°C and 800°C there were changes in colour, fragmentation and fracturing. There was a high prevalence of longitudinal, patina and delamination fractures (Appendix D1), at 600°C and 800°C, the fracture patterns were difficult to assess due to fragmentation (Appendix D2.2). Bones cremated at 800°C showed excessive fragmentation which prevented further analysis. Dry bones cremated at 400°C and 600°C did not fragment (Appendix D2.2). However, most of the fleshed and wet bones cremated at 600°C fragmented. These bone fragments were only partially aligned and too fragile to carry out the microscopic part of the experiment. As a result, the temperatures 200°C, 600°C and 800°C were excluded from the experimental study, with 300°C, 400°C and 500°C being the temperatures selected for subsequent experimentation (the experimental study).

Thermocouples allowed for monitoring of temperature within the furnace, the bone (and/or flesh), and the external environment. The ambient temperature remained relatively constant between

19°C - 30°C throughout the cremation processes whereas the furnace temperature and bone sample showed changes (Figure 3.1.2.1. A). The dry cremated bones showed a similar trend of gradual increase in temperature as the furnace temperature increased (phase I), followed by a plateau phase II, then increasing to approximately the specific maximum temperature for the trial (Figure 3.1.2.1 A phase III). While the furnace temperature was on hold for 30 minutes, the bone temperature continued to increase minimally, slowly plateauing until the trial end (Figure 3.1.2.1 A phase IV). When the cremation trial ended, after the 30 minutes hold, and the furnace was turned off, both the furnace and bone sample temperatures started decreasing (Figure 3.1.2.1 A phase V). The dry bone showed a tendency to increase in temperature beyond the maximum input temperature of cremation at 400°C (Figure 3.1.2.1 A) and 600°C (Figure 3.1.2.1 B) during phase IV. The wet bone followed a similar temperature trend as dry bones, but the wet bone increased above the input temperature of cremation less than dry bone did (Figure 3.1.2.1 B). However, fleshed cremated bone started with a slower gradual increase before the plateau phase I compared to wet and dry bones (Fig 3.1.2.1 B). The fleshed bone was increasing slowly to the specific maximum temperature (phase III) and kept on increasing during the 30 minutes hold (phase IV). In addition, the fleshed bones did not reach the maximum input temperature of cremation (Fig 3.1.2.1 B). The thermocouple readings were precise with a standard error of measurement of ±5°C (Appendix D3 A). Furthermore, the fleshed bone cooling rate after the cremation trial (phase V) was very slow compared to dry and wet bones. The cremation trials of fleshed and wet tibiae at 800°C were interrupted by the short circuiting of the furnace thus creating inconsistent spikes on the graphs (Appendix D3 B). The furnace could not hold both 800°C cremation trials for a longer period when the power came back and therefore the cremation trial was ended.

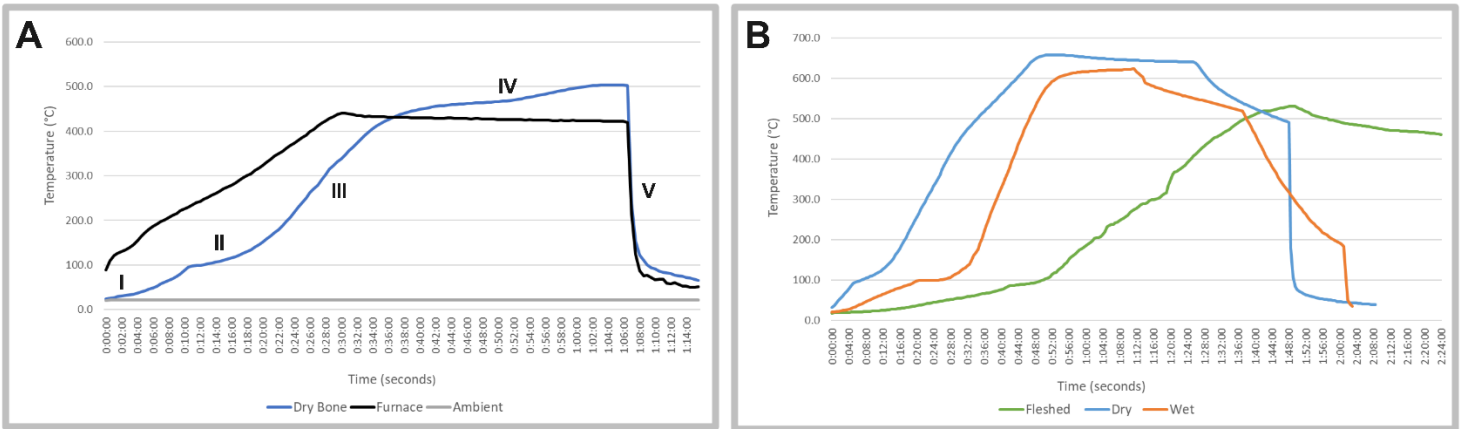


Figure 3.1.2.1: Graphs showing the cremation temperatures of samples, furnace, and the ambient temperature during cremation for 30 minutes at different maximum temperatures.

A) Representative graph of a burning trial of a dry bone at a maximum temperature of 400°C. Both the furnace and the bone sample with thermocouples were placed into the furnace when it had reached 100°C. Once the furnace temperature reached 400°C, the furnace was set to hold the temperature for 30 minutes. The trial was ended after the 30 minutes hold. **B**) Representative graph of cremation trials of bones in different taphonomic conditions (fleshed, wet and dry) cremated at a maximum temperature of 600°C.

3.1.3. Determination of optimal decalcification solution

Optimisation of decalcification solutions was done to test which solution was best suited for the study, being able to decalcify bone but particularly for burnt bone, maintain structural integrity for subsequent analysis. The unburnt (25°C) dry bone blocks had a mean decalcification time of 13 162 minutes (9 days, 15 hours and 40 minutes), when using formic citric acid (FCA), which took more time to decalcify than other decalcification solutions of interest and therefore it was eliminated. The rest of the decalcification solutions took less than half the time in comparison to FCA. The mean decalcification time for bone blocks decalcified with 10% formic acid (FA), 5% nitric acid (NA) and 3% nitric acid (NA) were 4 741 minutes (3 days and 7 hours), 4 218 minutes (2 days and 22 hours) and 2 163 minutes (1 day and 12 hours), respectively (Figure 3.1.3.1.). The 3% NA was used only on few unburnt dry bone blocks to test the effect of a lower NA concentration solution and had similar decalcification time as 5% NA.

Only 10% FA and 5% NA were further trialled to decalcify burnt bone blocks. About 60% of the burnt bone blocks decalcified with 5% NA and 40% burnt bone blocks decalcified with 10% FA

turned into powder during decalcification and/or during the tissue processing. Most of the blocks that turned into powder during decalcification were extracted from bones cremated at 500°C and 600°C while blocks from bones at 800°C could not be extracted due to being too fragmented and delicate (Appendix D4). Most of the bone blocks that were successfully embedded were decalcified with 10% FA (Appendix D4). Therefore, 10% FA was the decalcification solution chosen for the study.

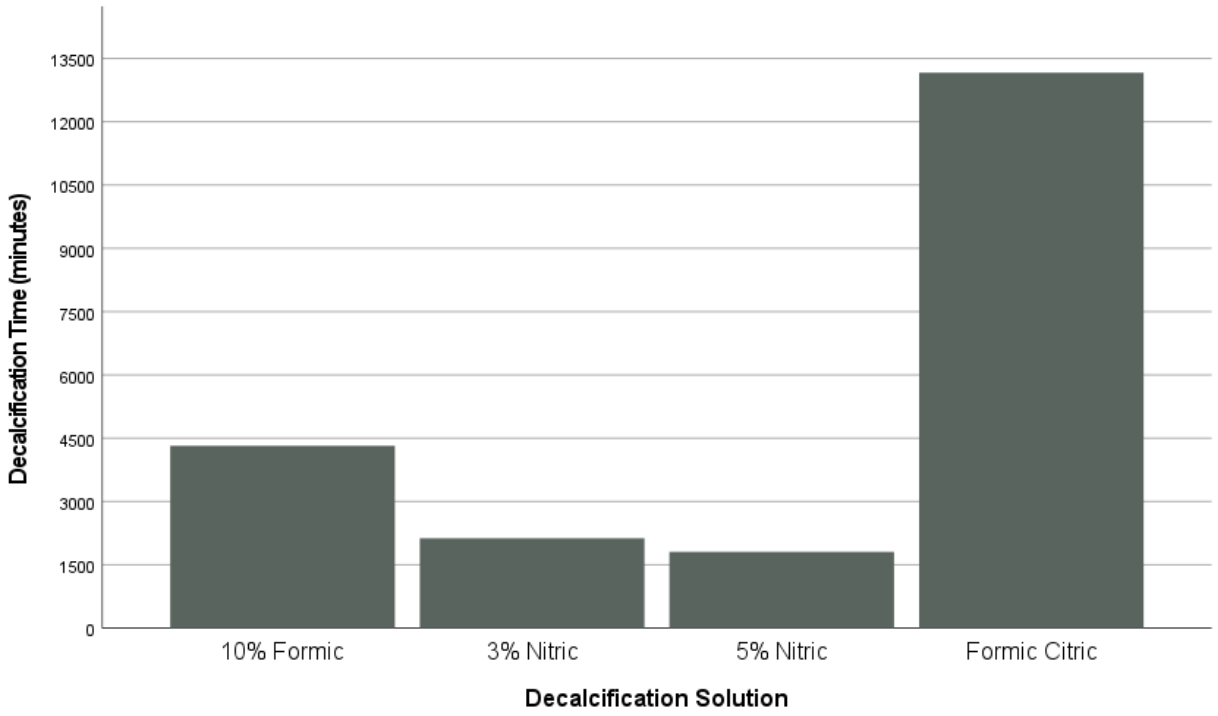


Figure 3.1.3.1: Decalcification time in relation to acid decalcification solutions and successful embedding of blocks.

Image showing the median of decalcification time, in minutes, of bone blocks decalcified using different decalcification solutions.

Following the completion of the pilot study and optimisation of the parameters for cremation (including air and furnace temperature) as well as determining the appropriate decalcification solution for histological analysis of fragile burnt bone, the experimental study was then conducted.

3.2. Experimental study - Macroscopic Results

The experimental study was conducted on a total of 33 tibiae bones at different taphonomic conditions (dry, wet, fleshed) at 300°C, 400°C and 500°C (Table 2.7.1). Thermocouple data demonstrated that the cremation trials of bone followed the same trend as during optimization where dry bone exceeded the maximum temperature while wet bones reached the maximum temperature, and the fleshed bones did not reach maximum temperature (Appendix E). Macroscopic heat-induced changes in colour, fragmentation and macrofractures were recorded and analysed.

3.2.1. Repeatability

Intra-observer repeatability was good to excellent ($\kappa = 0.7 – 0.9$) for most variables (colour change, total number of fractures per bone, number of fracture type present on each bone and number of fractures per location) (Appendix H1). Inter-observer agreement was poor for total number of fractures per bone location (ICC = 0.480) and only moderate (ICC = 0.555 and ICC = 0.517) for most variables (total number of fractures per bone and number of fracture type present on each bone) (Appendix H1), with the exception of colour changes which was good (ICC = 0.783) (Altman, 1999 adapted from Landis and Koch, 1977).

3.2.2. Heat-induced macroscopic colour change and fragmentation

A significant difference in heat-induced colour was identified between unburnt controls and experimental cremation temperatures ($\chi^2 = 34.929$, $p < 0.001$) (Appendix, F1.2). This difference in heat-induced colour was found for each tested temperature (300°C, 400°C and 500°C) compared to the unburnt controls ($p < 0.001$, Appendix F1.3), which retained the beige colour (Appendix F1.1). Heat lines and heat borders were present in all cremation temperature while charring was mostly present in bones cremated at 300°C and calcination was present in bones cremated at 400°C and 500°C (Appendix F1.1). There were significant differences in colour changes found between

bones cremated at different taphonomic conditions ($\chi^2 = 61.757$, $p < 0.001$) (Appendix F1.5). This difference in heat-induced colour was found across all the cremated bones at taphonomic conditions (fleshed, wet and dry) ($p < 0.001$) while the wet and dry controls did not have a statistical outcome (Appendix F1.6) as they retained beige colour (Appendix F1.4). Heat-induced colour change across bone taphonomic conditions showed that all fleshed bones presented with heat lines and heat borders, and only wet and dry bones presented charring and calcination (Appendix F1.4). There was no significant difference found across all the bones at different taphonomic conditions when cremated at different temperatures ($p = 0.100$, Appendix F1.8). In addition, there was no statistical outcome between wet and dry control, dry 400°C and dry 500°C, wet 400°C and wet 500°C, fleshed 300°C, fleshed 400°C and fleshed 500°C (Appendix F1.8). A qualitative analysis showed that regardless of cremation temperatures, all fleshed bones presented with the same colour change, heat lines and heat borders with partial charring (Appendix F1.7). The wet bones cremated at 300°C presented more charring with partial beige colour while wet bones cremated at 400°C and 500°C had less calcination with partial charring colour (Appendix F1.7). All the dry bones cremated at 300°C were completely charred while the dry bones cremated at 400°C and 500°C presented more calcination with partial charring colour (Appendix F1.7)

Qualitative analysis showed that as temperature increased, there were more fragmentation seen on both fleshed and wet bones. The fleshed and wet bones cremated at 400°C and 500°C had aligning fragments while one of the wet bones had fragments that aligned partially, nevertheless, there was no significant difference between different categories of fragmentation and cremation temperatures (300°C, 400°C and 500°C) ($\chi^2 = 8.546$, $p = 0.339$) (Appendix F2.2) ($p > 0.0083$, Appendix F2.3), or bone taphonomic conditions ($\chi^2 = 11.083$, $p = 0.746$) (Appendix F2.5) ($p > 0.005$, Appendix F2.6). Moreover, only two of the fleshed bones cremated at 500°C had fragments that did not align. All the dry bones cremated at different experimental temperatures did not fragment.

3.2.3 Heat-induced mass loss

The pre- and post-cremation test results showed that there was a significant decrease in the mass of bones after cremation irrespective of taphonomic condition ($Z = -4.542$, $p < 0.001$, Appendix G1). There was no significant difference on mass loss percentage of bone cremated at different taphonomic conditions ($F = 1.131$, $df = 26$, $p = 0.339$, Appendix G3). Greater mass loss percentage was seen at higher temperatures ($F = 7.312$, $df = 26$, $p = 0.003$, Appendix G2);

however, when combined, no significant difference was found between mass loss of bones at different taphonomic conditions across different cremation temperatures ($F = 1.131$, $df = 26$, $p = 0.339$, Appendix G3 and G4), increased temperatures appeared to have a greater effect in mass loss percentage over taphonomic condition. The greater difference in mass loss percentage was found between bones cremated at 300°C and 500°C ($p = 0.003$, Appendix G2). There was less mass loss at lower temperatures and more mass loss at higher temperatures (Figure 3.2.3.2). Dry bones had the least mass loss followed by wet bones, while fleshed bones had the greatest mass loss.

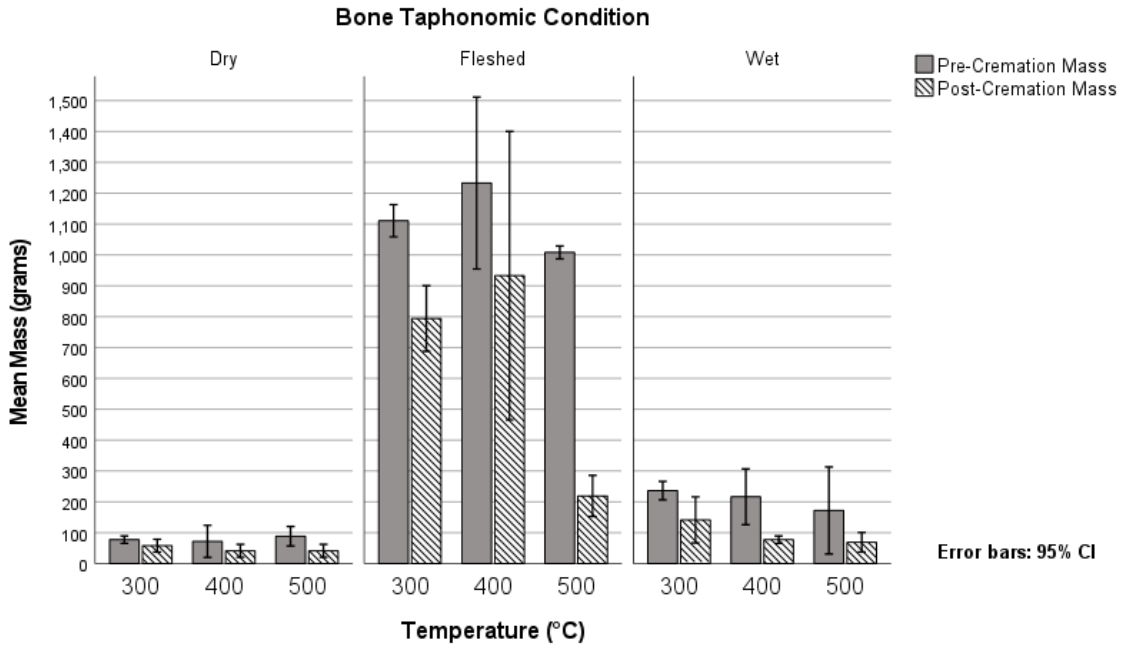


Figure 3.2.3.2: Pre- and post-cremation mass of bone cremated at specific temperature under different bone conditions.

Figure showing the mean pre-cremation mass (grey) and mean post-cremation mass (light pattern) for each taphonomic condition and cremation temperature group. The mean mass is clustered with different bone conditions (dry, fleshed, and wet bones) at different cremation temperatures to demonstrate the amount of mass loss. There error bars represent standard error of mean at a 95% confidence interval.

3.2.4. Heat-induced macroscopic fracturing

There was a significant increase in the total number of macro-fractures observed as the temperatures increased (Kruskal-Wallis $H = 23.023$, $df\ (n=33) = 3$, $p < 0.001$, Appendix H2).

Bones cremated at 400°C and 500°C had a significantly higher number of fractures compared to unburnt controls (25°C) ($p < 0.001$ and $p = 0.023$, respectively, Appendix H2). Bones cremated at 500°C had significantly higher number of fractures than those cremated at 300°C ($p = 0.004$) (Appendix H2). The significant increase in total number of macro-fractures at higher temperatures was found between some bone taphonomic condition groups ($F = 8.516$, $p < 0.001$, Appendix H3). There was a significant increase in number of macro-fractures on cremated dry bones compared to the fleshed bones ($p = 0.010$, Appendix H3), wet control ($p = 0.002$, Appendix H3) and dry bone control, ($p = 0.032$, Appendix H3). Wet bones also had a significantly greater number of total fractures compared to wet controls ($p = 0.032$, Appendix H3) and dry controls ($p = 0.032$, Appendix H3).

The most prevalent fracture types were patina, followed by delamination then longitudinal (Figure 3.2.4.1. A). There were more macrofractures on the anterior side, followed by posterior and medial with lateral side having the least number of macrofractures (Figure 3.2.4.1. B). The prevalence of macro-fracture types on each of the four different sides of the bone was similar to that in Figure 3.2.4.1. A, where patina fractures were more prevalent followed by delamination then longitudinal.

The least prevalent fracture type, curvilinear, appeared twice and was only present in fleshed bones cremated at 500°C (Table 3.2.4.1) on the lateral (muscle attachment site) and medial (non-muscle attachment site) surfaces (Figure 3.2.4.1. B). Overall, there was a greater number of total fractures in dry bones followed by wet bone and the least in fleshed bones (Table 3.2.4.1). There were more patina fractures at 500°C in dry bone followed by fleshed bones and the least in wet bones. There was a higher prevalence of delamination fractures at 300°C in dry and wet bones than at 500°C. Transverse fractures were only present in wet and dry bone, while step fractures were the least numerous outside of curvilinear fractures. There were more longitudinal fractures on fleshed bones than in dry and least on wet bones.

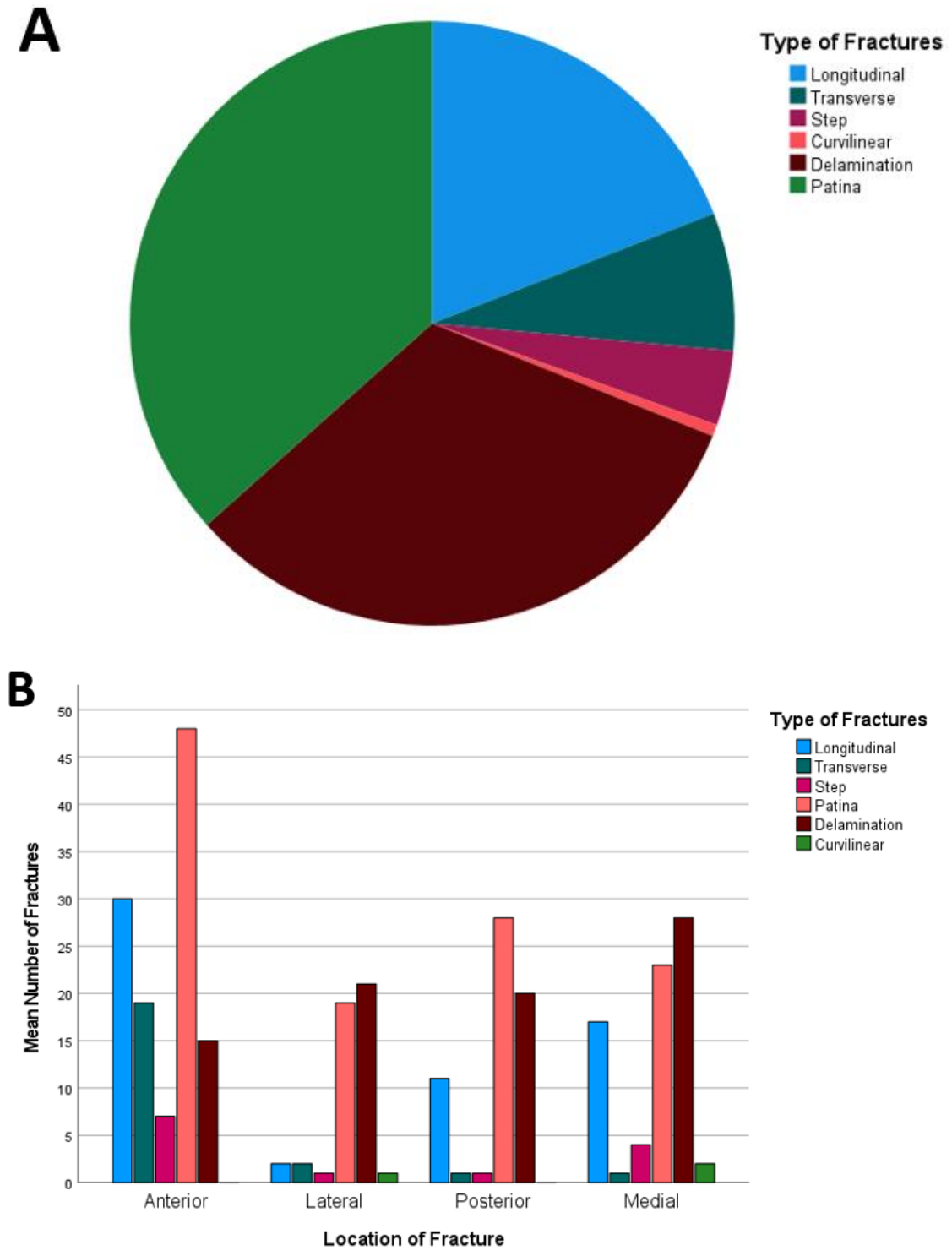


Figure 3.2.4.1: Macrofracture type prevalence and location across all experimental parameters (taphonomic conditions and temperatures).

A) Pie chart showing the prevalence of macrofracture types and **B)** the mean number of fractures present on the anterior, lateral, posterior and medial sides of the bone across all experimental bone samples, irrespective of taphonomic condition and temperature.

Table 3.2.4.1.: Frequency of fractures and fracture type for bones at different taphonomic conditions cremated at different temperatures.

Condition	Temperature	Longitudinal	Transverse	Step	Curvilinear	Delamination	Patina	Total
Controls	*25°C*	No fractures						0
	300°C	No fractures						0
Fleshed	*400°C*	2	0	0	0	0	5	*7*
	500°C	15	0	4	2	12	19	*52*
	300°C	0	0	0	0	21	9	*30*
Wet	*400°C*	6	8	2	0	14	11	*41*
	500°C	12	7	4	0	5	17	*45*
	300°C	3	1	1	0	22	5	*32*
Dry	*400°C*	11	4	0	0	20	12	*47*
	500°C	13	4	2	0	11	41	*71*

3.3. Experimental study - Microscopic Results

Post-cremation, two bone blocks were extracted from three groups (total of 66 bone blocks), decalcified, and processed for haematoxylin and eosin (H&E), and Sirius Red-Fast Green (SRFG) staining. There were sections that detached from the microscopic slides during the staining process, mainly the sections extracted from wet bones cremated at 400°C and 500°C, and some dry bones cremated at all three temperatures. In these cases, only a few pieces of scattered section fragments remained attached to the slide. Regarding ground bone sections, several sections were destroyed during the sample processing. Therefore, only sections that had more than a qualitatively assessed of 80% of the bone tissue morphology clearly visible were included for micro-fracture analysis. As a result, the histological sample was incomplete, hence, conducting any quantitative statistical analysis would be inaccurate and not truly representative of the expected outcomes of the study. As such, a qualitative evaluation of the micro-fracturing and collagen presence was conducted instead.

3.3.1. Repeatability

The analysis of microfractures was conducted on ground bone sections based on presence (none; low, medium and high extent of fracturing) and arrangement of microfractures (Table 2.8.4). Intra-observer agreement was good ($\kappa = 0.685$) and inter-observer agreement was moderate ($\kappa = 0.541$) (Appendix I1) (Altman, 1999, adapted from Landis and Koch 1977).

3.3.2. Histological Morphology of bone, tendon and muscle

In haematoxylin and eosin (H&E) stained tendon sections, collagen fibres stained light eosinophilic with the flat fibroblast nuclei staining basophilic (Figure 3.3.2.1 A-B). Muscle fibres stained more intensely eosinophilic, with striations evident, and the nuclei staining basophilic (Figure 3.3.2.1 C-D). The collagen fibres in the connective tissue sheaths stain light eosinophilic compared to muscle fibres (Figure 3.3.2.1 C-D). H&E staining of decalcified bone showed the nuclei of the osteocytes in the lacunae stained basophilic while the rest of the bone tissue stained eosinophilic (Figure 3.3.2.2 A-D). In many sections osteocytes were lost and lacunae appeared empty. Osteons, which were evident by concentric lamellae surrounding an osteon canal, stained more intensely eosinophilic compared to the interstitial lamellae (Figure 3.3.2.2 C-D). Plexiform bone was identified by a band of vascular canals forming rows of bone matrix (Figure 3.3.2.2 A-B). Internal borders of the areas surrounding resorption lacunae and vascular canals stained more intensely eosinophilic (Figure 3.3.2.2 A-D).

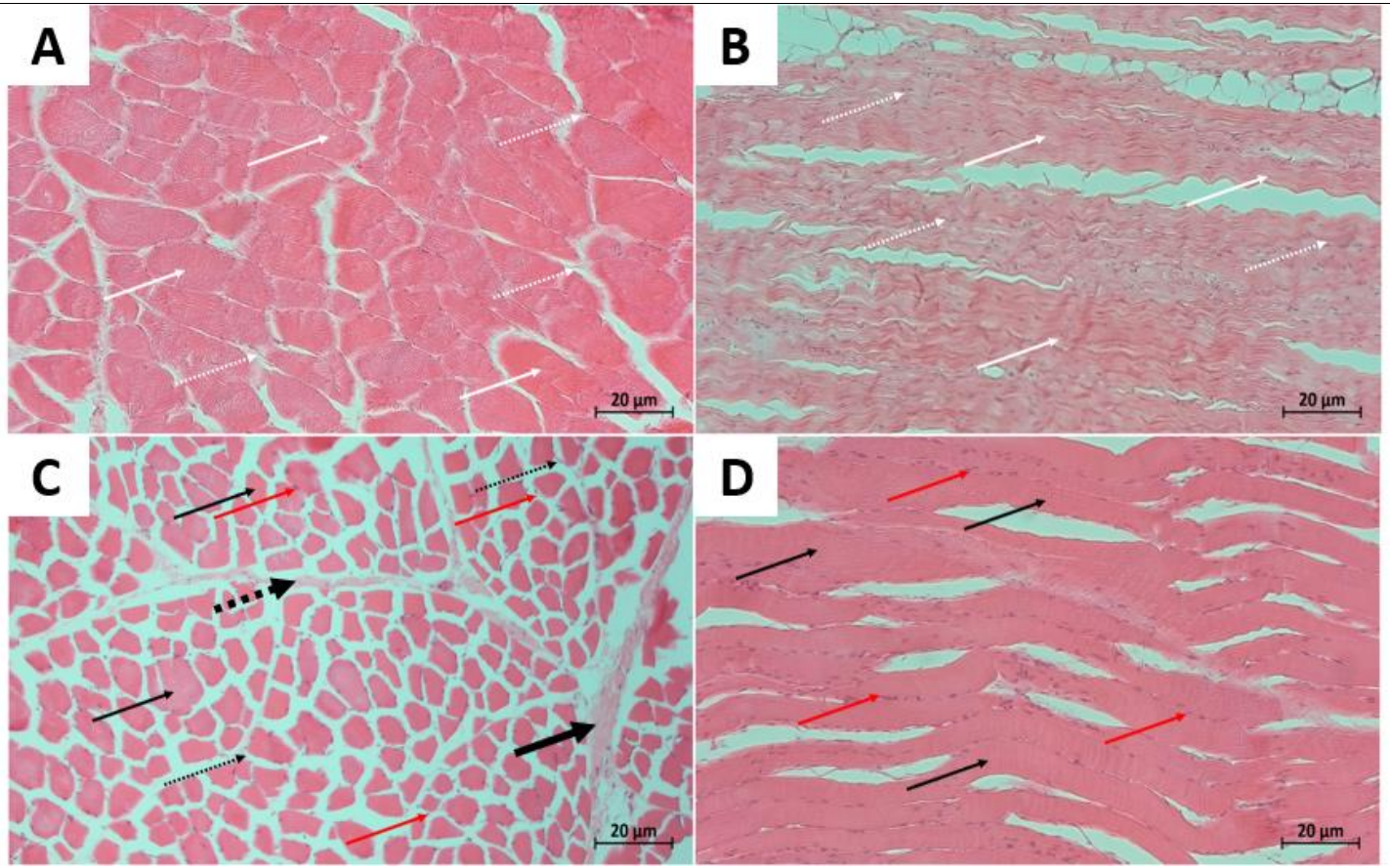


Figure 3.3.2.1: Representative photomicrographs of tendon and muscle stained with Haematoxylin and Eosin

A) Representing transverse section while **B)** representing longitudinal section of long digital extensor tendon showing the tendon collagen fibres (white arrow) with flat fibroblasts (white dashed arrow). **C)** Representing transverse section and **D)** representing longitudinal section of long fibular muscle showing muscle fibres (black thin arrow) surrounded by muscle connective sheaths, endomysium (black thin dashed arrow), perimysium (black thick dashed arrow) and epimysium (black solid arrow) with the nuclei of muscle cells (red thin arrow). Photomicrographs were taken at 5x magnification except image B that was taken at 10x magnification.

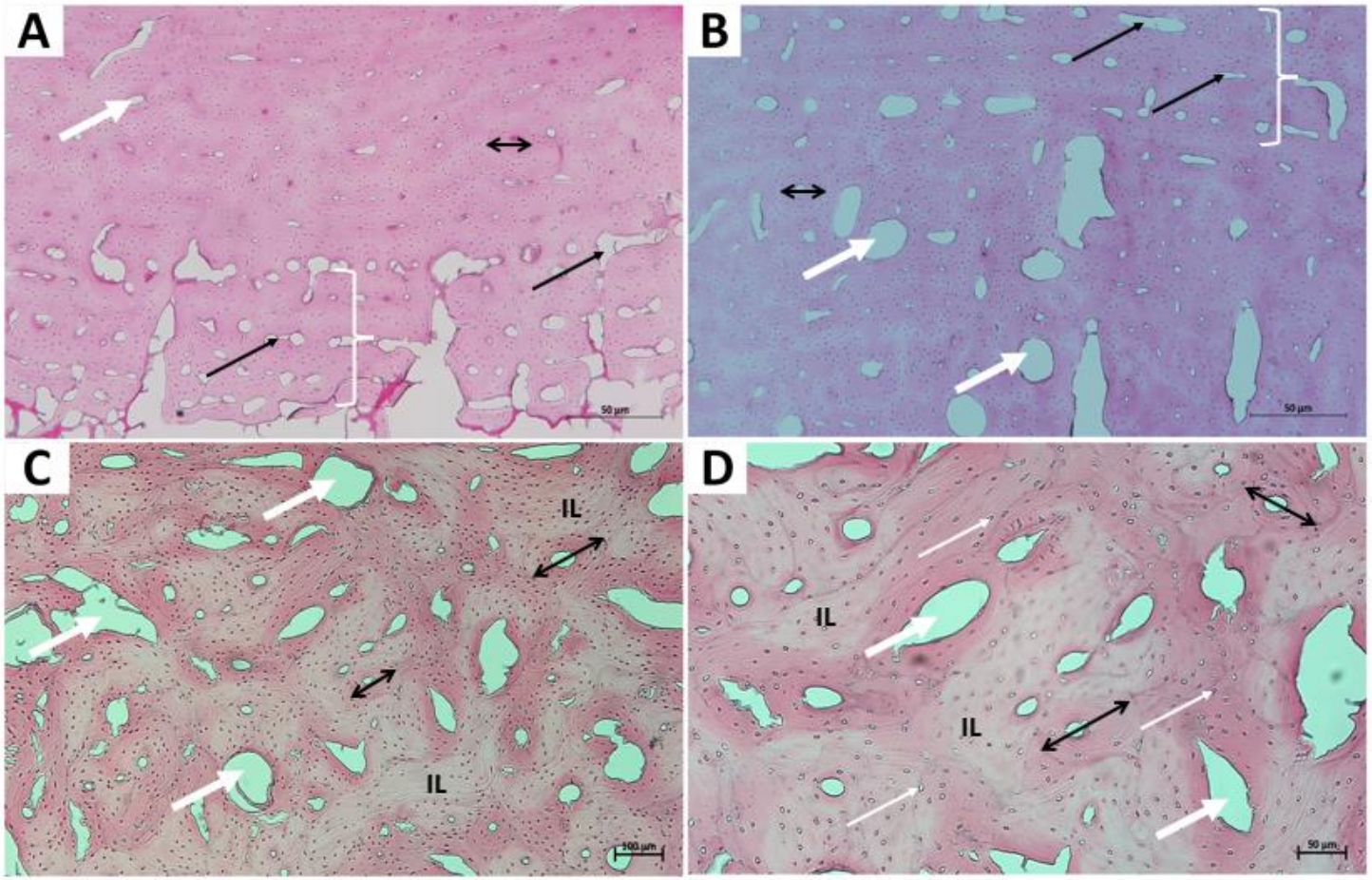


Figure 3.3.2.2: Representative photomicrographs of bone stained with Haematoxylin and Eosin

A) and **B)** represents dry control (unburnt) bones; **C)** and **D)** fleshed bone cremated at 300°C showing the osteons (black double arrowhead), osteocytes (thin white arrow) and resorption lacunae (thick white arrow) surrounded by interstitial lamellae (IL). Plexiform structures (white bracket) with vascular canals (thin black arrow). Photomicrographs A and B were taken at 5x magnification, C and D were taken at 10x magnification.

3.3.3. Qualitative assessment of collagen

The Sirius Red-Fast Green (SRFG) stains was used for qualitative analysis of collagen by staining collagen red and non-collagenous proteins green. Muscle was used as negative control, SRFG stained the muscle contractile fibres green and the surrounding connective sheaths red (Figure 3.3.3.1.B). The tendons, as positive controls being comprised primarily of collagen stained red, however, there were some areas of the tendon that stained green in between the red collagen fibres (Figure 3.3.3.1. A). The polarised photomicrographs showed birefringent colours which are all associated with collagen. Specifically, the colours yellow, yellowish-orange, yellowish-red, and red are associated with type I collagen while the colours green to greenish-yellow are associated with type III collagen (Montes and Junqueira, 1991; Hirshberg *et al*., 1999; Allon *et al*., 2006). The tendon birefringence presented the colours yellow, pink and blue-green (Figure 3.3.3.1. A2). The polarised images of muscle tissue also presented the pink birefringent colour which is associated with collagen within the connective sheaths (Figure 3.3.3.1. B2). However, the muscle fibres have shades of birefringence in blue-green colour, although this was difficult to discern (Figure 3.3.3.1. B2).

The SRFG stain on decalcified sections from dry control bones stained more red and less green, reflecting greater collagen content (Figure 3.3.3.2. A and B). The green staining on sections from dry controls mostly appeared around osteons, in the concentric lamellae and the red staining in the interstitial lamellae. Interestingly, the two dry bone controls showed different birefringent colours (Figure 3.3.3.2. A2) of blue-green and pink or blue-green and yellow, indicating more variation than had been expected (Figure 3.3.3.2. B2). Under polarised light, the histological structure was difficult to discern.

The cremated bones stained with SRFG showed similar staining to bone controls for sections obtained from fleshed bones cremated at lower temperatures. The interstitial lamellae of the fleshed bone cremated at 300°C stained red-pink and the osteons stained lighter green (Figure 3.3.2.2. A). However, the green staining around osteons was more consistent than in controls bones that were not cremated (Figure 3.3.3.3 A). The polarised images of sections obtained from fleshed bone cremated at 300°C showed the birefringent colours (pink and blue-green) (Figure 3.3.3.3 A2). Similar to muscle fibres, the green staining on the concentric lamellae of some osteons birefringed blue-green colour (Figure 3.3.3.3 A2). As the cremation temperatures increased, sections obtained

from the fleshed bones cremated at 400°C and 500°C stained primarily red with no green staining (Figure 3.3.3.3. B), meanwhile the areas that were intensely red staining had matched yellow birefringent colour, indicating type I collagen. The polarised image of sections obtained from the fleshed bones cremated at 400°C and 500°C showed little to no red-pink birefringent colours but more yellow with shades of blue-green associated with collagen, respectively (Figure 3.3.3.3 B2 – C2). In addition, sections from the fleshed bone cremated at 500°C had brighter yellow birefringence (Figure 3.3.3.3. C2) compared to samples obtained from fleshed bone cremated at 400°C (Figure 3.3.3.3. B2) while at 300°C there was no yellow birefringence (Figure 3.3.3.3. A2). Most of the sections from wet bone cremated at 300°C detached from the slide, a limitation noted that requires further optimisation, however, the remnants stained red only (Figure 3.3.3.4. A), while the matched polarised image showed few areas of the section that are birefringent with yellow and pink colours (Figure 3.3.3.4. A2). Increase in temperature, at 400°C and 500°C, for both wet and dry bones, where bone sections appeared charred with carbon deposition within the tissue, resulted in no staining (Figure 3.3.3.4. B and C) or birefringence (Figure 3.3.3.4. B2 and C2).

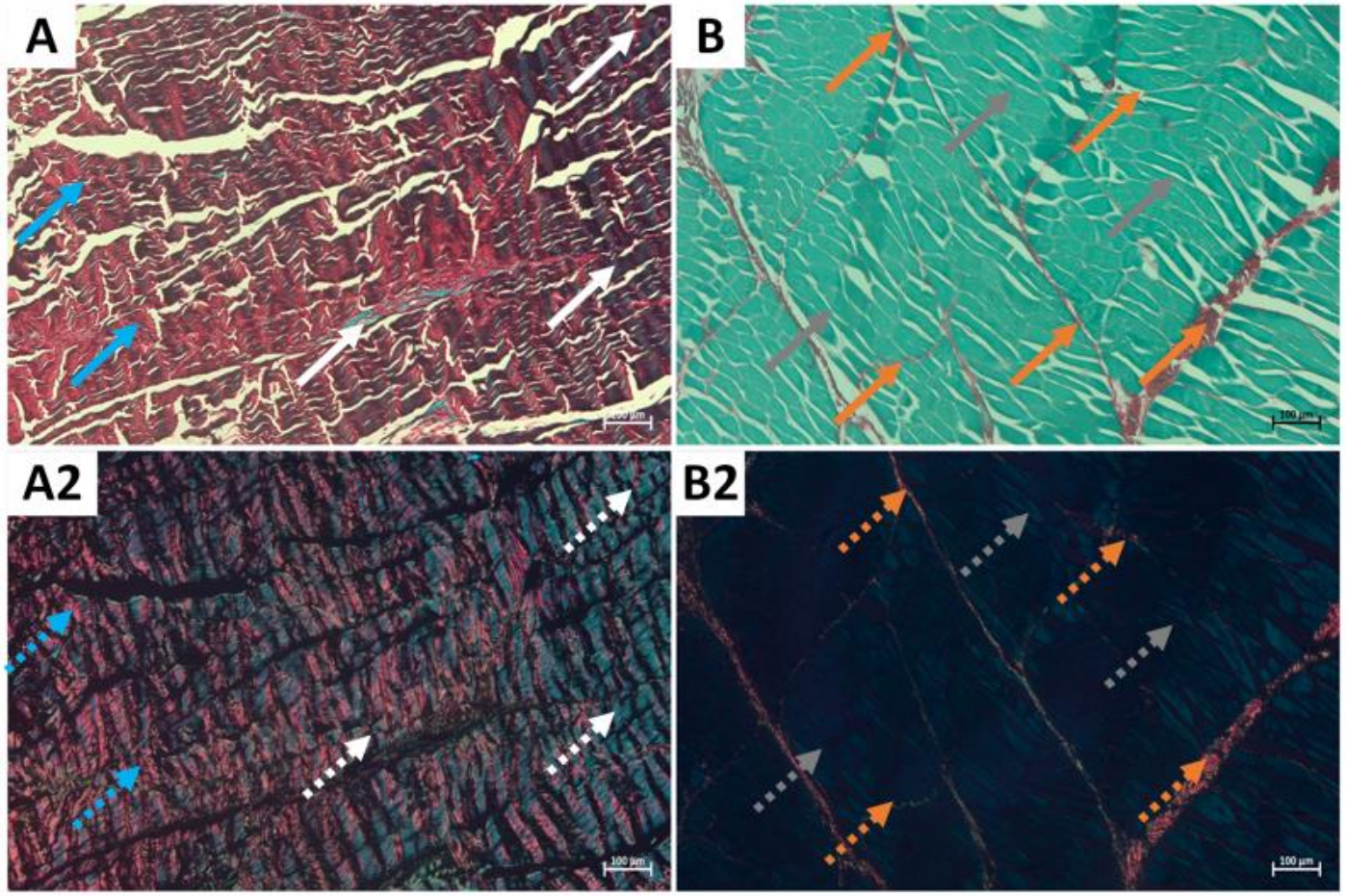


Figure 3.3.3.1: Representative photomicrographs showing sections of tendon and muscle stained with Sirius Red – Fast Green

A) SFRG stained tendon, and **B)** muscle under bright field microscopy. **A2) - B2)**: Matched SFRG stained sections under polarised light microscopy showing the birefringence. **A)** and **A2)** Showed the Achilles tendon where some areas stained red (blue arrow) and birefringed red-pink (dashed blue arrow), while the some areas that stained green (white arrow) and birefringed blue-green (white dashed arrow). **B)** and **B2)** Showed the cranial tibial muscle where the muscle contractile proteins stained green (grey arrow) and appear dark with shades of blue-green (dashed grey arrow) birefringence, while the connective tissue sheath stained red (orange arrow) and birefringed red-pink (dashed orange). Photomicrographs were taken at 5x magnification with 50µm scale bar.

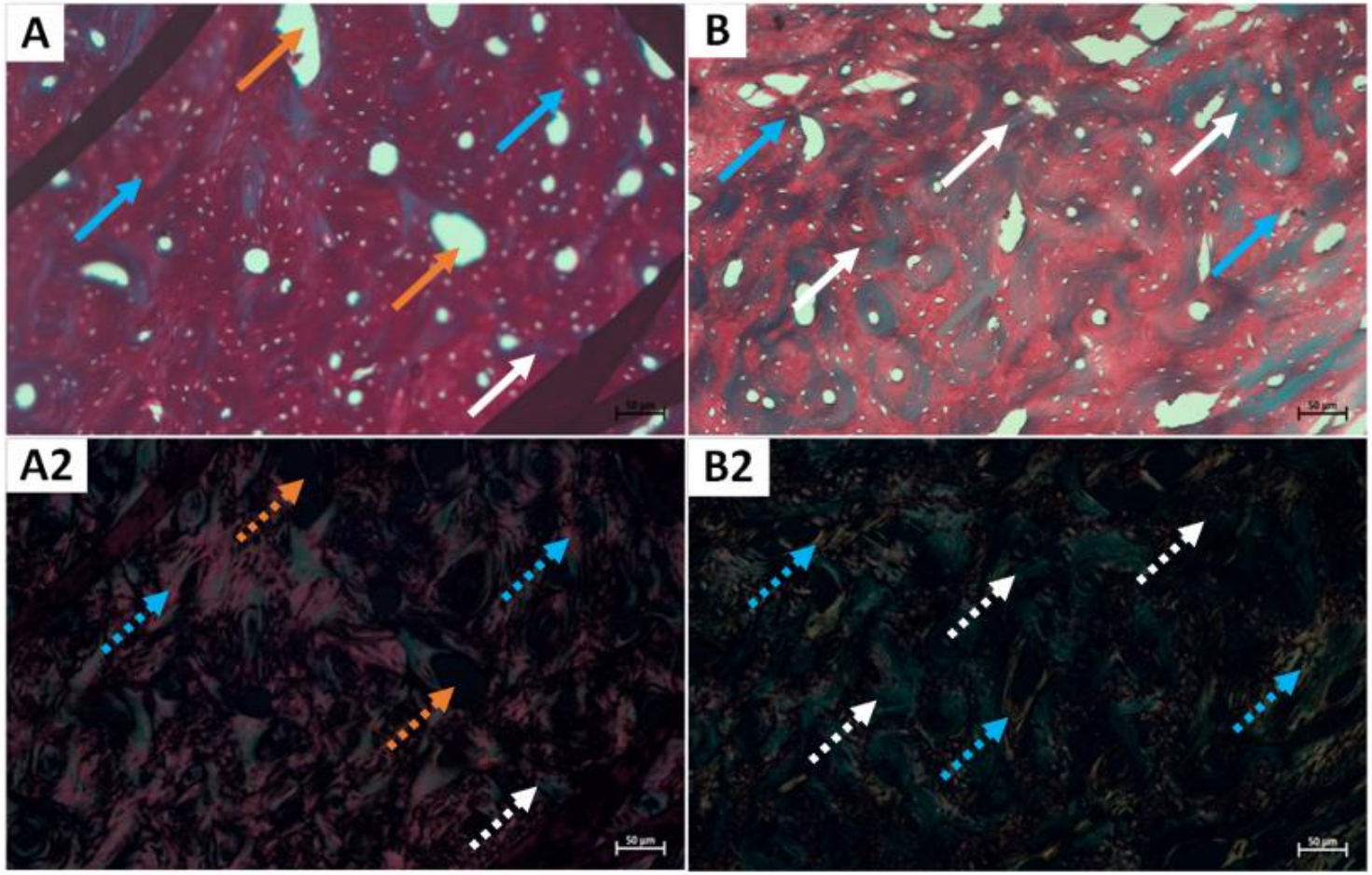


Figure 3.3.3.2: Representative photomicrographs showing Sirius Red – Fast Green stained sections of decalcified unburnt bone (control).

A) - B): Photomicrographs of SRFG stained sections under light microscopy from bone blocks extracted from two separate dry bone on the medial midshaft, decalcified with 10% FA. **A2) - B2)**: Photomicrographs of SRFG stained sections under polarised light microscopy showing the birefringence of staining colours from light microscopy. A) and B) showed the concentric lamellae of osteons staining green (solid white arrow) which birefringed blue-green (dashed white arrow), in between them is the interstitial lamella which stained red (solid blue arrow) and birefringed red-pink on **A2)** and blue-green on **B2)** (dashed blue arrow). The resorption lacunae (solid orange arrow) appear black (dashed orange arrow) due to polarised light. Photomicrographs were taken at 5x magnification with 50µm scale bar.

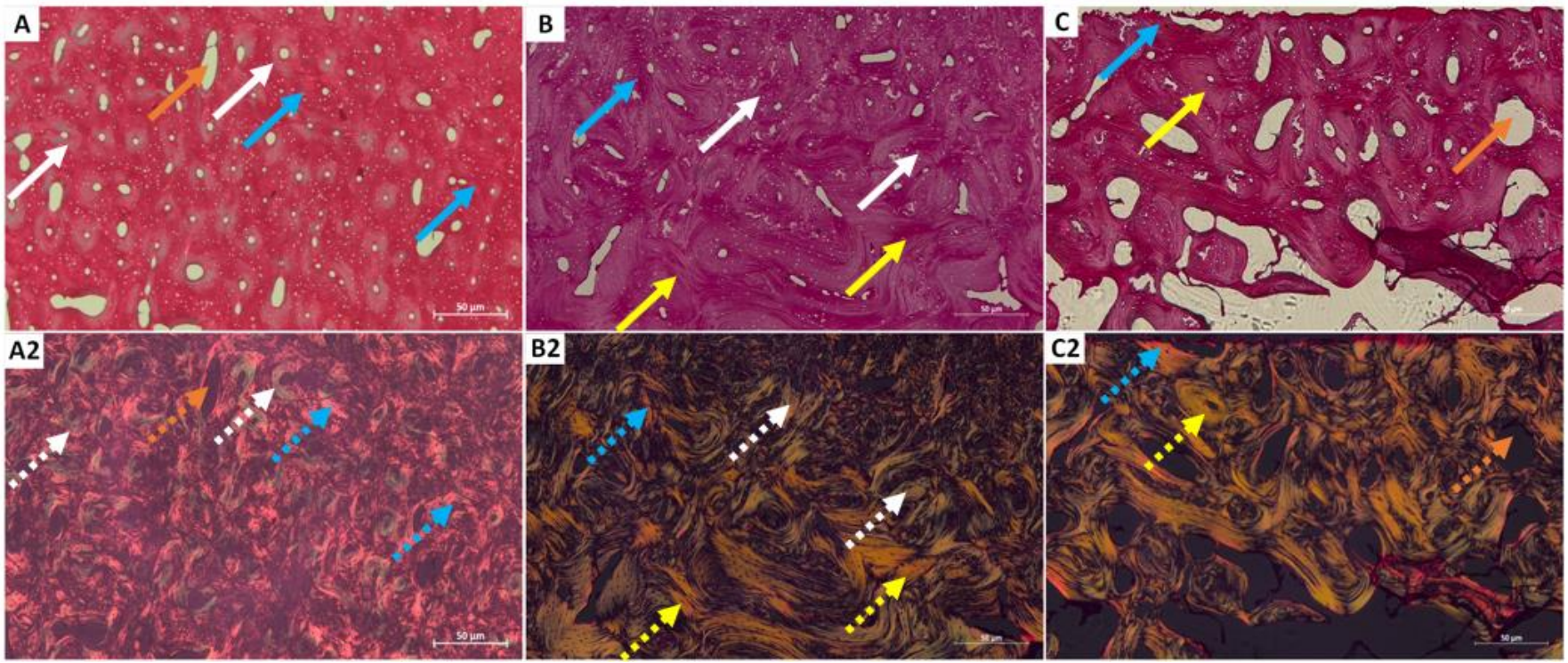


Figure 3.3.3.3: Representative photomicrographs of Sirius Red – Fast Green stained decalcified bone sections obtained from fleshed bones cremated at different temperatures.

A)-C): Photomicrographs of stained sections under light microscopy. **A2)-C2)**: Sections under polarised light microscopy. Sections originated from fleshed bones cremated at 300°C **A),** 400°C **B)** and 500°C **C)**. The osteons (solid white arrow) stained in varying faint shades of green and birefringed blue-green (dashed white arrow) while the interstitial lamellae (blue arrow) stained red and birefringed red-pink (dashed blue arrows). **B)** and **C)** Some areas of the interstitial lamellae stained intensely red (solid yellow arrow) and birefringed yellow (dashed yellow arrow). The spaces in the sections (solid orange arrow) appeared black (dashed orange arrow) due to polarised light. Photomicrographs were taken at 5x magnification with 50µm scale bar.

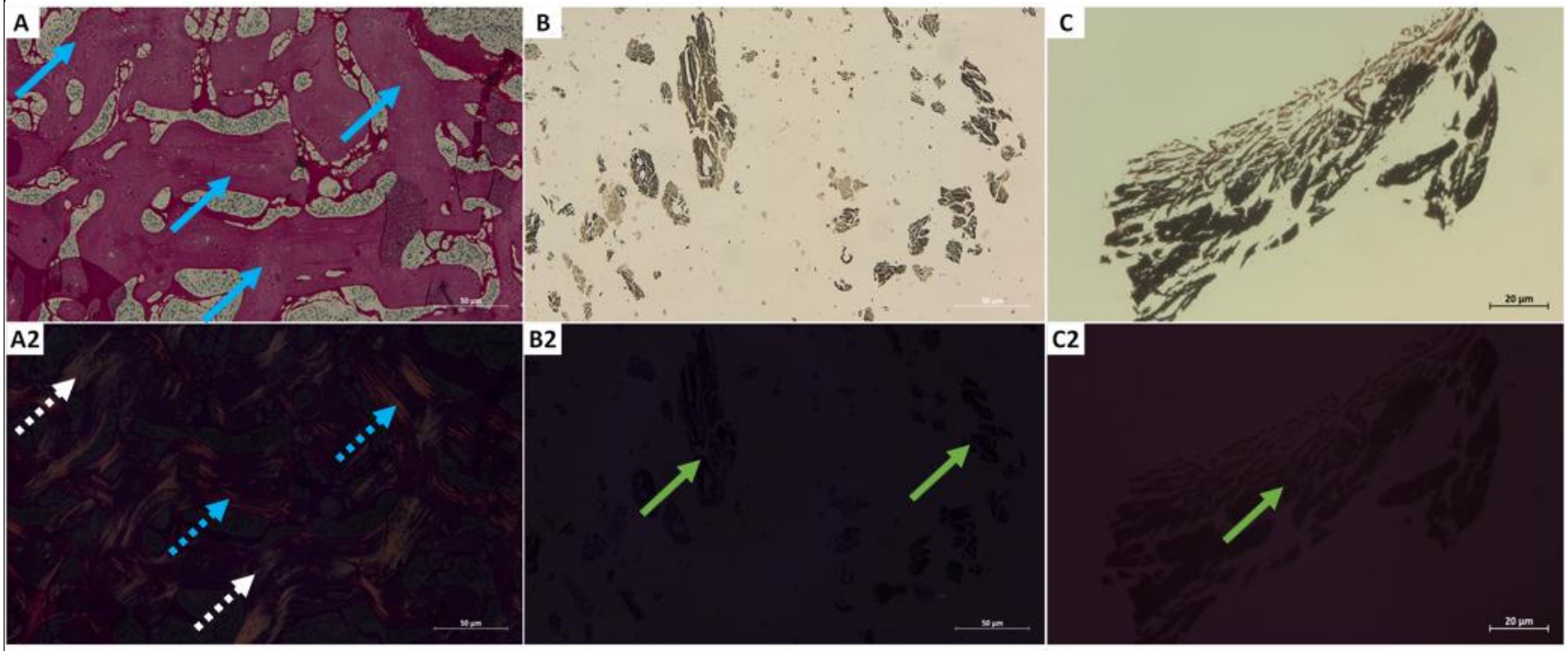


Figure **3.3.3.4: Representative photomicrographs showing the Sirius Red – Fast Green staining of decalcified sections from wet and dry bones cremated at different temperatures.**

A)-C): Photomicrographs of stained sections under light microscopy. **A2)-C2)**: Sections under polarised light microscopy. Photomicrographs showing **A)** and (B) wet bone cremated at 300°C and **B)** at 400°C, and **C)** dry bone cremated at 400°C. **A)** shows different areas of the bone staining red (solid blue arrow) with different birefringence colours, yellow (dashed white arrow) and red-pink (dashed blue arrow). **B)** and **C)** sections lifted off during staining and the remnants did not stain (solid green arrow) or show birefringence. Photomicrographs were taken at 5x magnification with 50µm scale bar.

3.3.4. Micro-fracture assessment

Descriptive qualitative histological micro-fracturing assessment of ground bone sections prepared as per Section 2.8.3 was also conducted. In brief, ground bone sections obtained from bones in all taphonomic conditions showed discernible osteon and plexiform structures coexisted in most of the bone sections, with osteons appearing as concentric lamellae around a canal (Figure 3.3.4.1. A, B, and F) and plexiform appearing as brick-like layering of the bone tissue (Figure 3.3.4.1. A and D). The vascular canals were found across the bone tissue extending in both osteons and plexiform structures (Figure 3.3.4.1. A and D). As the temperature increased, micro-fractures began to appear. Micro-fractures were similar in appearance to vascular canals, and thus caution in identification was noted (Figure 3.3.4.1. B and G). As temperature increased, bone tissue began to change in colour (Figure 3.3.4.1. A, D and G) appearing brown at lower cremation temperatures (Figure 3.3.4.1. B), and brown-black at higher temperatures (Figure 3.3.4.1. H). As the temperature increased, the colour intensity increased and covered more bone tissue (Figure 3.3.4.1. D-F) thus making the morphology and micro-fracture patterns less visible (Figure 3.3.4.1. G-I). Most of the tissue on the sections of wet and dry bones at higher temperatures were lost during ground bone section preparation (Figure 3.3.4.1. H-I) thus, further limiting the visibility of the sections in addition to black colouration.

These limitations are identified as caveats for assessing the extent of micro-fracturing, described as absent, low, moderate, or high (Table 2.8.4). Sections obtained from wet and dry control bones had a high frequency of sections with no micro-fractures, although some sections presented with few microfractures (low extent of micro-fracturing) (Figure 3.3.4.2). Exposure to furnace temperatures showed an increase in the extent of micro-fracturing observed.

The majority of ground bone sections obtained from fleshed bones cremated at 300°C presented with no or low extent of micro-fracturing. As the temperature increased, more sections from fleshed bones started showing micro-fracturing. Specifically, a greater number of sections presented with low -moderate micro-fracturing (400°C), and at 500°C, a few sections also showed evidence of a high extent of micro-fracturing (Figure 3.3.4.2). This suggests a temperature-dependent pattern of micro-fracturing.

When assessing other taphonomic conditions, the majority of ground sections obtained from wet bones even at 300°C, contrastingly presented with high extent of fracturing, with the frequency of

low and moderate micro-fracturing evident. At 400°C, there was an equivalent frequency of moderate and high fracturing evident, with an increase in temperature to 500°C showing only an increase in the frequency of sections with a high extent of micro-fracturing present (Figure 3.3.4.2). Dry bones followed a similar trend to wet bones (an increase in the presence of moderate and high extent of fracturing); however, in dry bones there was more high fracturing at 400°C than at 500°C (Figure 3.3.4.2). The results indicate that the extent of micro-fracturing observed was influenced not only by the temperature, but also by the taphonomic condition of the bone, with flesh perhaps having a protective effect.

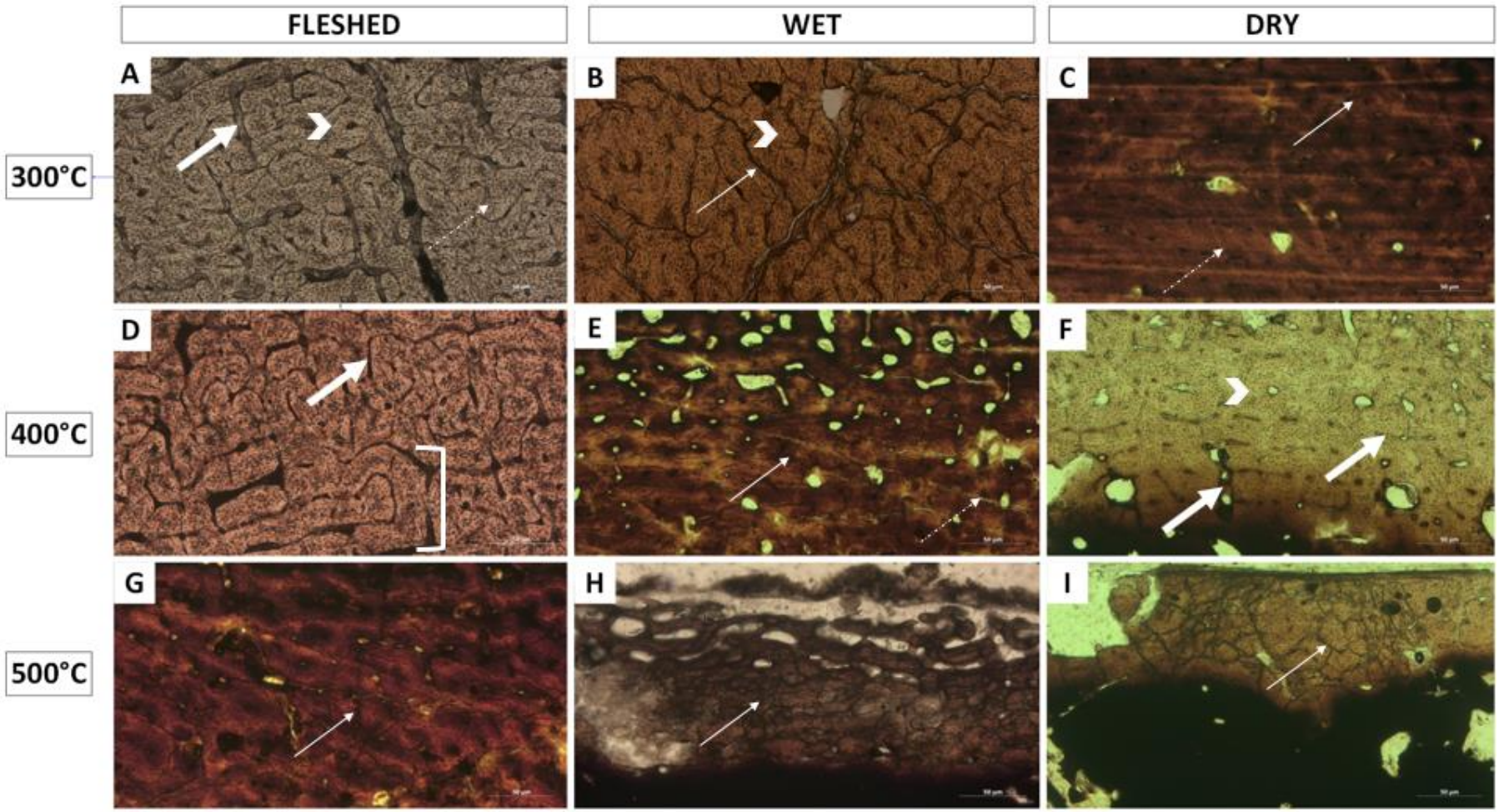


Figure 3.3.4.1: Representative photomicrographs of ground bone sections at different temperatures and taphonomic conditions showing micro-fracturing.

Images represent fleshed, wet and dry bone conditions by column arrangement and different temperatures (300°C, 400°C and 500°C) by rows arrangement. The images show vascular canals (thick arrows) extending from the osteons (arrowheads) and plexiform structures (right bracket). the distinction between micro-fractures (thin arrows) and artefactual superficial scratches from ground bone preparation (thin dashed arrows) was visible in the images. Photomicrographs were taken at 5x magnification.

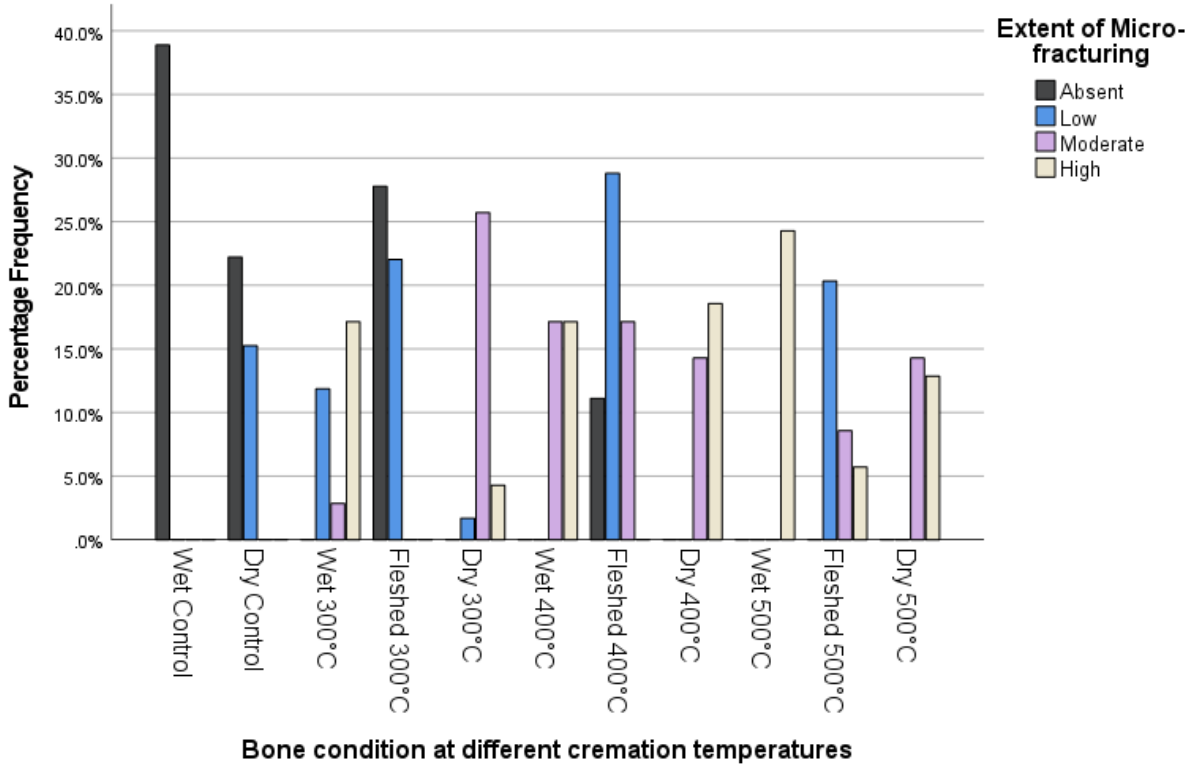


Figure 3.3.4.2: Graph showing the micro-fracturing extent on bones at different taphonomic condition cremated at different temperatures.
The graph indicates the percentage frequency of each category of micro-fracturing extent absent (black); low (blue); moderate (purple); high (beige) across bone sections from each taphonomic condition and cremation temperature. All sections categorised as absent micro-fracturing (black bars) total to 100%; all low extent of micro-fracturing sections (blue bars); all moderate micro-fracturing sections (purple bars) come to 100%; all high extent of micro-fracturing sections (beige bars) total 100%.

Chapter 4: Discussion

Fire as a result of heat can lead to burn injuries/fatalities, altering the critical morphological indicators used in forensic anthropometric analysis of sex, age, stature, and trauma and pathology interpretations. Hence, it is crucial for biological and forensic anthropologists to understand the macro and microstructural changes to the composition of bone and associated taphonomic conditions (fleshed, wet and dry) of the bone prior to heat exposure. Heating can result in macroscopic (colour, fracturing and warping) and microscopic (micro-fracturing, osteon size and bone matrix rearrangement) changes of bone (Imaizumi *et al.,* 2014; Gonçalves *et al*., 2015; Reidsma *et al*., 2016; Vassalo *et al*., 2016, 2019). Moreover, it is postulated that the underlying organic and inorganic molecular structure of bone plays a role in microscopic and macroscopic changes (Zioupos *et al*., 1998; Wang *et al*., 2001; Gonçalves *et al*., 2011; Horocholyn, 2013; Lambri *et al*., 2018; Marques *et al*., 2018). The results of the current closed-system study demonstrate an association between heat-induced colour changes in bone and cremation at different temperatures (300°C, 400°C and 500°C) across different taphonomic conditions (fleshed, wet and dry), whereas a larger extent of heat-induced fragmentation was associated with cremation but no direct significant difference was identified between the actual temperatures tested. Interestingly, mass loss was more strongly associated with higher cremation temperatures irrespective of bone taphonomic condition. There was a significant increase in total number of fractures when bones were exposed to greater temperatures (400°C and 500°C) across different taphonomic conditions, with dry bones showing significantly more macro-fracturing than wet and fleshed bones. Through qualitative analysis, the results showed that there was an increase in the macro-fracturing and extent of micro-fracturing as the temperature increased across different bone taphonomic conditions. Control tendon sections, rich in collagen, stained with Sirius Red- Fast Green (SRFG) and viewed under standard light microscopy showed red staining. In decalcified bone sections the red staining was variable, and the blue-green staining, indicative of non-collagenous proteins, more so. However, with the aid of polarised light, colours indicating both type I and type III collagen were identified even in sections cremated at higher temperatures (400°C and 500°C) obtained from fleshed bones, while sections from cremated wet and dry bones did not stain clearly, likely due to tissue carbon depositions.

4.1. Cremation trials in closed and open systems

Conducting representative actualistic experimentation to mimic cremation conditions of a real-world setting of fire affecting skeletal remains is difficult and different to accidental or natural occurring fires. Natural and accidental fires occur in an open system with no control of variables such as oxygen flow, duration and temperature of heat exposure. These factors mainly depend on where the fire occurs and how it started. The present study conducted cremation trials in a closed system using a muffle furnace thus limiting the amount of oxygen, maintaining a consistent temperature (Moore and Yamada, 1998), controlling heating rate, duration and direction of heating, during cremation. A closed system like this, while permitting control of the temperature to obtain repeatable data, may not accurately reflect realistic scenarios. This is particularly the case when considering that in these controlled trials combustion generally does not occur due to limited oxygen availability within the furnace (Raja *et al*., 2023). Certain studies conducted cremation trials in open systems attempted controlling some variables (oxygen flow) and mimicked certain settings (archaeological) (Carrolla and Smith, 2018) (modern) (Glazewski, 2006; Keough *et al*., 2015), while others did not control any variables and used realistic fuel samples (Glazewski, 2006; Keough *et al*., 2015). However, studies that conducted cremation trials in a closed systems using an oven (Reidsma *et al*., 2016) or furnaces (Shipman *et al*., 1984; Walker *et al*., 2008) also presented similar heat-induced changes. Each of these systems has its own limitations. In an open system, increase in wind speed increases the oxygen supply to the cremation process (Huang and Rein, 2017). Oxygen is crucial in starting and sustaining fire spread (Howell and Belmont, 2023; Raja *et al*., 2023). An increase in oxygen concentration results in more fuel molecules being able to oxidise, therefore accelerating the combustion reaction and enhancing complete combustion, while lower concentration of oxygen results in incomplete combustion (Raja *et al*., 2023). Increased oxygen concentration also increases thermal intensity, described as the total amount of energy radiated in a specific area during a fire (McGrattan *et al*., 2013), increasing peak cremation temperature (Raja *et al*., 2023). Hence the cremation trials conducted in an open system can easily reach temperatures above 800°C (Raja *et al*., 2023; Howell and Belmont, 2023). Closed systems allow for better control of unpredictable variables (e.g., oxygen and temperature fluctuations) in order to establish baseline data on the thermodynamic effects of bone and their biological implications, at the expense of mimicking real world settings. Without baseline data to understand what occurs in bone during heating, isolating which changes are caused by additional variables becomes impossible.

4.2. Bone heat transfer

When bone is exposed to heat, thermal energy is absorbed through heat transfer (Reidsma *et al*., 2016), hence, there is a slow increase in temperature when the bones are inserted inside the furnace during phase I. Thermocouple data allowed visualisation of how much heat can be absorbed by the bone (fleshed, wet and dry) at different temperatures. The short period of plateau on phase II that occurred reflected heat radiation transfer, as the bone material absorbs heat causing the bone temperature to increase (Braadbaart *et al*., 2007; Reidsma *et al*., 2016). During this plateau phase, there was balance in heating temperature due to bone absorbing and releasing heat at the same time (US Energy Information Administration, 2014). Lipids inside the bone marrow cavity, can serve as a source of fuel hence, the steep increase in bone temperature has been postulated to occur as a result of the rising temperature and melting and/or evaporating of lipids (Rendina-Ruedy and Rosen, 2020). In the current study's system a steep increase in temperature over shorter duration, phase III, was evident in dry bone, while wet bone required a greater time to reach similar temperatures and fleshed bone, with presumably more bone marrow, showed a gentler slope compared to both dry and wet bones. During the second plateau, phase IV, the temperature was constant due to the controlled furnace temperature and the bones matched the furnace temperature suggesting that it was releasing a similar amount of heat as it was receiving (US Energy Information Administration, 2014). We propose that marrow, fat (and flesh) takes time to heat explaining why the first phase of plateau in dry bones was short compared to wet and fleshed bones. Porcine marrow fat from the tibia has a melting point ranging between 30°C – 45°C (Morin *et al*., 2022). This temperature was exceeded during maceration of dry bones (55 °C for 24-48 hours), suggesting that dry bones would have little to no fat left in the marrow cavity.

However, dry bone temperature exceeded beyond the set furnace temperature during the second plateau phase and further increased towards the end of the cremation trial. If fat was acting as a fuel to rapidly increase temperature (Rendina-Ruedy *et al*., 2020) dry bones should have had the lowest temperature considering that fat content would be absent or reduced. Since fleshed bones were protected by soft tissue and an unaltered water content, potentially delaying the heating of fat, it is possible that they would have a lower temperature while the boiling point of water and soft tissues (including fats) was not yet reached (Holman, 2011; Su *et al*., 2020). This suggests that

the overlying soft tissue and water content protective effect play a bigger role than lipids melting and increasing heat transfer into the bone.

4.3. Heat-induced bone macroscopic changes and proposed associated microstructural mechanisms

4.3.1 Colour changes

The heat-induced colour change in all fleshed bones cremated at 300°C, 400°C and 500°C presented heat lines and heat borders with partial charring colour change. These results occurred due to diagenesis where heat alters the bone chemically and physically resulting in thermal decomposition of the organic materials of the bone (Book, 2014; Ellingham *et al*., 2015). Dehydration first occurs at temperatures between 25°C and 250°C where the water in the bone structure is lost (Ellingham *et al*., 2016) followed by water in between the hydrogen bonds holding the molecules that bind the crystalline structures together, as well as molecules that hold the collagen bonds together (Ellingham *et al*., 2016; Etok *et al*., 2007; Reidsma *et al*., 2016). This results in weakening of the molecular bonds as the hydrogen bonds stabilise the collagen molecules thus leading to triple helix structure collapsing (Bozec and Odlyha, 2011). Collagen is one of the most abundant proteins in the extracellular matrix and it is made up of triple helical structures held together by hydrogen bonds (Mandal, 2023; Exposito *et al*., 2002; Myllyharju, and Kivirikko, 2004). The helical structure is less susceptible to processes such as proteases compared to non-collagenous proteins (Franc *et al*., 1995; Wick *et al*., 2001), as non-collagenous proteins denature at temperatures between 40°C - 80°C (Ishiwatari *et al*., 2013) while the collagen begins to denature at temperatures between 120°C - 150°C (Wang *et al*., 2001; Lambri *et al*., 2018). As the cremation temperature increases reaching 236.85°C (510K), conformational changes of the collagen triple helix structure begin to occur (Lambri *et al*., 2018).

In bone, heat-induced changes such as shrinkage occurs as a result of the combination of losing collagen (Fredericks *et al*., 2015; Fredericks *et al*., 2012) and recrystallisation of hydroxyapatite which increases crystallinity (Fairgrieve, 2008; Fredericks *et al*., 2012). As fleshed bone is exposed to more heat, shrinkage and retraction of the tissue occurs thus exposing the bone surface to heat (Shipman *et al*., 1984; DeHaan, 2018). This results in the separation of tissue from shielding the

bone thus causing heat lines and heat borders formed clearly delineating between burnt and unburnt bone (Keough *et al*., 2015).

When bone is exposed to heat for longer periods, the dehydration of bone tissue further results in colour gradients (Symes *et al*., 2008; Reidsma *et al*., 2016). At 300°C, the chemical reactions begin to occur gradually changing the nature of the organic materials of the bone (Braadbaart *et al*., 2007). Thermal alterations occur faster at lower temperatures on wet and dry bones as heat transfer is no longer impeded by moisture and soft tissue presence. Hence, the degradation of the molecular bonds led to decomposition of the organic molecules at a faster rate (Keough *et al*., 2015). This is deposited on the surface of the bone, appearing as darkening of the bone to a black colour as the decomposed organic materials carbonise in an oxygen deprived environment, also known as charring process (Herrmann, 1970; Reidsma *et al*., 2016). Wet bones had similar bone composition as fleshed bones with the exception of the overlying soft tissue and underwent the same process of breaking fat and molecular bonds when exposed to heat compared to dry bones. Dry bones lost fat and moisture from maceration which altered how they responded to heat. Hence the dry bones cremated at 300°C presented with complete charring colour, as did the distal ends of fleshed bones that were exposed to heat due to retraction of soft tissues while wet bone mostly presented charring but with the presence of beige colour.

This charring process occurs at lower temperatures of heating that is followed by combustion of organic materials where the chemicals of the molecules begin to react as they are being heated (Reidsma *et al*., 2016; Marques *et al*., 2018). Further heating at 400 and 500°C resulted in different shades of colour such as brown, blue and grey as the carbon is beginning to deplete (Shipman *et al*., 1984; Correia, 1996) corresponding to the partial calcination and more charring seen on wet bones at those temperatures. More heat led to grey-white colour that is known as calcination, where the organic components are lost and the bone crystals fuse, (Shipman *et al*., 1984; Buikstra and Swegle, 1989) seen in dry bones cremated at 400°C and 500°C. However, there was no complete calcination because it usually occurs at higher temperatures (800°C), mostly in open system where carbon from organic materials is able to react with oxygen more freely (Correia, 1996).

The significant difference between colour and cremation temperature, as well as across different bone taphonomic conditions suggests that colour may be evident of heat-induced changes in

estimating the suspected cremation temperatures and the pre-burning conditions of the deceased (Shipman *et al*., 1984; Walker *et al*., 2008; Whyte, 2013; Keough *et al*., 2015; Reidsma *et al*., 2016). In addition, this method of heat-induced change in colour assessment was found to be repeatable as indicated by the good to excellent agreement in both inter and intra-observer. However, until further testing and refinement in real-world scenarios it cannot be used as a reliable factor as bone colour changes are known to be affected by a variety of factors including contact with materials surrounding the remains (clothing, metals such as bronze and zinc from the coffins having colours red, yellow and pink) (Gejvall, 1969; Lisowski, 1968; Corriea, 1996), duration of heat exposure, position of heat source, distance from the heat source, oxygen availability as well as the surrounding medium which influences the degree of combustion (Correia, 1996; Bennett, 1999; Walker & Miller, 2005; Imaizumi *et al*., 2014; Krap *et al*., 2017a).

4.3.2 Mass changes

The presence of soft tissue (skin, muscle, tendons and ligaments) covers and protects the bone from heat (Ellingham *et al*., 2016). As the soft tissue of the fleshed bones is exposed to more heat, the skin separates and burns quickly exposing the subcutaneous fat beneath (Ubelaker, 2009; Spitz *et al*., 2005; Ellingham *et al*., 2015). The fat acts as a good thermal insulator and good fuel which can sustain flaming combustion (Correia, 1996; Spitz *et al*., 2005; Ellingham *et al*., 2015). The thermal insulation of the soft tissue explains the slow increase in temperature in the beginning of the trial graph on figure 3.1.2.1 phase I followed by a steep increase in temperature as the fat has melted and evaporated in phase III.

As temperature increases, during the 400°C and 500°C fleshed bones cremation trials, a greater amount of soft tissue shrinks and retracts as tissues and components denature or undergo phase changes and are removed from the sample (lipids ≈ 30-45°C, water ≈ 100°C, myosin ≈ 180°C) (Agafonkina *et al*., 2019; Szpicer *et al*., 2023), thus the samples lost mass. Considering that even 300 °C are above the denaturation temperature of myosin (Agafonkina *et al*., 2019), this suggests that 30 minutes of heating at that temperature, may not be enough time to transfer enough heat into the sample to denature and reduce protein in the overlying soft tissues in order for the heat to have an effect on the underlying bone. This process explains the significant increase in mass loss as temperature increases, specifically between bones cremated at 300°C and 500°C. The wet and dry

bones are covered with minimal to no presence of soft tissue resulting faster and greater thermal alteration than fleshed bones covered with more soft tissues (Symes *et al*., 2013). This faster heat transfer occurs as a result of the dehydration process occurring quicker in bones with less moisture and earlier in the stages of burning. Although there was no significant difference in mass loss across different bone conditions, the presence of soft tissue has been found to have a significant impact on heat-induced changes of the bone matrix at both lower (< 300°C) and higher (> 800°C) temperatures (Ellingham *et al*., 2016). Due to minimal covering of soft tissue on the wet and dry bones, there was less total mass difference compared to fleshed bones. Furthermore, the cremated dry bones experienced the least mass difference due to being macerated which resulted in loss of fat and water that was initially present in the bone before maceration (Triaca *et al*., 2022). However, mass loss percentage was associated to temperature, suggesting that temperature overall played a bigger part in the ratio of mass lost, irrespective of initial sample mass.

4.3.3 Fragmentation and fracturing

The relationship between a force and deformation (warping) is one of the main primary principles in understanding bone fracture mechanics (Christensen *et al*., 2022). Different materials are arranged based on ability to deform and absorb energy (Christensen *et al*., 2022). Bone is made up of brittle material, which is the bioapatite mineral, a biologically composed variant of hydroxyapatite, and collagen with acts as a ductile material thereby balancing brittleness with the needs for overall strength (Christensen *et al*., 2022). The material's reaction to loading force is visualised as loading-deformation curve, which is a function of stress and strain, where stress is the load per unit area and strain is the change in dimension of the loaded body while the slope represents elastic modulus (Christensen *et al*., 2022 Martin *et al*., 1998). The load and deformation are proportional for materials such as bone until it reaches a yielding point, where plastic or permanent deformation occurs (Christensen *et al*., 2022). However, heat alteration in hydroxyapatite crystals affect the change in shape and size of the bone which further affects the stress and strain (Waterhouse, 2013; Symes *et al*., 2008; Correia, 1996; Thompson, 2005). In addition, dehydration as a result of heating results in decreased bone toughness due to loss of water in the collagen, and the loss of water is also associated with bone mineral which decreases both the bone strength and toughness (Nyman *et al*., 2006). This is notwithstanding heats effects on the molecular parameters of bone, including reduction in water content and the breakdown of collagen

fibres which in turn (Nyman *et al*., 2006) causes substantive changes in the bone's capacity to respond to stress and strain (Correia, 1996; Christensen *et al*., 2022).

In a pig study, juvenile bones have more trabecular bone (low compact bone density) and a greater amount of organic material (e.g., collagen) compared to mature adult bones which could alter how bone responds to heat (Waterhouse, 2013). Juveniles would require longitudinal growth as well as growth in mass over time, rates of which vary in different skeletal elements. This growth is reflected as greater cellular activity and matrix remodelling in juvenile bone, under the effects of growth hormone (Bachrach, 2005; Kawai and Rosen, 2012; Stagi *et al*., 2013). In the present study, decalcified sections stained with H&E, showed the presence of intense eosinophilic on the resorption pits between the osteon systems and the lamellae surrounding the vascular canals in the plexiform bone, as result of the cellular activity reflecting the high turnover of bone development in comparison to other artiodactyls (Martiniaková *et al.*, 2006a; Martiniaková *et al.*, 2006b). Bone fragility is affected by the loss of collagen, which occurs particularly in later adulthood, which reduces elasticity and thus the ability to withstand pressure as well as change in shape and size (Waterhouse, 2013). The high level of collagen content in juveniles provides more tolerance to elastic and plastic deformation resulting in better resistance to fragmentation (Waterhouse, 2013).

In the present study, the amount of fragmentation seen on wet and fleshed bones at higher temperatures (400°C and 500°C) suggests that there likely was heat-induced alteration of bioapatite and collagen. These microstructural thermochemical changes to the bone material would, hence, explain the fleshed and wet bones experiencing a greater extent of fragmentation with partial alignment and no alignment. The possible recrystallisation of hydroxylapatite at higher temperatures may have caused strengthening of the bone (Thompson, 2004). In addition, moisture loss and shrinkage continue after the bone has lost mass, even at higher temperatures, resulting in collagen becoming stiffer (Nyman *et al*., 2006) thus making the bone to be harder, and therefore more brittle (Imaizumi, 2015). This may have caused all dry bones cremated (300°C, 400°C and 500°C) to not deform to the same extent. Fragments that resulted tended to align when present, highlighting cremated dry bones becoming more brittle superficially, where most of the heat transfer would have occurred, resulting in a high number of delamination and patina (minimal superficial cracking) macro-fractures.

In comparison to humans, pigs are artiodactyls with shorter and thicker bones adapted for quadrupedal weight bearing (Arifakis *et al*., 2021). Long bone circumference scales isometrically with body mass meaning larger animals have more robust limb bones (Campione and Evans, 2012; Hutchinson, 2021). Therefore, the degree of bone warping and fragmentation are also affected by the body mass and locomotion, reflected in the bone architecture as insertions of collagen fibres, and the arrangement thereof. In the present study, it is thus possible that these factors of porcine bone led to the lack of identified warping. However, warping has been primarily seen in human bones cremated at temperatures exceeding 800°C (Castillo *et al*., 2013; Vassalo *et al*., 2019), a temperature not tested or reached by the experimental samples in the current study. As warping and shape changes have been observed to alter interpretation of forensic anthropological techniques such as age, sex and stature (Corriea, 1996; Gonçalves *et al*., 2011, 2015; Vassalo *et al*., 2019), it is noteworthy that at lower cremation temperatures, standards and techniques used in forensic anthropology may not be as affected.

A material's ability to absorb energy, also known as toughness, is an important bone biomechanical property, that depends on tensile strength (Nyman *et al*., 2006; Christensen *et al*., 2022) and ductility that permits resistance to fracturing (Christensen *et al*., 2022). In the present study it is postulated that macro-fractures and micro-fractures increased as the cremation temperature increased, since bone moisture was lost, resulting in collagen stiffens, thereby reducing the tensile strength and ductility, effectively decreasing the bone toughness (Nyman *et al*., 2006). The number of macro-fractures across different taphonomic conditions increased as the cremation temperature increased (Table 3.2.4.1). The high number of delamination and patina macro-fractures points to these fractures being associated with dry bones in the current study. This is in agreement with Reidsma *et al.* (2016) findings that bones that are in early to complete skeletonization undergo the same type of fracturing when heated. This further explains why on fleshed bones, the delamination and patina macro-fractures appear at 400°C as a result of shrinkage and soft tissue retraction exposing the bone surface. There were more delamination and patina fractures on dry and wet bones indicating that the bones were skeletonized and brittle, due to dehydration and increased crystallisation causing the bone surface cracks (patina) and cortical layers to flake off (delamination) (Symes *et al*., 2008; Işcan and Steyn, 2013). Additionally, both the delamination and patina fractures occurred on all sides (anterior, lateral, posterior and medial) supporting that the whole sample had skeletonised evenly. The prominent presence of delamination fractures on

wet and dry bones early at lower temperatures is suggested to be due to dehydration occurring early in the cremation process.

Curvilinear macro-fractures, also known as thumbnail fractures, were only present on fleshed bones specifically on the lateral and medial sides. The lateral side of tibia, specifically the extensor groove, has multiple muscle attachment sites that contain collagen fibres inserting into to the bone while the medial side has no muscle attachments. This shows that the macro-fracturing, specifically curvilinear, does not only occur due to muscle attachments, as has been proposed in biological anthropology studies (Baby, 1954; Binford, 1963; Symes *et al*., 2008). Curvilinear fractures have been associated with the preservation and contraction of collagen-apatite bonds at the enthesis (Zioupos *et al*., 1999; Gonçalves *et al*., 2011, 2015; Vassalo *et al*., 2016), a complex interface at which tissue microstructure alters to permit the transfer of forces to the bone itself. This tissue gradient considers the change from organic, unmineralized connective tissue to mineralised bone matrix. In the present study, fleshed bone was protected by soft tissue while, wet and dry bones were directly exposed to heat thus collagen-apatite bonds were less protected, and thus potentially broken at lower temperatures, through heat and dehydration (Bartsiokas, 2000; Gonçalves *et al*., 2011). The fact that these fractures did not appear on the posterior aspect of the bones, that has more pronounced muscle attachment sites, may suggest that muscle attachments in themselves may not be the only factor involved in curvilinear fractures formation.

Longitudinal fractures are thought to occur along the longitudinal axis very early in the heating process in dry (macerated) bone (Varvares, 2016). In the present study, longitudinal fractures were found on all sides of the wet and dry tibia but mostly on the non-muscle attachment sides (medial and anterior). On the fleshed bones, most longitudinal fractures were at 500°C while there were no fractures at 300°C and at 400°C, only two longitudinal fractures were present on the distal metaphysis of the medial side. Transverse fractures have been found to occur late in the cremation stage or during cooling stage where the soft tissue has been retracted (Varvares, 2016), in the present study they were found on wet and dry bones but not on fleshed bones.

Fractures propagate along weak interfaces (a point where two systems or objects meet) providing low energy path of fracturing (Hull, 1999). While lamellar bone is tough, by virtue of the arrangement of the bone matrix, collagen fibres and mineralisation, this is also balanced by the

need as a dynamic tissue to contain a distinct blood supply (Ross and Pawlina 2016; Sanz *et al*., 2023). Specifically, in lamellar compact bone, collagen fibres are arranged circumferentially around the periphery of the bone (Ross and Pawlina 2016), with more intricate arrangements around osteons (Sanz *et al*., 2023). In cross-section this appears as a circular arrangement around the canal and moving into the interstitium the fibres also run longitudinally and obliquely (Ross and Pawlina 2016). It has been proposed that such varied arrangements permit collagen to respond to the forces generated by load (i.e., tension, compression and shear forces), in different planes (Leng *et al*., 2013; Sanz *et al*., 2023). Elastic modulus and yield strength are also affected by fibre orientation and may thus explain, why most fractures propagate longitudinally instead of transversely (Pope and Outwater, 1972; Morgan *et al*., 2018) resulting in more longitudinal fractures compared to transverse fractures. The presence of less transverse fractures would explain why there were less step fractures (a combination of transverse fractures extending between two longitudinal fractures) (Symes *et al*., 2008). The stronger interfaces in the transverse plane and the deviation of force longitudinally (Christensen *et al*., 2022) likely resulted in less transverse fractures and therefore less step fractures.

Overall, most fractures were found on the anterior side, followed by posterior and medial with lateral side having the least number of macro-fractures. It is suggested that the lateral side of the bone in this study is more protected from fracturing, due to the muscle attachment sites and therefore the enthesis (Ross and Pawlina, 2006), the structure of which is specific to transmitting load. The anteromedial side of the bone used in this study, is a non-muscle attachment region and least protected making it easily exposed to heat and subsequently macro-fractures. In addition, in the current experimental set-up, the furnace heating elements are located on the sides and at a higher placement than the sample within the furnace, as such the heat would emanate towards the bone from these locations affecting the anterior aspects of the bone more (placed facing the ceiling of the furnace), with an expected greater exposure to direct heat.

The development of both macro and micro-fracturing in bone are less understood. However, other biological material such as teeth and geological material (soil sediments, rocks and coal) show similar patterns of micro-fractures (Boskey, 2007; Saiang and Miskovsky, 2012; Siratovich *et al*., 2013). All these biological materials contain bioapatite and semi-crystalline structures which are made up of different materials, including geological materials (soil sediments, rocks and coal), and

they all react similarly to heat providing a better understanding on how heat-induced micro-fractures are formed.

Bones and teeth are both made up of similar bioapatite and extracellular matrix proteins (Boskey, 2007). Bioapatite is carbonated hydroxyapatite and consist of calcium phosphate nanocrystals formed in spaces between collagen (Vallet-Regi and Navarrete, 2015) The physical and chemical properties of teeth and bone bioapatite crystals are slightly similar to those found in geological hydroxyapatite (de Jong, 1926; Reidsma *et al*., 2016). One of the main differences between these materials is that, in bone (remodelling is done by cellular activity while geologic hydroxyapatite is modified by physiochemical processes such as dissolution, precipitation and incorporation of foreign ions (Boskey, 2007). When these materials (such as rock and coal) are exposed to heat, they also undergo dehydration where water loss occur between crystals which decreases the strength of the minerals by breaking the covalent bonds (Boskey, 2007; Saiang and Miskovsky, 2012). This has similarly been seen in bone, where as a result of thermal expansion, collagen fibrils are denatured in bone (Bozec and Odlyha, 2011), affecting the mechanical behaviour reducing the strength and increasing stiffness therefore leading to micro-fracturing.

The present study showed that there were more macro and micro-fractures as the cremation temperature increased which was a consistent pattern throughout different bone taphonomic conditions. The increase in micro-fracturing extent is postulated to be due to the development of more and larger microfractures which increased the porosity within bone and decreasing the matrix density (Siratovich *et al*., 2013), as well as the increase in oxidation processes that occur at higher temperatures (Kus and Misz-Kennan, 2017). These micro-fracturing process can be equated to studies done on geological materials, despite the lack of specific criteria for defining different types of micro-fractures. In teeth, micro-fractures were identified by length, width, range and depth (Dumbryte *et al*., 2022) while in coal they were identified as micro-fissures that had a width of < 1 µm and microcracks which had a width of > 1µm (Kus and Misz-Kennan, 2017).

In bone research, there was a recent study by Bacci *et al*. (2021) that defined and provided clear descriptions on different type of micro-fractures, which were modified from Brain (1991). The study defined the fractures as interstitial, circumferential, irregular circumferential, radiating and irregular fractures which had specific descriptions on how to identify each fracture. Moreover, the

study was conducted on adult human bones that were treated with high impulse current mimicking lightning impact on bone. The bones were not damaged, to the extent that the present study did, by the impulse current nor did the samples have the same level of damage to the microstructure, making it easier to visualize the different types of micro-fractures; however, the interobserver repeatability of the study was low, indicating the difficulty in identifying and classifying micro-fractures. This method of micro-fracture analysis was initially applied to this study but porcine bones firstly, have a different histological organisation to human bone (Horochlyn, 2013; Brits *et al*., 2014) and when heated presented complex networks of micro-fractures which made identifying each micro-fracture type reliably, difficult. Hence, using this method of micro-fracture analysis (Bacci *et al*., 2021, derived from Brain, 1991) led to good inter-observer but poor intra-observer agreement in heat-induced bone (Appendix I3). Since this method could not be applied on a burnt bone analysis, the current study used a broader approach of rating the extent of micro-fracturing instead which had a moderate to good repeatability rate. As a result, this micro-fracturing extent approach, may be more applicable in forensic anthropology when conducting analyses of more destructive contexts, such as with burnt remains, than more specific methods like the one used by Bacci and colleagues (2021). However, more testing is required at greater variations of heating temperatures to ensure relationships between micro-fracturing extent and cremation temperature.

The fracture patterns observed in our study showed that some micro-fractures were radiating through vascular canals separating the bone tissue while other micro-fractures were propagating from the vascular canals to the interstitial lamellae. It is proposed that the presence of plexiform structures and vascular canals have an effect on the propagation patterns of micro-fracturing, which is different in humans as they do not possess plexiform structures (Horocholyn, 2013; Brits *et al*., 2014). Despite that, the current study's results highlight the importance of microstructure to fracture propagation. The present study showed that the fleshed bones cremated at 300°C and 400°C, from both muscle and non-muscle attachment sites, had little to no micro-fractures, and this is suggested to be due to being protected by soft tissues, including the muscle, periosteal tissues or tendons. However, the retraction of soft tissue at higher temperatures (500°C) led to direct exposure of the diaphysis and distal metaphysis to heat, resulting in moderate to high extent of micro-fracturing on non-muscle attachment sites (midshaft). The bone blocks extracted from non-muscle attachment sites (medial side) presented a higher level of micro-fracturing compared to

bone blocks extracted from muscle attachment site. This relationship was observed across all bone taphonomic conditions (fleshed, wet and dry bones), suggesting that once a threshold of heat is absorbed by the bone, moisture and other protective factors are eliminated, bone responds similarly irrespective of location. This could justify why moderate to high micro-fracturing was seen in wet bones cremated at 300°C, and a further increase to moderate-high and high micro-fracturing at 400°C and 500°C, respectively. The resistance to micro-fracturing is determined by covalent and ionic bonds between molecules (Domanski and Webb, 1992), and the resulting change in mechanical behaviour dependent on different temperatures (Saiang and Miskovsky, 2012). The general relationship of micro-fractures showed that the extent of micro-fracturing increased with increasing temperature. This relationship is also seen in wet and dry bones cremated at 400°C and 500°C which had moderate to high extent of micro-fractures.

Bone colour at the histological scale also changes as the organic components of the bone are being decomposed (Hanson and Cain, 2007). The bone appeared brown at lower temperatures (300°C) in wet bones then as the temperature increased (400°C and 500°C), they turned brown-black, while the dry bones at 300°C began by changing to brown-black. Some areas of the wet bones at 400°C, and dry bones at both 400°C and 500°C had turned completely black while the rest of the area on wet bone sections remained brown-black and the dry bone sections became pale. The fleshed bone sections at 300°C had no change in colour while the 400°C bone sections began to have shades of brown colours and the entire area of the sections at 500°C were brown-black. The presence of soft tissue appeared to have a strong effect in protecting the bone tissue from carbonisation as the presence of brown carbonisation only appeared at 400°C, with less intensity and brown-black at 500°C. These change in colours are specifically associated with heat exposure specifically, indicated by carbon deposition on the bone surface. Although other forms of taphonomy such as weathering may also induce diagenesis on bone, carbonisation of microstructure is specific to heat-induced changes (Brain, 1993; Hanson and Cain, 2007). The extent of carbonisation has been found to have an impact on the ability to visualise the bone tissue morphology and heat-induced micro-fracturing and change in osteon dimensions (Brain, 1993; Hanson and Cain, 2007; Horocholyn, 2013). Unlike these studies which identified different arrays of colour changes at a histological level (from tan, to red, to brown and black) (Brain, 1993; Hanson and Cain, 2007; Horocholyn, 2013), the only colours identified in the present study included brown, black and pale. However, these studies were conducted in an open system (e.g., campfire) with small sample sizes

(Hanson and Cain, 2007; Horocholyn, 2013) or from observations of archaeological sites (Brain, 1993) and not representative of the multiple variables that could have affected their findings. In Hanson and Cain (2007) brown and black were primarily seen in greasy and non-greasy bone burned between ≈480 and ≈620 °C, which roughly correspond to the higher temperatures where wet and dry bone of the current study found these colours. In the present study, some of the unburnt dry bone blocks were scored to have low extent of micro-fracturing meaning that there were few individual fractures observed. The process firstly of removing the bone block with a Dremel and then ground bone preparation on carborundum paper might have caused the control dry unburnt bones to develop micro-fractures. It has been found that drilling rotational speed can cause thermal impact (Davidson, 1999). Micro-fracturing, likely as a result of the ground bone preparation, was also found in another study in potentially pathologically weakened but experimentally untreated bone (Bacci, *et al*., 2021). It is thus a possibility that processing of samples may compounded the fractures present on the burnt bone sections.

Sections of burnt bone were also decalcified and stained with H&E and the SRFG stain to identify the general architecture and assess collagen changes during cremation. Collagen is a tropocollagen molecules consisting of triple helix of polypeptides (Zioupos *et al*., 1999; Lambri *et al*., 2018) which are stabilised by hydrogen bonds (Zioupos *et al*., 1999). The triple helical structure forms the fibrils which are arranged to form collagen fibres (Bozec and Odlyha, 2011), in which carbonated apatite crystals are embedded during the process of mineralisation (Mano, 2005; Lau *et al*., 2013; Lambri *et al*., 2016). Collagen consists of crosslinks which are produced by maturation of intermolecular bonds of the tropocollagen molecules (Eyre *et al*., 1988; Zioupos *et al*., 1999). These crosslinks can be affected by factors such as age and heat exposure (Zioupos *et al*., 1999). Collagen molecules are rich in amino acids which strongly react with acidic dyes such as Sirius Red (Montes *et al*. 1984; Montes and Junqueira 1991; Gopinathan *et al*., 2020).

Picrosirius red is an elongated molecule that has anisotropic organization that binds along the great collagen fibres axis via acidic sulfonic groups, enhancing the birefringence under polarized light (Lattouf *et al*., 2014; Gopinathan *et al*., 2020). Birefringence occurs in anisotropic structures as a measure of the difference of refractive indices that result from a beam of light splitting into two (Caamaño *et al*., 2010; Rittié, 2017; Liu *et al*., 2020). There are different colours that birefringe where yellowish orange represents thick collagen type I (Montes and Junqueira,1991; Hirshberg

et al., 1999; Allon *et al*., 2006) while green to greenish yellow represents collagen type III (Hirshberg *et al*., 1999; Allon *et al*., 2006). Other studies suggested that the birefringence is affected by the thickness and arrangement of collagen fibres (Pierard, 1989; Dayan *et al*., 1989; Rich and Whittaker, 2005; Coleman, 2011) where the loosely packed arrangement birefringe green-greenish to yellowish while the tightly packed fibres birefringe orange-red (Lattouf *et al*., 2014; Lambri *et al*., 2018; Liu *et al*., 2021). These colours are present under polarized light due to fibre size, alignment and packing, cross linking of fibres, interstitial ground substance and water content (Gopinathan *et al*., 2020). However, this study showed some inconsistencies of the SRFG staining under light microscopy where some areas of tendon fibres stained green. Tendon which contains type I and III collagen (López De Padilla *et al*., 2021), was used as a positive control to assess SRFG staining. Tendon stained red with SRFG but green staining was also evident, indicating other matrix proteins such as proteoglycans, proteases, and other proteins involved in cross-linking, were also present (Nielsen *et al*., 1997), albeit in greater proportions than expected (López De Padilla *et al*., 2021. SFRG staining of muscle as the negative control stained green where the contractile proteins were expected to be seen, while the connective sheaths that are made up of collagen fibres stain red as expected (Houghton *et al*., 1996).

Bone contains primarily collagen type I (90%) and smaller amounts of collagen Type III, V, XI and XIII (Ross and Pawlina, 2006). The SFRG stain stained the interstitial lamella and the osteons primarily red, with green staining, indicative of non-collagenous proteins evident particularly around the osteons. Non-collagenous proteins (such as calcium-binding proteins, multiadhesive glycoproteins) are secreted by osteoblasts, along with collagen, as the bone is being laid down and calcifying (Ross and Pawlina, 2006). However, the birefringence was difficult to visualise, with the amount of collagen and non-collagenous proteins variable between samples. Visualisation of collagen birefringence is also dependent on the plane in which the sections are taken (Liu *et al*., 2021).

Moreover, in normal brightfield microscopy, there was little to no presence of green staining on cremated bones stained with SRFG, which may be because of non-collagenous proteins denaturing at temperatures between 40°C – 80°C (Ishiwatari *et al*., 2013) while collagen, due to its triple helical structure and cross-linkage with fibrils (Zioupos *et al*., 1999), begins to denature at temperatures between 120°C – 150°C (Wang *et al*., 2001; Lambri *et al*., 2018). Notably, sections

obtained from dry bones cremated 300°C – 500°C, where collagen was expected to have denatured still stained with SRFG, as visualised under bright-field microscopy. This may be because SFRG is still capable of binding to amino acids within peptides, despite the degradation of the fibres. While it can be suggested that SRFG staining could also be due to some small amount of collagen being still present and in a good condition at lower temperatures, the intensity of the red staining is indicative of high levels of collagen arrangement and thickness (Dayan *et al*., 1989). At 400°C and 500°C; however, the matrix constituents birefringed more yellow as opposed to red. This may be due to collagen degrading as conformational changes had occurred at 236.85°C (Lambri *et al*., 2018) thus altering the arrangement of collagen which results in weak birefringence that may also birefringe greenish in colour (Lattouf *et al*., 2014). The weak birefringence has been explained by immature type III collagen fibres which are arranged in a disorderly manner thus causing decreased anisotropy (Puchtler *et al*., 1973). Meanwhile, most of the wet and dry bone sections were lost during the staining process but those that had remnants did not pick up the stain. This is possibly due to the complete charring of the sections, where sections appeared black, or the resulting change in ion composition, reflecting an inability to bind to the dye. Overall, we suggest that these inconsistencies in the bone SRFG staining may be because of the picrosirius red stain binds to amino acids (Montes *et al*., 1984; Montes and Junqueira, 1991) that may be part of peptides in denatured collagen, and which may also be present in non-collagenous proteins. This postulation is supported by a study where they also found Sirius Red staining proteins other than collagen (Puchtler *et al*., 1988; Nielsenl *et al*., 2009). Nielsen *et al*. (2009) suggested that the presence of molecules other than collagen should be considered when using picrosirius red for quantification of collagen. The histological finds of the present study highlight the importance of visualising the SRFG stain, without which quantification alone may overestimate the integrity of the collagen present. It is suggested that picrosirius red stain should not be used to quantify the amount of collagen since it is not specific enough, but other avenues sought to identify and validate collagen denaturation.

Chapter 5: Conclusion - limitations and findings

This study used a controlled, closed-system setting to investigate the relationship between bone macroscopic and microscopic heat-induced changes on bones at different taphonomic conditions (fleshed, wet and dry) cremated at different temperatures (300°C, 400°C and 500°C).

This study does not have immediate translational value in forensic anthropology; however, we have identified a definitive lack of studies on the effects of temperature on bone fracture patterns that present experimental data that is repeatable. Moreover, few studies have tested the underlying mechanisms that may be responsible for these fracture patterns. This study provided a controlled setting, using porcine bone, and demonstrated that macroscopic and microscopic heat-induced changes were related to one another as well as the taphonomic conditions and heating temperatures. The use of thermocouple data allowed the tracking of temperature changes during the cremation process. The data obtained suggests a protective role of soft tissue regarding heat transfer during bone burning and that the profile of heat-induced change may deviate, notably, based on the composition of cremated remains. Factors such as bone mineral composition, lipid and water content also have an effect on how heat is transferred which was seen as decreased damage suggestive of decreased heat transfer in fleshed bones. These postulations require further experimentation for validation. This study's implications for cremain analysis and further research specifically relate to the awareness and understanding of the complex and understudied biomechanic and histochemical changes that bone undergoes during heating.

5.1. Limitations

The use of porcine bone is a limitation to translational studies due to differences in bone maturity, composition, morphology (macroscopic and microscopic) and locomotory behaviour. Pigs are artiodactyls walking on their distal phalanges while humans are plantigrades, weight bearing on their entire foot. The difference in locomotion affects the morphology of the bone and muscle attachments that likely lead to different arrangement of collagen. This will therefore affect how heat-induced changes in collagen may result in different types, and propagation of fractures. In addition, the presence of vascular canals and plexiform arrangement of bone might influence both micro-fracture and micro-fracture distribution throughout the bone, which might be different in

humans with primarily osteonic bone. Nevertheless, the present study has provided an avenue to understand fracture pattens and heat-induced changes by creating an experimental system that can later incorporate the use of human bone.

While a muffle furnace allowed for definitive temperature control and the use of thermocouples to track temperature changes in the bone, a limitation for the study included it short-circuiting when cremating bones at higher temperatures thus making high temperature (600 and 800 °C) trials non-viable. This furnace limitation led to a smaller experimental temperature range thus limiting the observation of heat-induced changes such as warping, colour, and fragmentation as some of these changes occur at a higher temperature (400°C and 500°C). Future studies could make use a larger well-insulated furnace that protects the heating elements from the samples. This will allow to increase the temperature range to study heat-induced changes in a closed system more holistically.

Sampling cremated bone also proved challenging. During extraction of blocks from bones cremated at higher temperatures using a Dremel resulted in separation of cortical bone layers and damaged extracted blocks, making sampling inconsistent and thus led to caution on interpretation of microscopic data. Future studies should attempt extracting bone blocks using an EXACT diamond bladed saw, employ resin embedding and undecalcified bone sectioning to prevent tissue damage from tissue processing. Ensuring that the resin-embedded bone sections adhere appropriately to microscopic slides would allow to better observe histological changes occurring at higher temperatures. Lastly, since SRFG was found not specific enough to collagen, future studies should investigate alternative methods of studying collagen content and type distribution, by utilising, for example higher magnification microscopy that can visualise collagen fibrils (e.g., scanning electron microscopy, atomic force microscopy) or immunohistochemistry techniques.

The repeatability results of both macrofracture and microfracture were affected by several factors including observer variability and fracture complexity. Despite the training provided, the observers were not experienced enough to accurately differentiate between each type of fracture which further became more interconnected and superimposed as the cremation temperature increased. Thus, hindering the ability to isolate and identify each fracture pattern. The study carried out a controlled cremation environment while forensic cases maybe be a result of uncontrolled environment which have higher temperatures and even more complex fractures. In addition, the irregular cutting of the distal end of the distal metaphysis could have contributed to being bias

during the assessment. It is suggested that future studies should focus more on classifying the rate at which fractures extend at different temperatures in different cremation conditions in a clear and concise manner.

5.2. Findings

From this study, the assessment of heat-induced changes such as colour change and fracturing (both macro and micro) can broadly provide baseline information in forensic anthropology or archaeology cases, in relation to soft tissue presence and cremation temperatures. This was seen by the presence of heat lines and heat borders on fleshed bones while the bone that was exposed to heat, as a result of tissue shrinkage and retraction at 400°C and 500°C, became completely charred. Meanwhile, the wet and dry bones that were not covered with soft tissue experienced these heat-induced changes (complete charring) at lower temperatures (300°C) as a result of dehydration and other process of diagenesis occurring at an earlier stage. This is further evidenced by the suggested protective effect of soft tissues identified at lower temperatures on most heat-induced changes (colour, fracturing, fragmentation). At higher temperatures, however, the soft tissues and moisture were lost, as shown by the mass loss percentage being associated to heating temperature across all bones, irrespective of condition. Once lost, greater heat transfer into the bone was allowed and a higher extent of damage from temperatures of 400°C - 500 °C. Hence bones cremated a higher temperature, would likely display more extensive heat-induced damage and changes, irrespective of soft tissue presence, provided enough heat transfer over the time occurred. Yet bones with soft tissues and moisture may demonstrate some changes in heat-induced change patterns as certain processes occur at different times in the burning process.

In addition, there were more macroscopic and microscopic fractures, with presence of carbonisation and less visibility of the tissue, on wet and dry bones compared to fleshed bones. An increase in fractures as temperature increased was also noted irrespective of bone taphonomic condition. Curvilinear fractures, although rare, were only seen on fleshed bones, on both muscle and non-muscle attachment site, suggesting that they are not dependent on the presence of soft tissue insertions as suggested in the scientific literature. Greater number of delamination and patina fractures at higher temperatures were found in all bone conditions. Transverse fractures and step fractures were not as prevalent. This is suggested to be due to the strong histological and structural

interface at the transverse plane, therefore resulting in fractures propagating through the longitudinal axis, as a less resistant path, potentially explaining the greater number of longitudinal fractures.

The tensile strength and ductile properties of collagen have been associated with the macroscopic changes to withstand pressure from warping and fragmenting as seen in dry bones where there were no misaligned fragments across all cremation temperatures. Dehydration that led to loss of water associated with collagen molecules further resulted in shrinkage and loss in bone matrix integrity and thus decreased the bone's ability to resist microstructural changes. The decreased ductility and increased fragility are suggested to be expected in cremated archaeological remains, if they were exposed to heat after significant viable collagen loss. Moreover, the presence of curvilinear fractures in fleshed bones supports the hypothesis of the preservation and gradual contraction of collagen; however, these were few and also found in association with sites that were not associated with enthesis, contrary to propositions by other studies. Moreover, in understanding the mechanisms of microstructural change, it has been identified in other studies that the breaking of the hydrogen bonds in collagen compromises its helical structure. In the present study, as the temperature increased and the complete chemical decomposition of collagen and other organic components occurred, visualisation of the bone histomorphology was negatively impacted. Moreover, while the SRFG stain under brightfield and polarised light microscopy showed collagen staining in positive controls (red), a significant amount of green was also evident, indicating staining of non-collagenous proteins. The decreased birefringence of the SRFG stain in higher temperature cremated samples is suggested to reflect the degradation of collagen. However, the birefringence while evident as more intense and larger areas of birefringence of greenish-yellow, and yellow-red colour as temperature increased, showed variation between samples. Given than non-collagenous proteins also birefringed green, the specificity of the SFRG stain in identifying collagen and collagen degradation remains to be established with additional techniques. Giving these concerns, the SFRG was not quantified using spectrophotometric analysis; however, it is suggested that both qualitative, spectrophotometric and other more targeted techniques to visualise and track collagen fibril degradation (such as scanning electron microscopy, atomic force microscopy or immunohistochemistry techniques to identify collagen and other bone matrix proteins), be explored to understand the mechanisms of collagen degradation on microstructural changes, and how these lead to macroscopic fractures. Such technical advances would permit a

greater understanding of heat-induced changes to bone that would ultimately assist in forensic anthropology.

REFERENCES

Adamus, A. (2001). Technical note: review of nitrogen as an inert gas in underground mines. *Journal of the Mine Ventilation Society of South Africa* 54(3), 60-61.

Aerssens, J., Boonen, S., Lowet, G. and Dequeker, J. (1998). Interspecies Differences in Bone Composition, Density, and Quality: Potential Implications for in Vivo Bone Research. *Endocrinology*, 139(2), 663-670.

Agafonkina, I. V., Korolev, I. A. and Sarantsev, T. A. (2019). The study of thermal Denaturation of beef, pork, chicken and turkey muscle proteins using diferential scanning calorimetry. *Theory Pract meat Process 4*(3), 19-23.

Alabdalall, A. H., Al-Anazi, N. A., Aldakheel, L. A., Fatma H., Amer, F. H. I., Aldakheel, F. A., Ababutain, I. M., Alghamdi,A. I. and Al-Khaldi, E. M. (2021). Application and characterization of crude fungal lipases used to degrade fat and oil wastes. *Scientifc Reports* 11, 19670.

Allon, I., Vered, M., Buchner, A. and Dayan, D. (2006). Stromal differences in salivary gland tumors of a common histopathogenesis but with different biological behavior: A study with picrosirius red and polarizing microscopy. *Acta Histochem*. 108(4), 259-64.

Altman, D. G. (1999). Practical statistics for medical research. New York, NY: Chapman & Hall, CRC Press.

Arifakis, D., Muraca, J., Singh, A. and Granatosky, M. C. (2021). 'Artiodactyla Locomotion', in Vonk, J. and Shackelford, T. K. (eds.), Encyclopedia of Animal Cognition and Behavior, Switzerland, *Springer Nature*, 1-9.

Baby, R. S. (1954). Hopewell cremation practices. In: Papers in Archaeology. Ohio Historical Society, Columbus, 1-7.

Bacci, N. (2016). Traumatic Effects of Lightning Strike on Human Bone Morphology and Ultrastructure. MSs thesis. University of the Witwatersrand, Johannesburg.

Bacci, N., Augustine, T. N., Hunt, H. G. P., Nixon, K. J., Hoffman, J., Bam, L., de Beer, F. and Randolph-Quinney, P. (2021). Harnessing Thor's Hammer: Experimentally

induced lightning trauma to human bone by high impulse current. *Forensic Science International: Synergy 3*, 100206.

Bachrach, L. K. (2005). Assessing bone health in children: who to test and what does it mean? *Pediatr Endocrinol Rev* 2(3), 332-336.

Bancroft, J. D and Layton, C. (2019). 'The hematoxylins and eosin', in Survana, S. K., Layton, C. and Bancroft, J. C. (8th ed.), *Bancroft's Theory and practice of histological techniques.* Oxford, Elsevier, 126-138.

Bartsiokas, A. (2000). The eye injury of King Philip II and the skeletal evidence from the Royal Tomb II at Vergina. *Science* 288(5465), 511-514.

Bennett, J. L. (1999). Thermal alteration of buried bone. *J. Archaeol. Sci*. 26(1), 1–8.

Binford, L. R. (1963). An analysis of cremations from three Michigan sites. *Wisconsin Archaeologist* 44(2), 98-110.

Boaks, A., Siwek, D. and Mortazavi, F. (2014). The temporal degradation of bone collagen: A histochemical approach. *Forensic Science International* 240, 104–110.

Book, G. (2014). Compendium of chemical terminology. International Union of Pure and Applied Chemistry, 528.

Boskey, J. A., Gokhale, A. L. and Robey, P. G. (2001). 'The biochemistry of bone', in Marcus, R., Feldman, D., Kelsey, J. (2nd ed.), *Osteoporosis*, California, Academic Press, 107-188.

Bozec, L., van der Heijden, G. and Horton, M. (2007). Collagen fibrils: nanoscale ropes. *Biophys. J.* 92, 70–75.

Bozec, L. and Odlyha, M. (2011). Thermal denaturation studies of collagen by microthermal analysis and atomic force microscopy. *Biophysical Journal* 101(1), 228-36.

Braadbaart, F., Wright, P. J., van der Horst, J. and Boon, J. J. (2007). A laboratory simulation of the carbonization of sunflower achenes and seeds. *J. Anal. Appl. Pyrolysis* 78, 316-327.

Brain, C. K. (1991). 'The occurrence of burnt bones at Swartkrans and their implications for the control of fire by early hominids', in Brain, C. K., Sillen, A. and Hoering, T. (ed), *Swartkrans: a cave's chronicle of early man*, Pretoria, South Africa, The Transvaal Museum 8, 229–235

Brits, D., Steyn, M. and L'Abbé, E. N. (2014). A histomorphological analysis of human and nonhuman femora. *International journal of legal medicine*, *128*, 369-377.

Brushlinsky, N., Sokolov, S. and Wagner, P. (2022). Center of Fire Statistics World Fire Statistics. Available online: https://www.ctif. org/sites/default/files/2022-08/CTIF_Report27_ESG.pdf (accessed on 5 January 2023).

Byers, S. N. (2004). 'Postmortem changes to bone', in Byers, S. N. (2nd ed.), *Introduction to Forensic Anthropology*, Boston, Pearson, 383-405.

Caamaño, J. N., Muñoz, M., Diez, C. and Gómez, E. (2010). Polarized light microscopy in mammalian oocytes. *Reprod Domest Anim*. 45, 49-56.

Campione, N. E. and Evans, D. C. (2012). A universal scaling relationship between body mass and proximal limb bone dimensions in quadrupedal terrestrial tetrapods. *BMC Biol.* 10, 1-22.

Carrolla, E. L. and Martin Smith, M. (2018). Burning questions: Investigations using field experimentation of different patterns of change to bone in accidental vs deliberate burning scenarios. *Journal of Archaeological Science: Reports* 20, 952-963.

Castillo, R. F., Ubelaker, D. H., Acosta, J. A. L., de la Rosa, R. J. E. and Garcia, I. G. (2013). Effects of Temperature on Bone Tissue: Histological Changes. *J Forensic Sci.* 58(3), 578-582.

Cho, Y. I., Ganic E. N., Hartnett, J. P. and Rohsenow, W. M. (1998). 'Basic concepts of heat transfer in Rohsenow', W. M., Hartnett, J. R. and Cho, Y. I, (3rd ed.), *Handbook of heat transfer*, New York, McGraw-Hill books, 1-37.

Coleman, R. (2011). Picrosirius red staining revisited. *Acta Histochem* 113, 231-233.

Correia, P. M. M. (1996). 'Fire modification of bone: a review of the literature', in Haglund, W. D. and Sorg, M. H. (ed.), *Forensic Taphonomy: The Postmortem Fate of Human Remains*, Boca Raton, CRC Press, 275-286.

Correia, P. M. M. and Beattie, O. A. (2002). 'Critical look at methods for recovering, evaluating, and interpreting cremated human remains', in Hagland, W. D. and Sorg, M. H. (ed.). *Advances in Forensic Taphonomy – Method, Theory, and Archaeological Perspectives*. Boca Raton, CRC Press, 435-450.

Christensen, A. M., Isa, M. I., Smith, M. A., Hefner, J. T., Berryman, H. E., Saginor, I. S. and Webb, J. B. (2022). A guide to forensic fractography of bone. https://doi.org/10.5281/zenodo.6013748

Currey, J. D. (1990). 'Biomechanics of mineralized skeletons', in Carter, J. G. (ed.), *Skeletal Biomineralization: Patterns, Processes and Evolutionary Trends*, Van Nostrand Reinhold, New York *5*, 11-25.

Currey, J. D. (2003). Role of collagen and other organics in the mechanical properties of bone, *Osteoporosis Int.* 14, 29-36.

Currey, J. D., Zioupos, P., Davies, P. and Casinos, A. (2001). Mechanical properties of nacre and highly mineralized bone. *Proc. R. Soc. Lond. B 268*(1462), 107-111.

Dayan, D., Hiss, Y., Hirshberg, A., Bubis, J. J. and Wolman, M. (1989). Are the polarization colors of picrosirius red-stained collagen determined only by the diameter of the fibers? *Histochemistry* 93, 27-29.

Davidson, S. R. H. (1999). Heat transfer in bone during drilling. MSc Thesis. University of Toronto. Canada.

DeHaan, J. D. (2007) 'Fire and Bodies', in Schmiot, C. W. & Symes, S. A. (ed), *The analysis of burned human remains*, California, Vallejo, 1-13.

DeHaan, J. D. (2018). Post-Mortem Repositioning of Human Bodies in Fires. *Int J Cri & For Sci*. 2(3), 62-78.

de Klerk, M. and de Villiers, C. (2012) The value relevance of corporate responsibility reporting: South African evidence. *Meditari Accountancy Research* 20(1), 21-38.

de Oliveira Coelho, J. P. (2015). Unwarping heated bones: A Quantitative Analysis of Heat-induced Skeletal Deformations Using 3D Geometric Morphometrics. MSc Thesis. Coimbra, Portugal: University of Coimbra.

de Jong, W. F. (1926). La substance minérale dans les os. *Recueil des Travaux Chimiques des Pays-Bas* 45(6), 445-449.

Dirkmaat, D. C. (2002). 'Recovery and interpretation of the fatal fire victim: the role of forensic anthropology', in Hagland, W. D. and Sorg, M. H. (eds), *Advances in Forensic Taphonomy – Method, Theory, and Archaeological Perspectives,* Boca Raton, CRC Press, 451-472.

Domanski, M. and Webb, J. A. (1992). Effect of Heat Treatment on Siliceous Rocks Used in Prehistoric Lithic Technology. *Journal of Archaeological Science* 19, 60l-614.

Dumbryte, I., Narbutis, D., Vailionis, A., Juodkazis, S. and Malinauskas, M. (2022). Revelation of microcracks as tooth structural element by X-ray tomography and machine learning. *Scientific reports* 12(1), 224-289.

Eckert, W. G., James, S. and Katchis, S. (1988). Investigation of Cremations and Severely Burned Bodies. *American Journal of Medicine and Pathology* 9, 188-200.

Ellingham, S. T. D., Thompson, T. J. U. and Islam, M. (2016). The effect of soft tissue on temperature estimation from burnt bone using fourier transform infrared spectroscopy. *J. Forensic Sci.* 61(1), 153-159.

Ellingham, S. T. D., Thompson, T. J. U., Islam, M. and Taylor, G. (2015). Estimating temperature exposure of burnt bone-A methodological review. *Science and Justice* 55, 181-188.

Emmons, H. W. (1986). The needed fire science. In *Fire Safety Science-Proceedings of the First International Symposium,* 33-53

Enlow, D. H. (1966). 'An evaluation of the use of bone histology in forensic medicine and anthropology', in Evans, F. G (ed), *Studies on the anatomy and function of bone and joints*, Verlag, Heidelberg, Springer, 93-112.

Etok, S. E., Valsami-Jones, E., Wess, T. J., Hiller, J. C., Maxwell, C. A., Rogers, K. D., Manning, D. A., White, M. L., Lopez-Capel, E., Collins, M. J. and Buckley, M. (2007). Structural and chemical changes of thermally treated bone apatite. *J Mater Sci* 42(23), 9807–9816.

Exposito, J. Y., Cluzel, C., Garrone, R. and Lethias, C. (2002). Evolution of collagens. *Anat. Rec*. 268, 302–316.

Eyre, D. R., Dickson, I. R. and van Ness, K. (1988). Collagen crosslinking in human bone and articular cartilage: Age-related changes in the content of mature hydroxypyridinium residues. *Biochem J* 252, 495–500.

Etxeberria, F. (1994). Aspectos macroscópicos del hueso sometido al fuego: Revisión de las cremaciones descritas en el País Vasco desde la arqueologia. *Munibe Anthropologia-Arkeologia* 46, 111–116.

Fairgrieve, S. I. (2008). 'Heat-induced alterations of bone microstructure', in Fairgrieve, S. I, (ed.), *Forensic Cremation – Recovery and Analysis*, Boca Raton, CRC Press, 131–140.

Forster, R. E. (2006). Diffusion of gases. University of Pennsylvania, Philadelphia, PA, USA.

Franc, S., Marzin, E., Boutillon, M. M., Lafont, R., Lechéne de la Porte, P. and Herbage, D. (1995). Immunohistochemical and biochemical analyses of 20,000–25,000-year-old fossil cartilage. *Eur. J. Biochem*. 234, 125-131.

Francillon-Vieillot, H., de Buffrénil, V., Castanet, J., Géraudie, J., Meunier, F. J., Sire, J., Zylberberg, L. and de Ricqlès, A. (1990). 'Microstructure and mineralization of vertebrate skeletal, in Carter, J. G. (ed), *Skeletal biomineralization: patterns, processes and evolutionary trend*, Van Nostrand Reinhold, New York, 471-530.

Fredericks, J. D, Bennett, P., Williams, A., Rogers, K. D. (2012). FTIR spectroscopy: a new diagnostic tool to aid DNA analysis from heated bone. *Forensic Sci Int Genet*. 6, 375–380.

Fredericks, J. D., Ringrose, T. J., Dicken, A., Williams, A., Bennett, P. A. (2015). Potential new diagnostic tool to aid DNA analysis from heat compromised bone using colorimetry: a preliminary study. *Sci Justice* 55, 124–130.

Frost, H. M. (1973). Bone remodelling and its relationship to metabolic bone disease. Springfield, Charles C. Thomas.

Galtés, I. and Scheirs, S. (2019). Differentiation between perimortem trauma and heat-induced damage: the use of perimortem traits on burnt long bones. *Forensic Science, Medicine and Pathology* 15, 453-457.

Gevaart-Durkin, A., Swart, D. and Chowdhury, Z. (2014). A study of energy-related injuries from hospital admissions among children and adults in South Africa. *Burns* 40(6), 1209-1218.

Gejvall, N. G. (1969). 'Cremations', in Brothwell, D. and. Higgs, E. (2nd ed.), *Science in Archaeology*, New York, Praeger, 468–479.

Glazewski, M. (2006). Experiments in Bone Burning. University of Wisconsin Oshkosh, Oshkosh Scholar, 17–25.

Gopinathan, P. A., Kokila, G., Salman Siddeeqh, S., Prakash, R. and Pradeep, L. (2020). Reexploring picrosirius red: A review. *Indian Journal of Pathology and Oncology* 7(2), 196-203.

Gonçalves, D., Cunha, E. and Thompson, T. J. U. (2015). Estimation of the pre-burning condition of human remains in forensic contexts. *International Journal of Legal Medicine* 129, 1137-1143.

Gonçalves, D., Thompson, T. J. U. and Cunha, E. (2011). Implications of heat-induced changes in bone on the interpretation of funerary behaviour and practice. *Journal of Archaeological Science* 38, 1308–1313.

Hackman, L. (2016). 'Forensic Anthropology and Missing Persons Investigations', in Morewitz, S. J. and Colls, S. C (ed.), *Handbook of Missing Persons*, Switzerland, Springer International Publishing 415–425.

Hanson, M. and Cain, C. R. (2007). Examining histology to identify burned bone. *Journal of Archaeological Science* 34, 1902-1913.

Herrmann, B. (1970). Anthropologische Bearbeitung der Leichenbränden von Berlin-Rudow. *Ausgrabungen in Berlin* 1, 61-71.

Herrmann, N. P. and Bennett, J. L. (1998). The differentiation of traumatic and heat-related fractures in burnt bone. *J Forensic Sci* 44, 461-469.

Hillier, M. L. and Bell, L. S. (2007). Differentiating human bone from animal bone: a review of histological methods. *J Forensic Sci* 52, 249-263.

Hirshberg, A., Sherman, S., Buchner, A. and Dayan, D. (1999). Collagen fibres in the wall of odontogenic keratocysts: a study with picrosirius red and polarizing microscopy. *J Oral Pathol Med*. 28, 410-412.

Holman, J. P. (2011). Heat Transfer. McGraw-Hill Higher Education 46, 121–130.

Horocholyn, K. (2013). Comparative Histology of Burned Mammals Using Light Microscopy: Examining Heat-Induced Changes in Femoral Samples of Deer, Pig and Cow. MA thesis. University of Alberta.

Houghton, P. E., Keefer, K. A., Diegelmann, R. F. and Krummel, T. M. (1996). A simple method to assess the relative amount of collagen deposition in wounded fetal mouse limbs. *Wound Repair and Regeneration* 4(4), 489-495.

Howell, A. N. and Belmont, E. L. (2023). An Investigation of Oxygen Availability in Spreading Fires. *Fire Technology* 59, 2147–2176.

Huang, X. and Rein, G. (2017). Downward spread of smouldering peat fire: the role of moisture, density and oxygen supply. *International Journal of Wildland Fire* 26, 907–918.

Hull, D. (1999). Fractography: Observing, measuring and interpreting fracture surface topography. Cambridge, Cambridge University Press.

Hutchinson, J. R. (2021). The evolutionary biomechanics of locomotor function in giant land animals. *Journal of Experimental Biology* 224(11), jeb217463.

Imaizumi, K. (2015). Forensic investigation of burnt human remains. *Research and Reports in Forensic Medical Science* 5, 67-74.

Imaizumi, K., Taniguchi, K. and Ogawa, Y. (2014). DNA survival and physical and histological properties of heat-induced alterations in burnt bones. *Int. J. Legal Med.* 128, 439-446.

Işcan, M. Y. and Steyn, M. (2013). 'Perimortem trauma and thermal destruction', in Işcan, M. Y. and Steyn, M. (ed.), *The Human Skeleton in Forensic Medicine*, Charles C. Thomas, Springfield, IL, 317-360.

Ishiwatari, N., Fukuoka, M. and Sakai, N. (2013). Effect of protein denaturation degree on texture and water state of cooked meat. *Journal of Food Engineering* 117, 361-369.

Kawai, M. and Rosen, C. J. (2012). The insulin-like growth factor system in bone: basic and clinical implications. *Endocrinol Metab Clin North Am* 41, 323-33.

Keough, N., L'Abbe, E. N., Steyn, M. and Pretorius, S. (2015). Assessment of skeletal changes after post-mortem exposure to fire as an indicator of decomposition stage. *Forensic Science International* 246, 17-24.

Kerr, J. B. (2010). 'Skeletal Tissue', in McRitchie, D. and Natsis, C. (2nd ed.), *Functional Histology*, Australia, Elsevier, 223-256.

Kimemia, D. K. and van Niekerk, A. (2017). Energy poverty, shack fires and childhood burns. *SAMJ* 107(4), 289-291.

Kimemia, D., Vermaak, C., Pachauri, S., Rhodes, B. (2014). Burns, scalds and poisonings from household energy use in South Africa: Are the energy poor at greater risk? *Energy Sustain Dev* 18(1), 1-8.

Krap, T., Nota, K., Wilk, L. S., van de Goot, F. R. W., Ruijter, J. M., Duijst, W. and Oostra, R. J. (2017a). Luminescence of thermally altered human skeletal remains. *Int. J. Legal Med*., 1-13.

Krap, T., van de Goot, F. R. W., Oostra, R. J., Duijst, W. and Waters-Rist, A. L. (2017b). Temperature estimations of heated bone: A questionnaire-based study of accuracy and

precision of interpretation of bone colour by forensic and physical anthropologists. *Legal Medicine* 29, 22-28.

Kroeze, R. J., Helder, M. N., Govaert, L. E. and Smit, T. H. (2009). Biodegradable Polymers in Bone Tissue Engineering. *Materials* 2, 833-856.

Krogman, W. M. (1943a). Role of the Physical Anthropologist in the Identification of Human Skeletal Remains, I. *FBI Law Enforcement Bulletin* 12(4), 17-40.

Krogman, W. M. (1943b). Role of the Physical Anthropologist in the Identification of Human Skeletal Remains, II. *FBI Law Enforcement Bulletin* 12(5), 12–28.

Kus, J. and Misz-Kennan, M. (2017). Coal weathering and laboratory (artificial) coal oxidation. *International Journal of Coal Geology* 171, 12-36.

Labuschagne. L. (2020). The use of histological examination methods to distinguish between the burned remains of human and non-human bones. MPhil. Cape Town, University of Cape Town.

Lambri, M. L., Giordano, E. D. and Bozzano, P. B. (2016). Thermal Degradation of Type I Collagen from Bones. *Journal of Renewable Materials* 4(4), 251-257.

Lambri, M. L., Bozzano, P. B., Giordano, E. D. V., Bonifacich, F. G., Damián Gargicevich, D., Griselda Irene Zelada, G. I. and Lambri, O. A. (2018). Denaturation processes of collagen from cow bones as a function of temperature. *Revista Matéria* 23(2), 1–11.

Landis, J. R., & Koch, G. G. (1977). The measurement of observer agreement for categorical data. *Biometrics 33*, 159-174.

Lattouf, R., Younes, R., Lutomski, D., Naaman, N., Godeau, G., Senni, K. and Changotade, S. (2014). Picrosirius Red Staining: A Useful Tool to Appraise Collagen Networks in Normal and Pathological Tissues. *Journal of Histochemistry & Cytochemistry* 62(10), 751–758.

Lau, M., Lau, K., Ku, H. and Cardona, F. (2013). Analysis of heat-treated bovine cortical bone by thermal gravimetric and nanoindentation. *Composites Part B: Engineering* 55, 447-452.

Layton, C., Bancroft, J. C. and Survana, S. K. (2019). 'Fixation of tissues', in Survana, S. K., Layton, C. and Bancroft, J. C. (8th ed.), *Bancroft's Theory and practice of histological techniques*. Oxford, Elsevier, 40-63.

Lee, C. L. and Einhorn, T. A. (2001). 'The bone organ system – form and function', in Marcus, R., Feldman, D., Kelsey, J. (2nd ed.), *Osteoporosis*, California, Academic Press, 3-20.

Lee, C. H., Singla, A. and Lee, Y. (2001). Biomedical applications of collagen. *Int. J. Pharm*. 221, 1-22.

Lemmers, S. A. M. (2012). Burned culture: osteological research into Urnfield cremation technology and ritual in the South of the Netherlands, Lunula. *Archaeol Protohist* 20, 81-88.

Leng, H., Reyes, M. J., Dong, X. N. and Wang, X. (2013). Effect of age on mechanical properties of the collagen phase in different orientations of human cortical bone. *Bone* 55, 288–291.

Li, J., Yuan, S., Zhu, J., Li, S. and Zhang, W. (2020). Numerical Model and Experimental Validation for Laser Sinterable Semi-Crystalline Polymer: Shrinkage and Warping. *Polymers* 12, 1-23.

Liebenberg, M., Liebenberg, L., Krüger, G. C. and L'Abbé, E. N. (2023). Veldt fires in South Africa: Implications on osteometry and the biological profile. *J Forensic Sci*. 68, 586 – 595.

Liebich, H. G., König, H. E. and Maierl, J. (2020). 'Hindlimbs or pelvic limbs (membra pelvina)', in König, H. E and Liebich, H. G. (7th ed.), *Veterinary Anatomy of Domestic Animals Textbook and Colour Atlas*, Stuttgart, Thieme, 243-314.

Lisowski, F. P. (1968). The Investigation of Human Cremated Remains. *Anthropologie und Humangenetik* 4, 76–83.

Liu, J., Xu, M., Wu, J., Zhang, H., Yang, L., Lun, D., Hu, Y. and Liu, B. (2021). Picrosirius Polarization Method for Collagen Fiber Detection in Tendons: A Mini-Review. *Orthopaedic Surgery* 13, 701-707.

López De Padilla, M. C., Coenen, M. J., Tovar, A., De la Vega, R. E., Evans, C. H. and Müller, S. A. (2021). Picrosirius Red Staining: Revisiting Its Application to the Qualitative and Quantitative Assessment of Collagen Type I and Type III in Tendon. *Journal of Histochemistry & Cytochemistry* 69(10), 633–643.

Lowenstam, H. A. and Weiner, S. (1989). On Biomineralization, NY, Oxford University Press.

Ma, Z., Qiang, Z., Guo, C., Jiang, Y., Zhao, H., Wen, C. and Ren, L. (2021). Disparate micro-mechanical behaviors of adjacent bone lamellae through in situ SEM micropillar compression. *Materials Science & Engineering: A* 825, 141903.

Maat, G. J. R., Van Den Bos, R. P. M. and Aarents, M. J. J. (2001). Manual preparation of ground sections for the microscopy of natural bone tissue: Update and modification of frost's 'rapid manual method'. *Int. J. Osteoarchaeol.* 11, 366-374.

Mahon, T. J., Maboke, N. and Myburgh, J. (2021). The use of different detergents in skeletal preparations. *Forensic Science International* 327, 110967.

Mamede, A. P., Gonçalves, D., Marques, M. P. M. and de Carvailho, L. A. E. B. (2019). Burned bones tell their own stories: A review of methodological approaches to assess heat-induced diagenesis. *Australian Journal of Forensic Sciences* 51(2), 201-208.

Mandal, A. (2023). Collagen Molecular Structure. Available at: L: https://www.news-medical.net/health/Collagen-Molecular-Structure.aspx (Accessed: 17 February 2024).

Mano, J. F. (2005). Viscoelastic properties of bone: Mechanical spectroscopy studies on a chicken model. *Materials Science and Engineering: C* 25(2), 145-152.

Martin, R. B., Burr, D. B., Sharkey, N. A. (1998). Skeletal tissue mechanics. New York: Springer.

Martiniaková, M., Grosskopf, B., Omelka, R., Dammers, K., Vondráková, M. and Bauerova, M. (2006b). Differences among species in compact bone tissue microstructure of mammalian skeleton: use of a discriminant function analysis for species identification. *Journal of Forensic Sciences* 51(6), 1235-1239.

Martiniaková, M., Grosskopf, B., Vondráková, M., Omelka, R. and Fabiš, M. (2006a). Differences in femoral compact bone tissue microscopic structure between adult cows (*Bos taurus*) and pigs (*Sus scrofa domestica*). *Anatomia, Histologia, Embryologia* 35, 167-170.

Marques, M. P. M., Mamede, A. P., Vassalo, A. R., Makhou, C., Cunha, E., Gonçalves, D., Parker, S. F. and Batista de Carvalho, L.A. E. (2018). Heat-induced Bone Diagenesis Probed by Vibrational Spectroscopy. *Scientific Reports* 8, 1-13.

Matsuo, H., Tsurumoto, T., Maeda, J., Saiki, K., Okamoto, K., Ogami-Takamura, K., Kondo, H., Tomita, M., Yonekura, A. and Makoto Osaki, M. (2018). Investigating interindividual variations in cortical bone quality: analysis of the morphotypes of secondary osteons and their population densities in the human femoral diaphysis. *Anatomical Science International* 94,75–85.

McGrattan, K. B., McDermott, R. J., Weinschenk, C. G. and Forney, G. P., 2013. Fire Dynamics Simulator Users Guide. USA: US Department of Commerce, Technology Administration, National Institute of Standards and Technology. https://doi.org/10.6028/NIST.SP.1019

Montes, G. S., Bezerra, M. S. and Junqueira, L. C. (1984). 'Collagen distribution in tissues' in Ruggeri, A. and Motta, P. M. (eds.) *Ultrastructure of the connective tissue matrix*, Boston: Martinus Nijhoff Publishers, 65-88.

Montes, G. S. and Junqueira, L. C. (1991). The use of the Picrosirius-polarization method for the study of the biopathology of collagen. *Mem Inst Oswaldo Cruz 86 Suppl* 3, 1-11.

Moore, T. A. and Yamada, N. (1998). 'Nitrogen gas as a halon replacement'. *Halon Options Technical Working Conference*. 12 - 14 May. 330-338.

Morin, E., Soppela, P. and Chouinard, P. Y. (2022). Thermal adaptation and fatty acid profiles of bone marrow and muscles in mammals: Implications of a study of caribou (Rangifer tarandus caribou). *PLoS ONE* 17(12), e0268593.

Mundorff, A. Z. (2008) 'Anthropologist-directed triage: three distinct mass fatality events involving fragmentation of human remains', in Adams, B. J. and Byrd, J. E. (eds).

Recovery, Analysis, and Identification of Commingled Human Remains. Totowa (NJ), Humana Press, 123-144.

Murray, C. J. L. and Lopez, A. D. (1996). Global Health Statistics: A Compendium of Incidence, Prevalence and Mortality Estimates for over 200 Conditions, Harvard School of Public Health on behalf of the World Health Organization and the World Bank, Cambridge, MA, USA 2, 906. Available online: https://apps.who.int/iris/handle/10665/41848 (accessed on 13 November 2022).

Myllyharju, J. and Kivirikko, K. I. (2004). Collagens, modifying enzymes and their mutations in humans, flies and worms. *Trends Genet* 20, 33-43.

Nielsen H. S., Jonasson. L., Kalogeropoulos, K., Karsdal, M. A., Reese-Petersen, A. L., Auf dem Keller, U., Genovese, F., Nilsson, J. and Goncalves, I. (2020). Exploring the role of extracellular matrix proteins to develop biomarkers of plaque vulnerability and outcome. *J Intern Med* 287(5), 493–513.

Nielsen, L. F., Moe, D., Kirkeby, S. and Garbarsch, C. (2009). Sirius Red and Acid Fuchsin Staining Mechanism. *Biotechnic & Histochemistry* 73(2), 71–77.

Nymana, J. S., Royc, A., Shen, X., Acuna, R. L., Tyler, J. H. and Wang, X. (2006). The influence of water removal on the strength and toughness of cortical bone. *Journal of Biomechanics* 39, 931–938.

Parfitt, A. M. (1994). Osteonal and hemi-osteonal remodeling: the spatial and temporal framework for signal traffic in adult human bone. *J Cell Biochem* 55, 273-286.

Piérard, G. E. (1989). Sirius red polarization method is useful to visualize the organization of connective tissues but not the molecular composition of their fibrous polymers. *Matrix* 9, 68-71.

Pope, M. H. and Outwater, J. O. (1972). The fracture characteristics of bone substance. *Journal of Biomechanics* 5, 457-467.

Puchtler, H., Meloan, S. N. and Waldrop, F. S. (1988). Are picro-dye reactions for collagens quantitative? *Histochemistry* 88, 243-256.

Puchtler, H., Waldrop, F. S. and Valentine, L. S. (1973). Polarization microscopic studies of connective tissue stained with Picro-Sirius red FBA. *Beitr Pathol* 150, 174–187.

Raja, S., Tauseef, S. M. and Varadharajan, S. (2023). Investigating the impact of oxygen concentration on fire dynamics using numerical simulation with FDS. *Process Safety and Environmental Protection* 178, 195–203.

Reidsma, F. H., van Hoesel, A., van Os, B. J. H., Megens, L. and Braadbaart, F. (2016). Charred bone: Physical and chemical changes during laboratory simulated heating under reducing conditions and its relevance for the study of fire use in archaeology. *Journal of Archaeological Science: Reports* 10, 282-292.

Rendina-Ruedy, E., Clifford, J. and Rosen, C. J. (2020). Lipids in the Bone Marrow: An Evolving Perspective. *Cell Metabolism* 31, 219–231.

Rich, L. and Whittaker, P. (2005). Collagen and picrosirius red staining: a polarized light assessment of fibrillar hue and spatial distribution. *Braz J Morphol Sci* 22, 97-104.

Rittié, L. (2017). Method for Picrosirius red-polarization detection of collagen fibers in tissue sections. *Methods Mol Biol* 1627, 395–407.

Rosa, J., Marques, M. P. M., David Gonçalves, D. and Ferreira, M. T. (2023). Half a century of systematic research on heat-induced colour changes in bone. *A review. Science & Justice* 63, 573-580.

Ross, M. H. and Pawlina, W. (2006). Histology a text and atlas with correlated cell and molecular biology (5th ed). Baltimore, Lippincott Wiliams & Wilkins.

Saiang, C and Miskovsky, K. (2012). 'Effect of heat on the mechanical properties of selected rock types – a laboratory study', in Qian, Q. and Zhou, Y. (ed.). *Harmonising Rock Engineering and the Environment*. Taylor & Francis Group, London, 815-820.

Sanz, C. V., Rodríguez, I. V., Forriol, F., Tejado, E. and Lopez-Valdes, F. J. (2023). Variation in Juvenile Long Bone Properties as a Function of Age: Mechanical and Compositional Characterization. *Materials* 16, 1-13.

Schafer, A. (2001). The colour of the human skull**.** *Forensic Science International* 117(1-2), 53-56.

Schwebel, D. C., Swart, D., Hui, S. K. A., Simpson, J. and Hobe, P. (2009). Paraffin-related injury in low-income South African communities: Knowledge, practice and perceived risk. Bull World Health Organ 87(9), 700-706.

Segnani, C., Ippolito, C., Antonioli, L., Pellegrini, C., Blandizzi, C, Dolfi, A. and Bernardini, N. (2015). Histochemical Detection of Collagen Fibers by Sirius Red/Fast Green Is More Sensitive than van Gieson or Sirius Red Alone in Normal and Inflamed Rat Colon. *PLoS ONE* 10(12), e0144630.

Shipman, P., Foster, G. and Schoeninger, M. (1984). Burnt bones and teeth: an experimental study of color, morphology, crystal structure and shrinkage. *Journal of Archaeological Science* 11, 307-325.

Singh, D., Rai, V. and Agrawal1, D. K. (2023). Regulation of Collagen I and Collagen III in Tissue Injury and Regeneration. *Cardiol Cardiovasc Med.* 7(1), 5–16.

Siratovich, P. A., Villeneuve, M., Kennedy, B., Gravley, D., Cole, J. and Davidson, J. (2013). 'The geothermal stimulator: A high-temperature, high-pressure device for inducing thermal fracture in rocks', *35th New Zealand Geothermal Workshop*, 17 – 20 November. New Zealand, Rotorua, 1-6.

Snoeck, C., Schulting, R. J., Lee-Thorp, J. A., Lebon, M. and Zazzo, A. (2016). Impact of heating conditions on the carbon and oxygen isotope composition of calcined bone. *Journal of Archaeological Science* 65, 32-43.

Spearpoint, M. and Hopkin, C. (2021). Household cooking oil use and its bearing on fire safety. *J. Fire Sci.* 39, 265–284.

Spennemann, D. H. and Colley, S. M. (1989). Fire in a pit: the effects of burning on faunal remains. *Archaeozoologia,* 3(1–2), 51-64.

Spitz, W. U. and Spitz, D. J., (2005). 'Chapter XIII: Thermal Injuries', in Spitz, W. U. and Fisher, R. S. (eds), *Medicolegal Investigation of Death: Guidelines for the Application of Pathology to Crime Investigation*, Charles C Thomas Pub. Ltd, Springfield, 747–782.

Stagi, S., Cavalli, L., Iurato, C., Seminara, S., Brandi, M. L. and de Martino, M. (2013). Bone metabolism in children and adolescents: main characteristics of the determinants of peak bone mass. *Clinical Cases in Mineral and Bone Metabolism* 10(3), 172-179.

Stout, S. D. and Crowder, C. (2011). Bone remodeling, histomorphology, and histomorphometry. *Bone histology: an anthropological perspective*, 1-21.

Su, Y., Yang, J., Li, R., Song, G. and Li, J. (2020). Experimental study of moisture role and heat transfer in thermal insulation fabric against hot surface contact. *International Journal of Thermal Sciences* 156, 106501.

Symes, S. A., Rainwater, C. W., Chapman, E. N., Gipson, D. R., and Piper, A. L. (2008). 'Patterned thermal destruction of human remains in a forensic setting', in Schmidt, C. W. and Symes, S. A. (1st ed.), *The analysis of burned human remains*, London, Academic Press, 15-54.

Symes, S. A., Rainwater, C. W., Chapman, E. N., Gipson, D. R. and Piper, A. L. (2015) 'Patterned Thermal Destruction in a Forensic Setting', in Schmidt, C. W and Symes, S. A (2nd ed.), *The analysis of Burned Human Remain*, Oxford, Elsevier, 17-59.

Szpicer, A., Binkowska, W., Wojtasik-Kalinowska, I. and Poltorak, A. (2023). Prediction of protein denaturation and weight loss in pork loin (muscle Longissimus dorsi) using computational fluid dynamics. *European Food Research and Technology* 249, 3055–3068.

Taheri, P. (2015). An Integrated Approach from the Preliminary Design to the Final Proposal of Gaseous Fire Suppression Systems. MSc Thesis. Politecnico di Milano.

Thompson, T. J. U. (2004). Recent advances in the study of burned bones and their implications for forensic anthropology. *Forensic Sci. Int.* 146, S203-S205.

Thompson, T. (2005). Heat-induced dimensional changes in bone and their consequences for forensic anthropology. *J. Forensic Sci*. 50 (5), 1008–1015.

Thompson, T. J. U. (2015). 'The analysis of heat-induced crystallinity change in bone', in Schmidt, C. W. and Symes, S. A. (2nd eds.), *The analysis of Burned Human Remain*, Oxford, Elsevier, 323-337.

Triaca, A., Mahon, T. J. and Myburgh, J. (2022). A comparison of different maceration techniques on burnt remains. *J Forensic Sci.* 67, 676-682.

Ubelaker, D. H. (2009). The forensic evaluation of burned skeletal remains: A synthesis. *Forensic Sci. Int*. 183(1–3), 1-5.

Ulguim, P. (2015). 'Analysing cremated human remains from the southern Brazilian highlands: interpreting archaeological evidence of funerary practice at mound and enclosure complexes in the Pelotas River Valley', in Thompson, T. J. U. (ed), *The archaeology of cremation: burned human remains in funerary studies*, Oxford, Oxbow Books, 173-212.

US Energy Information Administration, *Primary Energy Consumption by Source and Sector, 2012*, http://www.eia.gov/totalenergy/data/monthly/pdf/flow/css_2012_energy.pdf. Data derived from US Energy Information Administration, *Monthly Energy Review* (January 2014).

Vallet-Regi, M. and Navarrete, D. A. (2015). 'Biological apatites in bone and teeth', in O'Brien, P. (2nd ed.), *Nanoceramics in Clinical Use: From Materials to Applications*, Cambridge, UK, Royal Society of Chemistry 1, 1–29.

Varvares, A. (2016). *Effect of Burning on Bones: Heat-Related Fractures in Burned Bone.* [Poster]. American Pathological Association. Saint Louis University and University of Florida.

Vassalo, A. R., Cunha, E., de Carvalho, L. A. E. B. and Gonçalves, D. (2016). Rather yield than break: assessing the influence of human bone collagen content on heat-induced warping through vibrational spectroscopy. *Int J Legal Med* 130, 1647-1656.

Vassalo, A. R., Mamede, A. P., Ferreira, M. T., Cunha, E. and Gonçalves, D. (2019). The G-force awakens: the influence of gravity in bone heat-induced warping and its implications for the estimation of the pre-burning condition of human remains. *Australian Journal of forensic sciences* 51(2), 201-208.

Virtual Slide 093B_HISTO_40X: Ground section of compact bone, cross section, 40X (osteons = Haversian systems, lacunae for osteocytes, canaliculus, Volkmann's =

nutrient canals). Photograph. Michigan Histology and Virtual Microscopy Learning Resources. University of Michigan Medical School, Michigan Medicine, 2024. https://histologyslides.med.umich.edu/Histology/Basic%20Tissues/Cartilage%20and%20Bone/093B_HISTO_40X.htm. 08 August 2024.

Walker, P. L. and Miller, K. P. (2005). Time, temperature and oxygen availability: an experimental study of the effects of environmental conditions on the color and organic content of cremated bone. *Am. J. Phys. Anthropol*. 40 (222), 216–217.

Walker, P. L., Miller, K. W. P. and Richman, R. M. S. (2008). 'Expeimental study of the effects of environmental conditions on the color and organic content of cremated bone', in Schmidt, C. W and Symes, S. A (1st ed.), *The analysis of Burned Human Remain*, Oxford, Elsevier, 17-59.

Wang, X., Bank, R. A., TeKoppele, J. M. and Agrawal, C. M. (2001). The role of collagen in determining bone mechanical properties. *Journal of Orthopaedic Research* 19, 1021-1026.

Waterhouse, K. (2013). The effect of victim age on burnt bone fragmentation: Implications for remains recovery. *Forensic Science International* 231, 409.e1–409.e7.

Wells, C. (1960). A Study of Cremations. *Antiquity* 34, 29–37.

Wick, G., Kalischnig, G., Maurer, H., Mayerl, C. and Müller, P. U. (2001). Really old-palaeoimmunology: immunohistochemical analysis of extracellular matrix proteins in historic and pre-historic material. *Exp. Gerontol*. 36, 1565-1579.

Whyte, T. R. (2013). Distinguishing remains of human cremations from burned animal bones. *J. Field Archaeol*. 28 (3/4), 437-448.

Wolman, M. (1975). Polarized light microscopy as a tool of diagnostic pathology. *J Histochem Cytochem* 23, 21–50.

World Health Organization (2016). Mortality and causes of death in South Africa, 2016: Findings from death notification. *Statistics South Africa: Statistical Release* P0309.3, 1-138.

Wynn, T. A. (2008). Cellular and molecular mechanisms of fibrosis. *J Pathol* 214, 199–210.

Zioupos, P., Currey, J. D. and Hamer, A. J. (1999). The role of collagen in the declining mechanical properties of aging human cortical bone. *Journal of Biomedical Materials Research* 45, 108-116.

Appendix A: Waiver from Animal Ethics Research Committee

A1: Waiver for using commercial pig bones.

ANIMAL RESEARCH ETHICS COMMITTEE

Registration number: AREC-101210-002

Date: 04/11/2021

Certificate reference: Waiver 04-11-2021-O
Category: O
Applicant: Thato Rathokane
Department: School of Anatomy
Tel: 011 717 2660; **Email**: 1689581@students.wits.ac.za

Re: Waiver from the Animal Research Ethics Committee of the University of the Witwatersrand

This letter is to confirm that Thato Rathokane, MSc (Med) #1689581 at the School of Anatomy under the supervision of Drs Nicholas Bacci, Tanya Augustine and Brendon Billings, does not require full Animal Research Ethics Committee clearance to undertake the work titled **'Heat-Induced Changes on Bone at Different Taphonomic Conditions'**.

Reason for waiver

The project is using commercially available pig bones.

Details of the study

Lot of controversy exists around how heat-induced fracturing and warping is affected by different taphonomic conditions (fleshed, wet, or dry) of cremains and the amount of collagen present on bones. The aim of the study is to investigate the relationships between heat-induced macroscopic fractures, bone warping and histological alterations at different taphonomic conditions (fleshed, wet and dry bone) and temperatures. The study will make use of domestic pig (Sus scrofa domesticus) tibiae. The tibia is selected due to its availability at butchers, as well as similar size and histology than human tibia. A total of 81 bones (n = 81) with different taphonomic conditions will be exposed 30 or 60 min to heat (200 to 800°C). Micro and macroscopic changes will then be determined.

The individuals covered by the waiver are Thato Rathokane and Drs Nicholas Bacci, Tanya Augustine and Brendon Billings.

Please contact me should you require further information.

Yours sincerely

Ass Prof Frederic Michel
Chair: Animal Research Ethics Committee
University of the Witwatersrand

A2: Waiver for using dry pig skeletal remains.

ANIMAL RESEARCH ETHICS COMMITTEE

Registration number: AREC-101210-002

Date: 02/08/2022

Certificate reference: Waiver 02-08-2022-O
Category: O
Applicant: Nicholas Bacci
Department: School of Anatomical sciences (WITS)

Tel: 011 717 2660; **Email**: nicholas.bacci@wits.ac.za

Re: Waiver from the Animal Ethics Research Committee of the University of the Witwatersrand

This letter is to confirm that Dr Nicholas Bacci (School of Anatomical Sciences), does not require full Animal Ethics Research Committee clearance to train his MSc candidate, Thato Rathokane - student #1689581, on the proposed bone histology methods.

Reason for waiver

The project is using historic pig skeletal material available from the School of Anatomical Sciences.

Details of the study

Bone samples will be sectioned into 3mm and 1mm blocks using Dremel rotary multi-tool (4000 Platinum) with cut-off wheels (n. 409). The 3mm bone block samples will be fixed in 10% neutral buffered formalin (Layton et al., 2019) and decalcified using different acid decalcification solutions (3% and 5% nitric acid, and 10% formic acid). The decalcification endpoint will be checked using a handheld Nomad portable dental X-ray (Aribex Inc., East Orem, USA) by monitoring calcium pockets initially visible as opaque white portions in the X-ray and when decalcification is complete, the bone will appear translucent. Only the preferred decalcifying solution will be used for the MSc study (Waiver No.: 04-11-2021-O). The samples

will then undergo tissue processing (Thermo Scientific Citadel 2000) followed by embedding into paraffin wax (Tissue-Tek Console, Miles Scientific) to enable 5µm thin-sectioning using a rotary microtome (Leica RM2125 RTS). The thin sectioned samples will be stained with a Sirius Red-Fast Green stain, which stains the collagenous protein red and non-collagenous protein green (Segnani et al., 2015). These stained sections will be firstly photographed using Zeiss Axioskop 2 plus with a Zeiss Axiocam 208 colour (Zen 2010) microscope. The stained sections will then be eluted using 1ml of 0.1N NaOH (sodium hydroxide) and absolute methanol solution for 20 minutes and transferred into a 96-well microplate for analysis using a spectrophotometer (Promega GloMax Explorer) (Houghton et al., 1996). The spectrophotometer will be used to record optical density at 540 nm and 600 nm wavelengths for collagen and non-collagenous proteins, respectively (Houghton et al., 1996). The 1mm blocks will be processed following Maat's et al. (2001) ground bone sectioning method using distilled water and 220-grid waterproof carborundum paper to obtain bone thin sections. The thickness will be monitored using a light microscope until histological features are resolved (Maat et al, 2001; following modification by Bacci, 2016). The sections will then be rinsed in distilled water thrice and placed in fresh distilled water prior to mounting to prevent dehydration (Maat et al, 2001). Photomicrographs of the ground bone sections will then be taken and used for training on how to measure microscopic fractures (Brain, 1991; Bacci et al., 2021) and osteon dimensions (area, length, and diameter) (Horocholyn, 2013) using ImageJ (v 1.53m) (Schneider et al., 2012).

The individuals covered by the waiver are Dr Nicholas Bacci and Thato Rathokane (School of Anatomical Sciences, WITS).

Please contact me should you require further information.

Yours sincerely



Prof Frederic Michel
Chair: Animal Research Ethics Committee
University of the Witwatersrand

APPENDICES B: Solutions

B1: Solution Constitution

10% Neutral Buffered Formalin Fixative Solution

The following recipe was taken from Bancroft's Theory and Practice of Histological Techniques 8th edition by Suvarna, S. K., Layton, C. and Bancroft, J. D. (2019):

For a 1-liter solution:

- 100 ml formaldehyde (40%)
- 900 ml distilled water
- 4g sodium phosphate, monohydrate, monobasic (Sodium dihydrogen orthophosphate ~ NaH_2PO_4)
- 6.5g sodium phosphate, dibasic, anhydrous (di-Sodium hydrogen orthophosphate ~ Na_2HPO_4)

Making Decalcification Solutions

The recipe for 100 ml solutions were taken from Theory and Practice of Histology Techniques by Bancroft, J., Stevens, D. and MRC Path, A. 2nd edition (1982):

1. 3% Nitric Acid
    - Nitric acid 3ml
    - Distilled water 97ml
2. 5% Nitric Acid
    - Nitric acid 5ml
    - Distilled water 95ml
3. 10% Formic Acid
    - 90% Formic acid 10ml
    - Distilled water 90ml
4. 10% Formic Citric Acid
    - 20% aqueous solution of trisodium citrate 65ml
    - 90% Formic acid 35ml

B2: Coating and Staining Solution

Coating slides with 3% 3-aminopropyltriethoxysilane (APES) in acetone

- Put microscopic slides in glass staining rack in a glass staining dish with 3% 3-aminopropyltriethoxysilane (APES) (6 ml) and 194 ml of acetone for 30 minutes.
- Dip slides 10 times in 200 ml acetone (repeat in a second clean dish of acetone)
- Dip slides 10 times in dish with distilled water.
- Let slides dry overnight and store in incubator (38 °C) for 2 days.

Hematoxylin and Eosin Stain for Bone

Hydration

1. Dewax in xylene for 10 minutes x 2
2. Immerse in 100% ethanol for 1 minute x 2
3. Immerse in 95% ethanol for 1 minute
4. Immerse in 70% ethanol for 1 minute
5. Wash in water for 1 minute

Nuclear Staining

1. Stain with Meyer's haematoxylin for 10 minutes
2. Wash in running tap water for 5 minutes
3. Differentiate in 1% acid alcohol (2 dips)
4. Wash in running tap water for 5 minutes
5. Stain in Scott's tap water for 5 minutes
6. Wash in running tap water for 5 minutes

Cytoplasm Staining

1. Stain in Eosin for 2 minutes
2. Rinse in tap water

Dehydration and Mounting

1. Immerse in 70% ethanol for 1 minute
2. Immerse in 95% ethanol for 1 minute
3. Immerse in 100% ethanol for 1 minute x 2
4. Immerse in xylene for 10 minutes x 2
5. Mount in Entellan

Results

Nuclei: Blue

Muscle fibers: deep pink-red

Cytoplasm: Varying shades of pink

Sirius Red-Fast Green Staining

After mounting, drying and incubating the slides, the following procedure from Houghton *et al*. (1996) will be done to stain the slides with Sirius Red-Fast Green dye:

All steps are done by moving slides in a metal slide rack through staining dishes filled with respective solutions for the time specified:

1. Deparaffinized slides:

   Xylene 15 minutes
   Xylene 15 minutes
   Hydrate slides

2. Hydrate slides:

   100% Ethanol 6 minutes
   100% Ethanol 6 minutes
   95% Ethanol 6 minutes
   95% Ethanol 6 minutes
   70% Ethanol 6 minutes
   Tap water 6 minutes
   Distilled water 1 minute

3. Stain slides with Sirius red and fast green dye mixture for 2 hours.
4. Wash slides with fresh water for each rack of slides:

   Distilled water 15 minutes
   Distilled water 15 minutes
   Distilled water 15 minutes

5. Let slides dry at room temperature overnight.

Appendix C: Ground Bone Sectioning and other methods (Maat *et al,* 2001; Bacci, 2016)

For preparation of ground bone sections of 1 mm blocks. Vaseline was applied on the back of the sandpaper then stuck to the glass sab so that it is stable during the ground bone sectioning. A drop of water was applied on the grid paper then ground down using index and middle finger. Once the section was thin and smooth, the Frost's gripping device was applied. Frost's gripping device is the section holder where a slip of fresh abrasive paper was folded, with its abrasive side outward, transversally across the central part of one side of a glass microscope slide. The two free ends of the slip were used to hold both the glass slide and abrasive paper tight during the grinding. This was done by putting the index finger in between the free ends on the center of the glass slide, and by positioning the thumb and middle finger of the same hand on the outward side of the same ends. Monitoring the visibility of microscopic structure under the microscope was done often to avoid destruction of the section. Once the light was passing through the section under the microscope and all the microscopic structures were clearly visible, then the sectioning was complete.

For the delicate bones burnt from 300°C-500°C, one side of the block was ground down on 220 grid paper until the section was flat then block was rinsed with sunlight liquid detergent and left to dry. The smooth side of the block was then placed onto a drop or two of Alcolin super glue that had been applied to a glass slide. The glue was permitted dry for 2 hours, with weight on its flat smooth side down directly on top of it. When sectioning, the microscopic slide was used as the holder to grind the section. Rotation movement was done by moistening the index and middle fingers with water and place them onto the centre of the glass slide to hold down the slide. The sectioned was also monitored under the microscope until microstructures were visible.

Appendix D: Optimisation Results

D1: Table showing the number of fractures and the fracture type from the bones cremated.

Tibial Bone Condition	Number of cremation trials	Temperature (C°)	Fracture Types						
			Longitudinal	Transverse	Step	Curvilinear	Delamination	Patina	Total
Fleshed	1	*200*	0	0	0	0	0	0	*0*
	0	*400*	0	0	0	0	0	0	*0*
	1	*500*	3	0	0	0	0	2	*5*
	2	*600*	15	3	3	0	5	11	*37*
	1	*800*	0	0	0	0	0	0	*0*
Wet	1	*200*	0	0	0	0	0	0	*0*
	1	*400*	2	1	0	0	0	2	*5*
	1	*500*	2	2	2	2	0	15	*23*
	4	*600*	16	11	9	2	22	46	*106*
	1	*800*	2	3	0	0	0	11	*16*
Dry	1	*400*	2	1	1	0	0	0	*4*
	0	*500*	0	0	0	0	0	0	*0*
	1	*600*	2	1	0	0	0	8	*11*
	0	*800*	0	0	0	0	0	0	*0*
Total	*15*	-	-	-	-	-	-	-	-

Appendix D2: Heat-induced colour change and fragmentation

D2.1: Table showing the level of heat-induced colour change across different bone condition cremated at different conditions.

		Temperature °C					
Heat-induced colours	**Bone Condition**	**200**	**400**	**500**	**600**	**800**	***Total***
Beige	*Fleshed*	1	0	0	0	0	***1***
	Wet	1	0	0	0	0	***1***
Heat line and heat borders with partial charring	*Fleshed*	0	0	1	0	0	***1***
Completely charred	*Fleshed*	0	0	0	2	0	***2***
	Wet	0	1	0	2	0	***3***
Less than half calcined and rest charred	*Dry*	0	1	0	0	0	***1***
	Fleshed	0	0	0	0	1	***1***
	Wet	0	0	1	1	0	***2***
More than half calcined and rest charred	*Dry*	0	0	0	1	0	***1***
	Wet	0	0	0	1	1	***2***
Total		***2***	***2***	***2***	***7***	***2***	***15***

D2.2: Table showing the heat-induced fragmentation on bones cremated at different temperatures.

		Temperature (C°)					
Fragments Alignment	**Bone Condition**	**200**	**400**	**500**	**600**	**800**	***Total***
No fragments	*Dry*	0	1	0	1	0	*2*
	Fleshed	1	0	1	0	0	*2*
	Wet	1	1	1	3	0	*6*
Fragments are present and aligned	*Wet*	0	0	0	1	0	*1*
Fragments are present and partially aligned	*Fleshed*	0	0	0	2	0	*2*
	Wet	0	0	0	0	1	*1*
Fragments are present and do not align	*Fleshed*	0	0	0	0	1	*1*
Total		*2*	*2*	*2*	*7*	*2*	*15*

D3: Thermocouple temperature graphs from optimisation

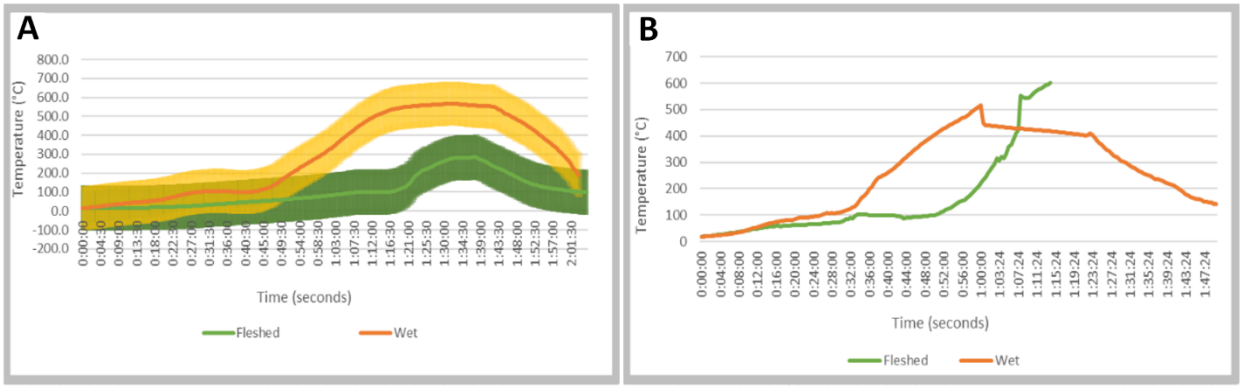


Figure D3: Graphs showing the cremation temperatures of bone samples for 30 minutes at different maximum temperatures.

A) The cremation trials of bones at different taphonomic conditions cremated at a maximum temperature of 500°C. The graph shows +/- 5°C error that could have been recorded by the thermocouple. **B)** shows the burning trial of wet and fleshed bones cremated at 800°C while the furnace was short circuiting.

D4: Decalcification graph

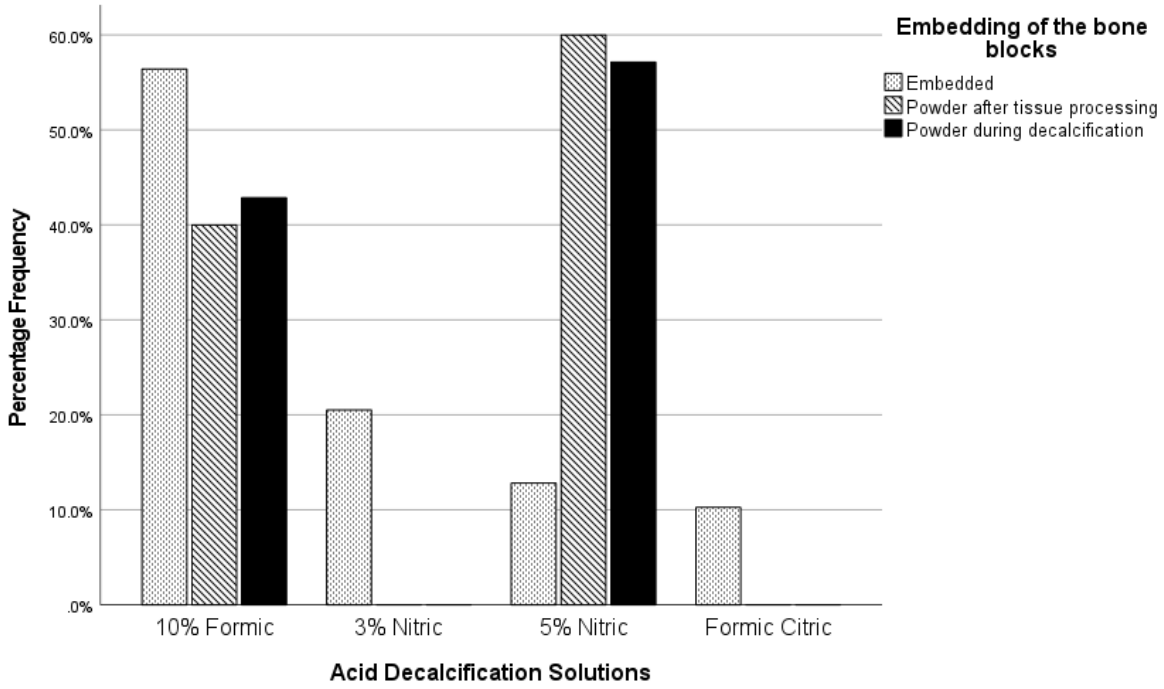


Figure D4: Decalcification time in relation to acid decalcification solutions and successful embedding of blocks.

Image showing the frequency at which bone blocks were successfully embedded (grey), turned into powder during decalcification (black) or tissue processing (pattern) based on the different decalcification solutions (10% FA, 5% NA and 3% NA) they were treated with.

Experimental Results Appendix

Appendix E: Thermocouples temperature graph

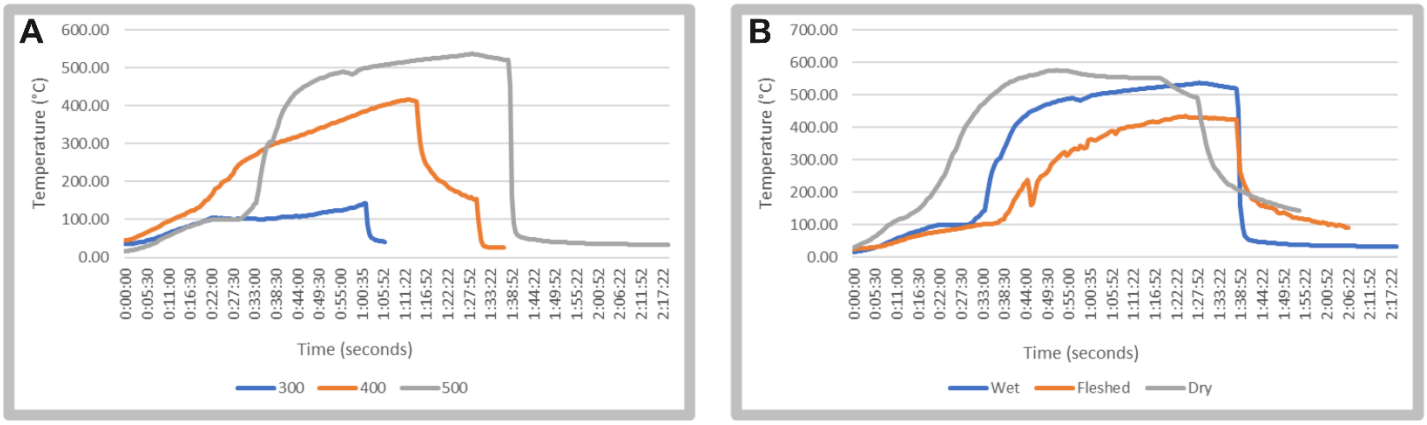


Figure E1: Graphs showing the cremation temperatures of the bone samples, furnace, and the ambient temperature during cremation for 30 minutes at different maximum temperatures.

A) Representative graph of a cremation trial of a wet bone at a maximum temperature of 300°C, 400°C and 500°C. **B**) Representative graph of cremation trials of fleshed, wet and cremated at a maximum temperature of 500°C.

Appendix F: Heat-induced colour change and fragmentation.

F1: Heat-induced colour change.

F1.1: Frequencies of bones with each heat-induced colour change in relation to cremation temperature

Colour	Temperature (°C)				Total
	25	300	400	500	
Beige	6	0	0	0	6
Heat lines and heat borders with partial charring	0	3	3	3	9
More than half charred and rest beige	0	3	0	0	3
Completely charred	0	3	0	0	3
Less than half calcined and rest charred	0	0	3	3	6
More than half calcined and rest charred	0	0	3	3	6
Total	6	9	9	9	33

F1.2: Table showing Fisher-Freeman-Halton Exact test results of heat-induced colour in relation to temperature.

	Value	Exact p-value (2-sided)
Fisher-Freeman-Halton Exact Test	34.929	< 0.001
N of Valid Cases	33	

F1.3: Table showing pairwise Fisher's Exact test of heat-induced colour in relation to temperature.

Temperature	**Pairwise Fisher's Exact test (Bonferroni corrected) ***
25 - 300	P < 0.001*
25 - 400	P < 0.001*
25 - 500	P < 0.001*
300 - 400	P = 0.016
300 - 500	P = 0.016
400 -500	P = 1.000

*Significant values based on the Bonferroni adjusted alpha of p = 0.0083

F1.4: Frequencies of bones with each heat -induced colour change in relation to bone condition.

Colour	Taphonomic Condition					Total
	Fleshed	Wet	Dry	Wet control	Dry control	
Beige	0	0	0	3	3	6
Heat lines and heat borders with partial charring	9	0	0	0	0	9
More than half charred and rest beige	0	3	0	0	0	3
Completely charred	0	0	3	0	0	3
Less than half calcined and rest charred	0	6	0	0	0	6
More than half calcined and rest charred	0	0	6	0	0	6
Total	9	9	9	3	3	33

F1.5: Table showing Chi-squared test of heat-induced colour in relation to bone condition.

	Value	Exact Sig. (2-sided)
Fisher-Freeman-Halton Exact Test	61.757	< 0.001
N of Valid Cases	33	

F 1.6: Table showing pairwise Fisher's Exact test of heat-induced colour in relation to bone condition.

Colour	**Pairwise Fisher's Exact test (Bonferroni corrected alpha = 0.005)**
Wet Control – Dry Control	. [1]
Wet Control - Wet	P = 0.005
Wet Control - Fleshed	P = 0.009
Wet Control - Dry	P = 0.009
Dry Control - Wet	P = 0.005
Dry Control - Fleshed	P = 0.009
Dry Control - Dry	P = 0.009
Wet - Fleshed	P < 0.001*
Wet - Dry	P < 0.001*
Fleshed- Dry	P < 0.001*

1 - There was no statistical outcome on SPSS
*Significant values based on the adjusted alpha of p = 0.005

F1.7: Frequencies of bones with each heat -induced colour change cross tabulation in relation to both colour and temperature.

	Taphonomic Condition																			
	Fleshed				Wet				Dry				Wet control				Dry control			
	25	300	400	500	25	300	400	500	25	300	400	500	25	300	400	500	25	300	400	500
Beige	0	0	0	0	0	0	0	0	0	0	0	0	3	0	0	0	3	0	0	0
Heat lines	0	0	0	0	0	0	0	0	0	0	0	0	0	0	0	0	0	0	0	0
Heat lines and heat borders	0	0	0	0	0	0	0	0	0	0	0	0	0	0	0	0	0	0	0	0
Heat lines and heat borders with partial charring	0	3	3	3	0	0	0	0	0	0	0	0	0	0	0	0	0	0	0	0
Less than half charred and rest beige	0	0	0	0	0	0	0	0	0	0	0	0	0	0	0	0	0	0	0	0
More than half charred and rest beige	0	0	0	0	0	3	0	0	0	0	0	0	0	0	0	0	0	0	0	0
Completely charred	0	0	0	0	0	0	0	0	0	3	0	0	0	0	0	0	0	0	0	0
Less than half calcined and rest charred	0	0	0	0	0	0	3	3	0	0	0	0	0	0	0	0	0	0	0	0
More than half calcined and rest charred	0	0	0	0	0	0	0	0	0	0	3	3	0	0	0	0	0	0	0	0
Completely calcined	0	0	0	0	0	0	0	0	0	0	0	0	0	0	0	0	0	0	0	0

F1.8: Table showing pairwise Fisher's Exact test of heat-induced colour in relation to taphonomic condition and temperature.

Test	Significance	Test	Significance	Test	Significance
Wet Control – Dry Control	. [1]	Wet 300°C – Wet 400°C	P = 0.100	Wet 500°C – Dry 400°C	P = 0.100
Wet Control – Wet 300°C	P = 0.100	Wet 300°C – Wet 500°C	P = 0.100	Wet 500°C – Dry 500°C	P = 0.100
Wet Control – Wet 400°C	P = 0.100	Wet 300°C – Fleshed 300°C	P = 0.100	Fleshed 300°C - Fleshed 400°C	. [1]
Wet Control – Wet 500°C	P = 0.100	Wet 300°C – Fleshed 400°C	P = 0.100	Fleshed 300°C - Fleshed 500°C	. [1]
Wet Control – Fleshed 300°C	P = 0.100	Wet 300°C – Fleshed 500°C	P = 0.100	Fleshed 300°C – Dry 300°C	P = 0.100
Wet Control – Fleshed 400°C	P = 0.100	Wet 300°C – Dry 300°C	P = 0.100	Fleshed 300°C – Dry 400°C	P = 0.100
Wet Control – Fleshed 500°C	P = 0.100	Wet 300°C – Dry 400°C	P = 0.100	Fleshed 300°C – Dry 500°C	P = 0.100
Wet Control – Dry 300°C	P = 0.100	Wet 300°C – Dry 500°C	P = 0.100	Fleshed 400°C - Fleshed 500°C	. [1]
Wet Control – Dry 400°C	P = 0.100	Wet 400°C - Wet 500°C	. [1]	Fleshed 400°C - Dry 300°C	P = 0.100
Wet Control – Dry 500°C	P = 0.100	Wet 400°C - Fleshed 300°C	P = 0.100	Fleshed 400°C - Dry 400°C	P = 0.100
Dry Control - Wet 300°C	P = 0.100	Wet 400°C - Fleshed 400°C	P = 0.100	Fleshed 400°C - Dry 500°C	P = 0.100
Dry Control - Wet 400°C	P = 0.100	Wet 400°C - Fleshed 500°C	P = 0.100	Fleshed 500°C - Dry 300°C	P = 0.100
Dry Control - Wet 500°C	P = 0.100	Wet 400°C – Dry 300°C	P = 0.100	Fleshed 500°C - Dry 400°C	P = 0.100
Dry Control - Fleshed 300°C	P = 0.100	Wet 400°C – Dry 400°C	P = 0.100	Fleshed 500°C - Dry 500°C	P = 0.100
Dry Control - Fleshed 400°C	P = 0.100	Wet 400°C – Dry 500°C	P = 0.100	Dry 300°C - Dry 400°C	P = 0.100
Dry Control - Fleshed 500°C	P = 0.100	Wet 500°C – Fleshed 300°C	P = 0.100	Dry 300°C - Dry 500°C	P = 0.100
Dry Control - Dry 300°C	P = 0.100	Wet 500°C – Fleshed 400°C	P = 0.100	Dry 400°C - Dry 500°C	. [1]
Dry Control - Dry 400°C	P = 0.100	Wet 500°C – Fleshed 500°C	P = 0.100		
Dry Control - Dry 500°C	P = 0.100	Wet 500°C – Dry 300°C	P = 0.100		

1 – There was no statistical outcome on SPSS

F2: Heat-induced fragmentation

F2.1: Frequencies of bones with each heat -induced fragmentation cross tabulation in relation to temperature

	Temperature				
	25	300	400	500	Total
No fragments	6	9	7	6	28
Fragments align	0	0	1	1	2
Fragments align partially	0	0	1	0	1
Fragments do not align	0	0	0	2	2
Total	6	9	9	9	33

F2.2: Table showing Chi-squared test of heat-induced fragmentation in relation to temperature.

	Value	Exact Sig. (2-sided)
Fisher-Freeman-Halton Exact Test	8.546	0.339
N of Valid Cases	33	

F2.3: Table showing paired-wise Fisher's Exact test of heat-induced fragmentation in relation to temperature.

Fragmentation	Paired-wise Fisher's Exact test[1]
25 - 300	. [2]
25 - 400	p = 1.000
25 - 500	p = 0.486
300 - 400	p = 0.471
300 - 500	p = 0.206
400 -500	p = 0.718

1 – The adjusted alpha from the paired-wise Fisher's Exact test p = 0.0083
2 - There was no statistical outcome on SPSS

F2.4: Frequencies of bones with each heat -induced fragmentation cross tabulation in relation to bone condition

	Condition Code					
	Fleshed	Wet	Dry	Wet control	Dry control	Total
No fragments	6	7	9	3	3	28
Fragments align	1	1	0	0	0	2
Fragments align partially	0	1	0	0	0	1
Fragments do not align	2	0	0	0	0	2
Total	9	9	9	3	3	33

F2.5: Table showing Chi-squared test of heat-induced fragmentation in relation to bone condition.

	Value	Exact Sig. (2-sided)
Fisher-Freeman-Halton Exact Test	11.083	0.746
N of Valid Cases	33	

F2.6: Table showing pairwise Fisher's Exact test of heat-induced fragmentation in relation to bone condition.

Fragmentation	Paired-wise Fisher's Exact test [1] (sign p = 0.005)
Wet Control – Dry Control	. [2]
Wet Control - Wet	P = 1.000
Wet Control - Fleshed	P = 1.000
Wet Control - Dry	. [2]
Dry Control - Wet	P = 1.000
Dry Control - Fleshed	P = 1.000
Dry Control - Dry	. [2]
Wet - Fleshed	P = 0.718
Wet - Dry	P = 0.206
Fleshed- Dry	P = 0.471

1 – The adjusted alpha from the paired-wise Fisher's Exact test p = 0.005
2 - There was no statistical outcome on SPSS

F2.7: Frequencies of bones with each heat -induced fragmentation cross tabulation in relation to temperature and bone condition.

	Condition Code																			
	Fleshed				Wet				Dry				Wet control				Dry control			
	25	300	400	500	25	300	400	500	25	300	400	500	25	300	400	500	25	300	400	500
No fragments	0	3	2	1	0	3	2	2	0	3	3	3	3	0	0	0	3	0	0	0
Fragments align	0	0	1	0	0	0	0	1	0	0	0	0	0	0	0	0	0	0	0	0
Fragments align partially	0	0	0	0	0	0	1	0	0	0	0	0	0	0	0	0	0	0	0	0
Fragments do not align	0	0	0	2	0	0	0	0	0	0	0	0	0	0	0	0	0	0	0	0

F2.8: Table showing paired-wise Fisher's Exact test of heat-induced fragmentation in relation to temperature and bone condition.

Test	Significance	Test	Significance	Test	Significance
Wet Control – Dry Control	.	Wet 300°C – Wet 400°C	P = 1.000	Wet 500°C – Dry 400°C	
Wet Control – Wet 300°C	.	Wet 300°C – Wet 500°C	P = 1.000	Wet 500°C – Dry 500°C	
Wet Control – Wet 400°C	P = 1.000	Wet 300°C – Fleshed 300°C	.	Fleshed 300°C - Fleshed 400°C	P = 1.000
Wet Control – Wet 500°C	P = 1.000	Wet 300°C – Fleshed 400°C	P = 1.000	Fleshed 300°C - Fleshed 500°C	P = 0.400
Wet Control – Fleshed 300°C	.	Wet 300°C – Fleshed 500°C	P = 0.400	Fleshed 300°C – Dry 300°C	.
Wet Control – Fleshed 400°C	P = 1.000	Wet 300°C – Dry 300°C	.	Fleshed 300°C – Dry 400°C	.
Wet Control – Fleshed 500°C	P = 0.400	Wet 300°C – Dry 400°C	.	Fleshed 300°C – Dry 500°C	.
Wet Control – Dry 300°C	.	Wet 300°C – Dry 500°C	.	Fleshed 400°C - Fleshed 500°C	P = 0.400
Wet Control – Dry 400°C	.	Wet 400°C - Wet 500°C	P = 1.000	Fleshed 400°C - Dry 300°C	P = 1.000
Wet Control – Dry 500°C	.	Wet 400°C - Fleshed 300°C	P = 1.000	Fleshed 400°C - Dry 400°C	P = 1.000
Dry Control - Wet 300°C	.	Wet 400°C - Fleshed 400°C	P = 1.000	Fleshed 400°C - Dry 500°C	P = 1.000
Dry Control - Wet 400°C	P = 1.000	Wet 400°C - Fleshed 500°C	P = 0.400	Fleshed 500°C - Dry 300°C	P = 0.400
Dry Control - Wet 500°C	P = 1.000	Wet 400°C – Dry 300°C	P = 1.000	Fleshed 500°C - Dry 400°C	P = 0.400
Dry Control - Fleshed 300°C	.	Wet 400°C – Dry 400°C	P = 1.000	Fleshed 500°C - Dry 500°C	P = 0.400
Dry Control - Fleshed 400°C	P = 1.000	Wet 400°C – Dry 500°C	P = 1.000	Dry 300°C - Dry 400°C	.
Dry Control - Fleshed 500°C	P = 0.400	Wet 500°C – Fleshed 300°C	P = 1.000	Dry 300°C - Dry 500°C	.
Dry Control - Dry 300°C	.	Wet 500°C – Fleshed 400°C	P = 1.000	Dry 400°C - Dry 500°C	.
Dry Control - Dry 400°C	.	Wet 500°C – Fleshed 500°C	P = 0.400		
Dry Control - Dry 500°C	.	Wet 500°C – Dry 300°C			

1 – There was no statistical outcome on SPSS

Appendix G: Heat-induced mass loss

G1: Pre- and post-cremation mass

Wilcoxon Signed Ranks test				
		N	Mean Rank	Sum of Ranks
Post-Cremation Mass - Pre-Cremation Mass	Negative Ranks	27	14.00	378.00
	Positive Ranks	0	0.00	0.00
	Ties	6		
	Total	33		

Wilcoxon Signed Ranks Test Statistics	
	Post-Cremation Mass - Pre-Cremation Mass
Z	-4.542
Asymp. Sig. (2-tailed)	$p < 0.001$

G2: Mass loss percentage in relation to temperature

ANOVA					
Mass Loss Percentage					
	Sum of Squares	df	Mean Square	F	Sig.
Between Groups	4477.724	2	2238.862	7.312	0.003
Within Groups	7348.761	24	306.198		
Total	11826.485	26			

Multiple Comparisons							
Dependent Variable: Mass Loss Percentage							
			Mean Difference (I-J)	Std. Error	Sig.	95% Confidence Interval	
	(I) Temperature	(J) Temperature				Lower Bound	Upper Bound
Bonferroni	300	400	-11.07506	8.24888	0.576	-32.3047	10.1546
		500	-31.11671*	8.24888	0.003 *	-52.3464	-9.8870
	400	300	11.07506	8.24888	0.576	-10.1546	32.3047
		500	-20.04166	8.24888	0.069	-41.2713	1.1880
	500	300	31.11671*	8.24888	0.003 *	9.8870	52.3464
		400	20.04166	8.24888	0.069	-1.1880	41.2713

*-Significant values based on adjusted alpha

G3: Mass loss percentage in relation to bone condition

ANOVA					
Mass Loss Percentage					
	Sum of Squares	df	Mean Square	F	Sig.
Between Groups	1018.294	2	509.147	1.131	0.339
Within Groups	10808.191	24	450.341		
Total	11826.485	26			

G4: Mass loss percentage in relation to temperature and bone condition

Sample 1-Sample 2	Test Statistic	Std. Error	Std. Test Statistic	Adj. p-value[a]
Fleshed 400-Dry 300	.167	6.480	.026	1.000
Fleshed 400-Fleshed 300	1.000	6.480	.154	1.000
Fleshed 400-Wet 300	5.000	6.480	.772	1.000
Fleshed 400-Dry 400	-5.667	6.480	-.875	1.000
Fleshed 400-Dry 500	-10.500	6.480	-1.620	1.000
Fleshed 400-Wet 500	-12.333	6.480	-1.903	1.000
Fleshed 400-Wet 400	14.667	6.480	2.263	0.850
Fleshed 400-Fleshed 500	-19.667	6.480	-3.035	0.087
Dry 300-Fleshed 300	.833	6.480	.129	1.000
Dry 300-Wet 300	4.833	6.480	.746	1.000
Dry 300-Dry 400	-5.500	6.480	-.849	1.000
Dry 300-Dry 500	-10.333	6.480	-1.595	1.000
Dry 300-Wet 500	-12.167	6.480	-1.878	1.000
Dry 300-Wet 400	-14.500	6.480	-2.238	0.909
Dry 300-Fleshed 500	-19.500	6.480	-3.009	0.094
Fleshed 300-Wet 300	4.000	6.480	.617	1.000
Fleshed 300-Dry 400	-4.667	6.480	-.720	1.000
Fleshed 300-Dry 500	-9.500	6.480	-1.466	1.000
Fleshed 300-Wet 500	-11.333	6.480	-1.749	1.000
Fleshed 300-Wet 400	-13.667	6.480	-2.109	1.000
Fleshed 300-Fleshed 500	-18.667	6.480	-2.881	0.143
Wet 300-Dry 400	-.667	6.480	-.103	1.000
Wet 300-Dry 500	-5.500	6.480	-.849	1.000
Wet 300-Wet 500	-7.333	6.480	-1.132	1.000
Wet 300-Wet 400	-9.667	6.480	-1.492	1.000
Wet 300-Fleshed 500	-14.667	6.480	-2.263	0.850
Dry 400-Dry 500	-4.833	6.480	-.746	1.000
Dry 400-Wet 500	-6.667	6.480	-1.029	1.000
Dry 400-Wet 400	9.000	6.480	1.389	1.000
Dry 400-Fleshed 500	-14.000	6.480	-2.161	1.000
Dry 500-Wet 500	1.833	6.480	.283	1.000
Dry 500-Wet 400	4.167	6.480	.643	1.000
Dry 500-Fleshed 500	9.167	6.480	1.415	1.000
Wet 500-Wet 400	2.333	6.480	.360	1.000
Wet 500-Fleshed 500	-7.333	6.480	-1.132	1.000
Wet 400-Fleshed 500	-5.000	6.480	-.772	1.000

Appendix H: Heat-induced macro-fracturing

H1: Inter- and intra-observer intra-class correlation coefficient test results.

		ICC Test		95% Confidence Interval	
		ICC	Sig.	Lower Bound	Upper Bound
Inter-observer	Colour change	0.783	<0.001	0.130	0.973
	Total number of fractures per bone	0.555	<0.001	0.108	0.853

	Number of fracture types present per bone	0.517	<0.001	0.353	0.660
	Number of fractures present on each location	0.480[1]	<0.001	0.222	0.681
Intra-observer	**Colour change**	0.978	<0.001	0.740	0.977
	Total number of fractures per bone	0.839	<0.001	0.605	0.953
	Number of fracture types present per bone	0.757	<0.001	0.657	0.837
	Number of fractures present on each location	0.749	<0.001	0.619	0.848

1-The ICC value less than 0.5 indicating that it is less than a good repeatability value.

H2: Total number of macrofractures in relation to temperature

Kruskal Wallis Test Statistics	
	Total Number of Fractures
Kruskal-Wallis H	23.023
df	3
Asymp. Sig.	p < 0.001

Mann Whitney U Post Hoc Test Pairwise Comparisons of Temperature (C°) [1]				
Sample 1-Sample 2	Test Statistic	Std. Error	Std. Test Statistic	Adj. Sig
25-300	-7.167	5.033	-1.424	0.927
25-400	-14.444	5.033	-2.870	0.025*
25-500	-22.389	5.033	-4.449	0.000*
300-400	-7.278	4.502	-1.617	0.636
300-500	-15.222	4.502	-3.382	0.004*
400-500	-7.944	4.502	-1.765	0.466

1-The adjusted alpha based on Mann Whitney U Post Hoc test pairwise p = 0.050
*-Significant value based on the adjusted alpha

H3: Total number of macrofractures in relation to bone condition

ANOVA					
Total Number of Fractures					
	Sum of Squares	df	Mean Square	F	Sig.
Between Groups	1163.616	4	290.904	8.516	p < 0.001
Within Groups	956.444	28	34.159		
Total	2120.061	32			

Post Hoc Multiple Comparisons Test [1]							
Dependent Variable: Total Number of Fractures							
	(I) Bone Condition	(J) Bone Condition	Mean Difference (I-J)	Std. Error	Sig.	95% Confidence Interval	
						Lower Bound	Upper Bound
Bonferroni	Fleshed	Wet	-6.000	2.755	0.380	-14.39	2.39
		Dry	-10.111	2.755	0.010 *	-18.51	-1.72
		Wet Control	6.556	3.896	1.000	-5.32	18.43
		Dry Control	6.556	3.896	1.000	-5.32	18.43
	Wet	Fleshed	6.000	2.755	0.380	-2.39	14.39
		Dry	-4.111	2.755	1.000	-12.51	4.28
		Wet Control	12.556	3.896	0.032 *	0.68	24.43
		Dry Control	12.556	3.896	0.032 *	.68	24.43
	Dry	Fleshed	10.111	2.755	0.010 *	1.72	18.51
		Wet	4.111	2.755	1.000	-4.28	12.51

		Wet Control	16.667	3.896	0.002 *	4.79	28.54
		Dry Control	16.667	3.896	0.002 *	4.79	28.54
	Wet Control	Fleshed	-6.556	3.896	1.000	-18.43	5.32
		Wet	-12.556	3.896	0.032 *	-24.43	-0.68
		Dry	-16.667	3.896	0.002 *	-28.54	-4.79
		Dry Control	0.000	4.772	1.000	-14.54	14.54
	Dry Control	Fleshed	-6.556	3.896	1.000	-18.43	5.32
		Wet	-12.556	3.896	0.032 *	-24.43	-0.68
		Dry	-16.667	3.896	0.002 *	-28.54	-4.79
		Wet Control	0.000	4.772	1.000	-14.54	14.54

1-The adjusted alpha based on Bonferroni Correction post hoc p = 0.050
*-Significant values based on adjusted alpha

Appendix I: Experimental microfracture

I1: Microfracture Intra-observer repeatability

Overall Agreement						
		Asymptotic			Asymptotic 95% Confidence Interval	
	Kappa	Standard Error	z	Sig.	Lower Bound	Upper Bound
Overall Agreement	0.685	0.107	6.407	<0.001	0.475	0.894

I2: Micro-fracture Inter-observer repeatability

Overall Agreement						
		Asymptotic			Asymptotic 95% Confidence Interval	
	Kappa	Standard Error	z	Sig.	Lower Bound	Upper Bound
Overall Agreement	0.541	0.108	4.992	<0.001	0.329	0.754

I3: Repeatability test for total number of micro-fractures based on definitions adapted from Bacci *et al*., 2021.

	Tests	ICC Test		95% Confidence Interval	
		ICC	Sig.	Lower Bound	Upper Bound
Inter-observer	Trial 1-Trial 2	0.703	< 0.001	0.588	0.790
	Trial 1-Trial 3	0.745	< 0.001	0.643	0.821
	Trial 2-Trial 3	0.721	< 0.001	0.612	0.803
Intra-observer	Observer 1- Observer 2	0.259	0.002	0.073	0.429
	Observer 1- Observer 3	-0.002	0.509	-0.144	0.154
	Observer 2- Observer 3	0.013	0.431	-0.121	0.161

Appendix J: Plagiarism – Turnitin Report

